CFD ANALYSIS OF TURBULENT SLURRY FLOW THROUGH THE SENSING REGION OF NEAR IR DIFFUSE TRANSMISSION AND REFLECTANCE PROBES MOUNTED IN A PIPE FLOW

By

GAURAV SHARMA

Bachelor of Engineering in Mechanical Engineering

Madhav Institute of Technology and Science

Gwalior, India

2006

Submitted to the Faculty of the
Graduate College of the
Oklahoma State University
in partial fulfillment of
the requirements for
the Degree of
MASTER OF SCIENCE
May, 2010

CFD ANALYSIS OF TURBULENT SLURRY FLOW THROUGH THE SENSING REGION OF NEAR IR DIFFUSE TRANSMISSION AND REFLECTANCE PROBES MOUNTED IN A PIPE FLOW

Thesis Approved:

Dr. Frank W. Chambers

Thesis Adviser

Dr. David G. Lilley

Dr. Andrew S. Arena

Dr. A. Gordon Emslie

Dean of the Graduate College

ACKNOWLEDGMENTS

First of all, I wish to extend sincere gratitude to my Adviser Dr. Frank Chambers for his esteemed guidance and untiring supervision. I extremely appreciate his caring attitude towards his students. Also, I would like to thank him for his precious suggestions during my research work. I am grateful to him for providing me the privilege to work on this research opportunity.

I also wish to extend my appreciation to Dr. A. Arena and Dr. D.G. Lilley for serving as the members of my Thesis committee. I wish to say thanks to my dear parents and my brothers Saurav and Pushkar for boosting me up with their love.

I would like to express my regards to my research group members Netaji, Krishna and Vamsee for their suggestions during my research study. At last, I am indebted to my friends Vineet, Ashish, Sam and Janae for their love and encouragement.

I am also thankful to all those people who directly or indirectly helped me through my thesis work.

TABLE OF CONTENTS

Chapter Page

LIST OF TABLES

Table

Page

LIST OF FIGURES

Figure Page

NOMENCLATURE

a	Acceleration in m/sec
f	Body forces
g	Acceleration due to gravity
I	Identity matrix
k	Turbulent Kinetic energy
L	Litres
m	Mass in Kg.
p	Pressure
r	Radial coordinate
R	Radius in meters.
Re	Reynolds number
Re_P	Particle Reynolds number
Δp	Pressure drop
t	Time in secs.
T	Temperature
u	Velocity in X direction
v	Velocity in Y direction
w	Velocity in Z direction
X	X-axis

Y	Y-axis
Z	Z-axis
α	Volume fraction
ε	Turbulence dissipation
κ	Log-law coefficient
ρ	Fluid density
τ	Stress tensor
μ	Dynamic viscosity
ν	Kinematic viscosity
ν_T	Turbulent viscosity
ω	Specific dissipation rate
∇	Del operator
θ	Angular distance

ABBREVIATIONS

ACH	Air Changes per Hour
AR	Aspect Ratio
ADP	2, Amino, 4, 6 Dimethyl Pyrimidine
ASM	Algebraic Slip Model
CFD	Computational Fluid Dynamics
DES	Detached Eddy Simulation
DNS	Direct Numerical Simulation
FTIR	Fourier Transformed Infrared Reflectance
LES	Large Eddy Simulation
LIF	Laser Induced Fluorescence
N-S	Navier Stokes
NIR	Near Infrared
NIRA	Near Infrared Reflectance Analysis
PDE	Partial Differential Equation
PEPT	Positron Emission Particle Technique
PIV	Particle Image Velocimetry
RANS	Reynolds Averaged Navier Stokes
RNG	Renormalization Group
RSM	Reynolds Stress Model
SA	Spalart Allmaras
S k- ε	Standard k- ε
SKW	Standard k-omega

SST	Shear Stress Transport k- omega
TI	Turbulent Intensity

CHAPTER I

INTRODUCTION

1.1 Background:

The flow of liquids through pipelines is a common process in industries as well as the households. The supply of water for household purposes involves the transport of water through pipes which have small diameters. In industries the water and other fluids supply is done through pipelines with comparatively larger diameter. The mechanics of the flow of fluids depends on the properties of the fluids being transported. These fluid properties include density, viscosity and surface tension. The mechanics of fluid flow is simpler when there is only one phase. Complexities in the flow are introduced when more than one number of phases is participating in the flow. The flow in which more than one phases is flowing together is known as multiphase flow. Examples of multiphase flow can be bubble or droplet flow, slug flow, pneumatic transport, hydrotransport or slurry flows. The multiphase flow of solid particles with liquids such that the presence of solid particles in the flow is considerable is termed slurry flow

Multiphase flows are complex flows and their complexity can be attributed to the interaction between the participating phases. Apart from this, there can be other sources which contribute to the complexity of the flow. These may include the physical aspects

like transition between different flow regimes, turbulent flow and the presence of some disturbed interface such as surface waves on a film to name a few. In the case of slurry flows liquid- particle interaction and turbulent characteristics of the flow are the factors which require special attention. In industrial applications, along with single phase flows, there are many multiphase flows in the form of particles and liquid flowing together. Most of the pharmaceutical and petrochemical industries involve the transportation of slurries through pipes using different type of pumping devices. These slurries have a complex composition consisting of chemical particles flowing in organic or inorganic solutions. The methods or the processes applied in the handling of slurries should be effective and efficient. The current research focus is to design better sampling techniques for measuring these chemical slurries used for industrial purposes. This study aims at providing a new methodology for the analysis of complex samples under industrial conditions. In the current study the flow of some specific slurries has been simulated using a CFD commercial software package.

1.2 Importance of computational methods: Experimental methods have always found wide applications in order to visualize the flow fields and the feature which are of real concern. Some of the flows can be very well described using experimental methods. However, it could be difficult to set up a multiphase flow experiment with the necessary degree of control. Such situations arise, for example, in the case of the breakup of a drop in a turbulent flow or precise characterization of the bubble or drop size distribution. There are many experimental techniques that can be easily implemented for single phase flows while multiphase flow systems poses severe difficulties. For example, bubbly flow may become opaque resulting in poor visualization even at low volume fractions. The

clustering of particles suspended in a slurry flow depends on the small scale details which are difficult to be resolved through experiments. In all these situations, numerical simulation stands out as an important tool for the study of multiphase flow systems. Computation techniques may be the best tools in some conditions. These conditions may be attributed to the presence of forces of gravity and surface tension. In case of experimental techniques, these aspects may be immeasurable. In the case of multiphase flows, there is always a requirement of reduced descriptions for modeling which is given sometimes through averaged equations. Thus such reduced models are greatly benefitted from the computational techniques.

1.3 Fluent and Gambit as CFD tools: As discussed in the preceding paragraphs computational methods have an edge over experimental techniques not only because of the ease of obtaining the end results but also because they are economical compared to the experimental set ups. In the present study, Fluent has been employed as the commercial software package in order to facilitate the analysis of chemical slurry flow through pipes with FTIR (Fourier transformed infrared reflectance) probes. Gambit has been used as the preprocessor used to construct and mesh the pipe and probe assembly. The meshed geometry is exported to Fluent for the actual analysis. The pipe Reynolds number for the flow is of the order of 100,000. The mixture model has been employed as the multiphase flow model while K-ε model has been used to account for the turbulence effects of the flow. Two different types of slurries have been considered for analysis. The first one is the flow of ADP particles in Xylene as the liquid and another is the Calcium Carbonate particles in water as the flowing liquid.

1.4 **Aims and objectives to accomplish:** The present study aims at the following tasks:

- To apply CFD to visualize the flow over and through the sensing gap of the FTIR probe.
- To determine the volume fraction profiles of the particles flowing through the sensing gap.
- To determine the velocity profiles of the particles flowing through the sensing gap.

CHAPTER II

REVIEW OF LITERATURE

2.1 Introduction:

This chapter deals with the studies and investigations done by researchers and scientists around the world in the field of Computational Fluid Dynamics (CFD). The discussion in the current study will be focusing on the multiphase flow consisting of solid particles and liquid fluids with turbulent characteristics. This chapter will also deal with a little discussion about the Fourier transformed infrared spectroscopic studies. In the current study the area to be given attention is the CFD simulations of turbulent slurry flows through pipe, hence major stress has been given on these keywords. Therefore this chapter includes the review of most relevant literature available. In the first part of the chapter, studies related to the CFD have been covered while the later part deals in brief about Fourier transformed spectroscopic studies and some of their applications.

2.2 Numerical simulation studies in two phase flow: As the present study deals with the flow of ADP particles with Xylene as the liquid fluid hence it is necessary that the particles should remain in suspension with the liquid while during the flow. Various studies have been conducted in order to determine the factors that are responsible to make the particles flow with the liquid fluid. This section will cover the previous studies and

researches made in order to discuss the effects of governing parameters on the flow characteristics and its behavior in a two phase flow. These parameters are particle size, particle concentration and particle velocities to name a few. Xu et al. (2004) have conducted numerical simulations in order to simulate the flow of solid hydrogen particles in liquid helium. They concluded that the flow must be turbulent else the hydrogen particles will form a sliding layer over the helium layer. The concentration profiles of hydrogen particles have been found to be dependent upon the size of particles, the velocity of flow and the inlet volume fraction of the hydrogen particles.

Similarly Oey et al. (2001) have simulated the flow of gas-liquid and solid flow in an internal loop airlift reactor. They have made use of the two phase flow approach in order to simulate a three phase mixture of solid, liquid and gas by treating the airlift loop as two phase system i.e. a gas-liquid two phase system. They were able to detect different flow regimes by varying the gas flow rate. They also concluded that turbulent dispersion of the solid particles is needed in order to prevent them from settling down at the dead corners. The solid particle distribution is found to be smooth with higher volume fraction of solids in the lower part of the lower comers when the turbulent dispersion is taken into consideration. When turbulent dispersion is taken into account equilibrium between settling and dispersion is found.

Kasat et al. (2008) developed a CFD model in order to evaluate the complex interaction between the solid particles and the liquid phase mixing in a stirred slurry reactor. They studied the characteristic behavior of mixing time of the solid liquid suspension as a function of the impeller speed. According to them the mixing time increases with the increment in impeller speed and then reaches a maximum value and

further increment in impeller speed brings a gradual decrease in the mixing time. They have attributed the delayed mixing of the solid and liquid phases to the low velocities in the upper clear liquid region in the reactor. Their CFD model can be used for large scale industrial studies which involve the suspension and mixing of solid particles into liquids.

2.3 Studies of two phase slurries in pipes: In this portion of the chapter, discussion is primarily focused on studies involving solid-liquid flow through pipelines.

Brown (1999) studied the abrasive nature of a slurry consisting of bauxite particles flowing with caustic liquid by predicting the erosion taking place in the pipelines. He developed a three dimensional CFD model bases on Eulerian- Eulerian continuum approach. He has used K-ε model to account for the turbulence effects at the Tee section. A swirling inlet flow condition has been preferred to be used to accurately predict the accumulation of particles and the position of accumulation. They have employed a multiphase model with the help of which a solution for the erosion problem has been obtained. The problem of erosion has been found to be decreased by using a pivoted elbow design in place of a Tee junction. They have shown the ability of applications of CFD to the industrial problems which occur due to erosion phenomenon.

It has been observed that deposition critical velocity plays an important role in the design of the pipelines made for the slurry flows. It is the magnitude of minimum flow velocity at which the flow of slurries can remain suspended in the pipeline. It has been found that the deposition velocity of flow depends on several factors including the size of the particles, the density of particles, the diameter of pipe and the solid concentration of the slurries. Kaushal et al. (2002) have conducted experiments to measure the

concentration at the pipe bottom at deposition velocity. They have utilized the data studied by Kaushal et al. (1995), Mukhtar et al. (1991), Seshadri et al. (1975) and Seshadri et al. (1980) with variable size iron ore particles, copper tailings and zinc tailings slurries flowing through pipes. The diameters of the pipelines which were considered are 55 mm and 105 mm. They have made modifications to Karabela's model (1977) on the basis of their studies. The original Karabela's model determines the solid concentration profiles in a slurry consisting of multisized particles with help of an equation. The Karabela's equation take into account the particle diffusivity, the particle size, and settling velocity. There are two assumptions involved in determining the solid concentration profiles in Karabela's model. Firstly, the dimensionless eddy diffusivity is taken constant and is independent of space coordinates and solid concentration. Second, the solid concentration is assumed to depend only on vertical coordinate. It has been found that the overall concentration profiles predicted by the modified Karabelas model for 30 sets of experimental data holds good agreement for almost all of them. The original Karabelas model gives large deviations particularly for higher concentrations. Thus it has been concluded that the modified Karabelas model is more accurate. This is due to incorporating the solid concentration effects on settling of particles and the turbulent eddy diffusivity. Thus it has been proved that turbulence is affected by solid concentration. Further, the deposition velocity can be obtained using the ratio of concentration at the bottom and static settled concentration. Also deposition takes place when solid concentration at the bottom becomes equal to three times the product of efflux concentration and static settled concentration.

Deposition critical velocity plays an important role in the flow of slurries through pipelines. However designing a pipeline also requires lot of parameters which needs to be considered. Pressure drop through the pipeline is one of the important factors that should be given importance. In order to design a pipeline carrying slurries it is necessary to know the pressure drop. Also it helps to choose the power of the pumping device. Kaushal et al. (2005) made an attempt to measure the pressure drop and concentration profiles in horizontal, vertical and 45^{o} inclined planes including the axis of the pipe. The diameter of the pipe was 54.9 mm. The concentration profiles were obtained by traversing isokinetic sampling probes. They have used two types of glass bead particles with mean diameters 440 μm and 125 μm respectivelly. They have developed the experimental set up as shown in the figure 2.1.

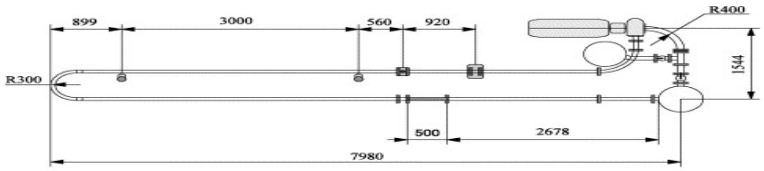

(a) Plan view (all the dimensions are in mm)

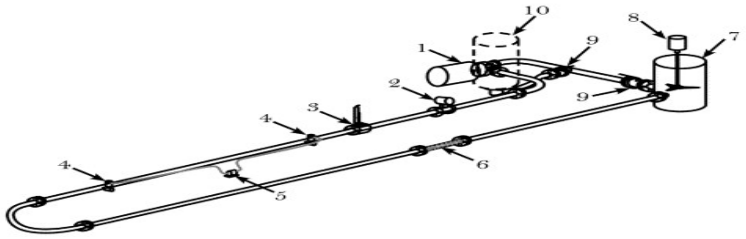

1. Slurry Pump 2. Electomagnetic flow meter 3. Isokinematic sampling probe
4. Pressure tapings 5. Differential pressure transducer 6. Observation chamber
7. Slurry Tank 8. Mixer 9. Valve 10. Water Tank

(b) Schematic diagram

Fig. 2.1 Test loop used by Kaushal et al. (2005)

Pipe diameter is 54.9 mm while the rig has a 22 m long recirculating pipe loop with slurry tank having capacity of 200 L. It also consists of 150 L capacity water tank along with a centrifugal pump to maintain the flow of slurry. The supply of slurry is done through tank 7 (Fig. 2.1) where proper mixing of water and solid particles are done

mechanically using an electric mixer. It is ensured with the help of the mixer that distribution of particles should be homogenous. The outlet of the tank is situated at 10 cm above the bottom i.e. almost 10 cm below the impeller. There is an additional water tank 10 (as shown in Fig. 2.1) connected in parallel with the slurry tank which has been employed to reduce the variation of mixture level in the tank at start up and shut down. The circulation of slurry in the loop is done with a centrifugal pump with the operating conditions of – 15 kW with a rate of 0.6 cubic meters per min at 22 m head. Slurry volumetric flow rate is measured with the help of an electromagnetic flow meter 2 (as shown in Fig. 2.1). A sampling probe 3 (as shown in Fig. 2.1) is used to measure the concentration profiles. It has a rectangular slot of area 5 mm x 6 mm which is 3 mm above the end. Samples were collected in horizontal, vertical and 45^{o} inclined planes at different locations ensuring the slurry flow is uniform and uninterrupted. On the basis of their results they have concluded that variation in flow velocity does not bring any significant variation in the concentration in horizontal plane. They have obtained a unique change of concentration profile for 440 μm particles which indicated a sliding bed regime. They also found that high frictional losses are associated with narrow grading particles (small diameter) and broad grading particles (larger diameter) have low frictional losses at higher concentrations.

In another study, Kaushal et al. (2002) have modified the model for solids concentration profiles and composites proposed by Kaushal and Tomita (2002). They have included the effect of particle size and efflux concentration of particle diffusivity. They have calculated the ratio of homogeneously distributed concentration and heterogeneously distributed concentration for each size of particles present in the slurry.

They have calculated the total pressure drop in the pipe by adding the pressure drop through the homogenously distributed and heterogeneously distributed portions of all the particle sizes. They have also done the experiments to calculate the pressure drop to validate the results. These pressure drop results obtained are found to be more accurate than those obtained by previous researchers and were found to be in good agreement with the experimental results. They calculated the mean square difference values between predicted and experimental values and have expressed as percentage of the measured value. Their comparison statistics have shown the variation for different models as Wasp et al. (1977) with 5-21.8%, Gillies model (1991) with 6-9.2 %, Kaushal and Tomita model (2002) with 1.7-3.5 % and the proposed model with just 1.6-2.0 %.

Kumar et al (2003) have also conducted studies with varied range of efflux concentration and particle size through slurry pipelines carrying liquid solid flows. They have measured the pressure drop and distribution of solid concentration. They have measured the particle size effects on pressure drop utilizing the solid distribution in the pipe. They have employed an integral flow model to determine the optimum particle size for which the specific energy consumption is minimum. They have used the integral flow model for predicting pressure drop and solid particle concentration. They have proved that there can be an optimum size of particles for which the energy required for transportation of slurry having that particle size will be lesser than the energy required for slurry having even smaller particle size. They have also concluded that modified Karabela's model is able to predict the solid concentration with good accuracy.

Ling et al. (2001) have used a horizontal pipeline having a fully developed solid liquid flow in order to perform the numerical investigations. They have employed an

algebraic slip model (ASM) in order to model two phase flow and RNG K-ε model for accurately modeling the turbulence effects. They have used an unstructured grid in order to discretize the flow domain. Finite volume method is used for the determining the solution of the governing equations. The pipeline used in the study has a length of 1.4 m with a diameter of 0.0221 m. They have used silica sand and Zirconia sand particles with densities of 2380 Kg per cubic meter and 4223 Kg per cubic meter respectively. They have displayed various slurry characteristics which include slurry density, volume fraction variations, slip velocity magnitude, slurry mean velocity variations and skin friction variation. Their results vary significantly for silica and zirconia sand particles as they have different densities. Their results have been found in good agreement with the experimental data when the slurry mean velocity has a magnitude higher than the critical deposition velocity. Their results are also found to match the results obtained in current research which are presented in Results and Discussion section. The effects of density of particles are clearly visible in the results obtained.

Lin et al (2007) have studied the developing slurry flow in the entrance region of a horizontal pipe. They have also used algebraic slip model (ASM) in order to model two phase flow and RNG K-ε model for modeling the turbulence effects. They have used an unstructured grid with 67200 cells. The turbulence intensity level used in their computations as a boundary condition is 4%. They have plotted the profiles for comparison of volume fraction, density distribution, mean velocity profiles and mean skin friction coefficients. They have also shown the variation of volume fraction in the vertical central plane of the pipe's cross section for volume fractions 0.172414 and 0.20689. This is shown in Fig. 2.2. The results obtained in the current research for

velocity profiles along the vertical axis in the entrance region of the pipe slurry flow are compared with those obtained by Lin et al in chapter 4. The results of Lin et al. for velocity profiles of slurry are shown in Fig. 2.3. They have concluded that volume fraction and mean density will be lower in the upper part compared to lower part of the pipe in the entrance region. In the fully developed region, in the upper part of pipe, the solid liquid density will be almost equal to primary fluid density and the volume fraction will be almost zero.

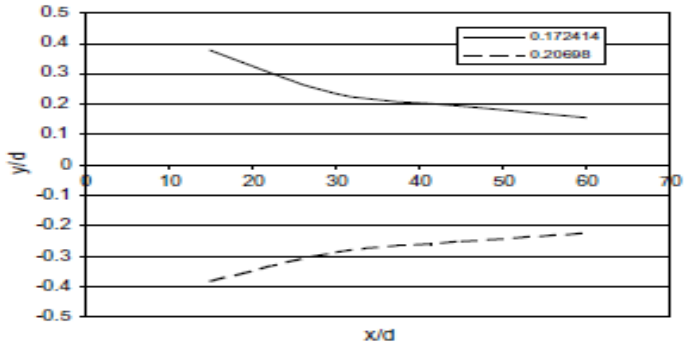

Fig. 2.2 Evolution of volume fraction of silica sand at the vertical central plane of the pipe's cross section (Source: Lin et al (2007))

Hossain et al (2003) have used the multiphase mixture model available in Fluent in order to study the particle deposition and suspension in a horizontal pipe flow. They have considered the diameter of particle, density of fluid and velocity of fluid as the decisive factors for the deposition of particles in the pipe flow. Similar to the current research, they have also considered the gravitational forces as well as hydrodynamic drag forces on the particles. They have quantified the gravitational settling velocities and free flight velocities. It has been concluded on the basis of same that those larger particles that have gravitational settling velocity more than twice their free flight velocities will be more likely to settle. Similarly, smaller particles with gravitational settling velocities less than half of their free flight velocities will be have dominance of turbulent diffusion and

hence are dispersed along the cross section of the pipe. The results obtained in the current research are compared with findings expressed by Hossain et al. in chapter 4.

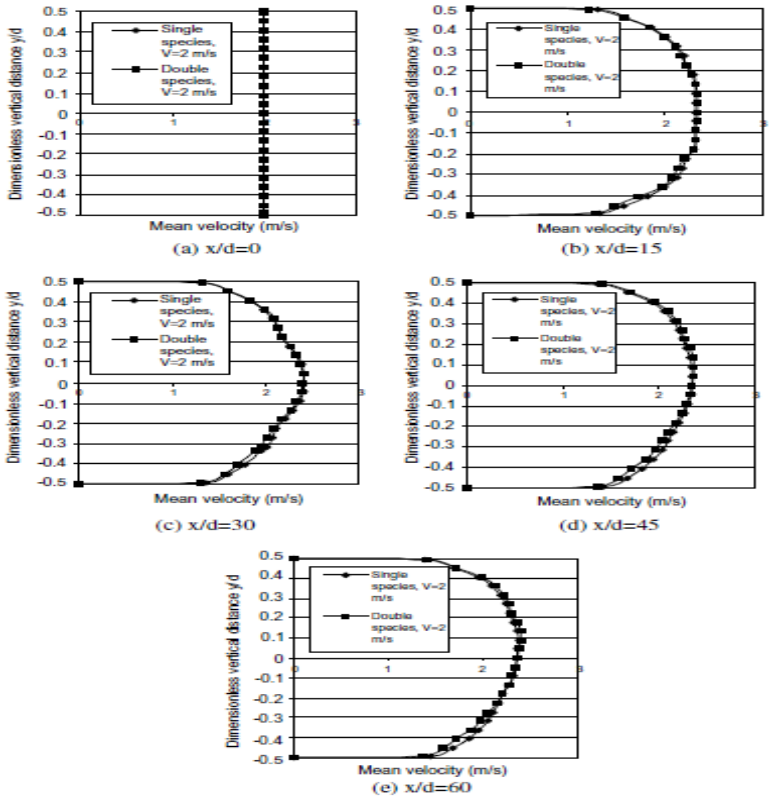

Fig. 2.3 Velocity profiles of single and double species slurry flow along the vertical centerline from the entrance region to fully developed slurry flow region (volume fraction=20%, particle diameter =100 microns, pipe diameter = 0.0221m (Source: Lin et al (2007))

Eesa et al. (2008) have conducted similar studies and have used a Eulerian-Eulerian Computational fluid dynamics approach for investigating the flow of coarse particles in a horizontal or vertical pipe. They also conducted experimental measurements in order to validate the results predicted through modeling. The positron emission particle technique (PEPT) has been utilized for the experimental verification. The results of the previous studies have been used in the validation of the pressure drop computations. The particles employed in the study can be considered neutrally buoyant. The solid and liquid phase velocities, pressure drop and particle concentration profiles are found to be

dependent upon the particle diameter and their concentration, mean flow velocity and the rheological properties that the carrier fluid possesses. Due to large particle diameters, asymmetry is found to arise in the solid as well as liquid velocity profiles. Pseudo-homogeneous flow takes place for smaller particles while the concentration profiles are distorted for particles with larger diameters as larger particles are more likely to settle during the flow. Higher solid concentrations result in increase in pressure drop along with more uniform radial distribution of particles. The non-dimensional solid and liquid phase velocities and particle concentration profiles were not dependent on the particle diameter and their concentrations.

Kaushal et al. (2002) have studied the concentration profiles along with the pressure drop through a pipe of diameter 105 mm for a zinc tailings slurry flow consisting of more than one size particle. The particle size in the slurry ranges from 38 μm to 739 μm. It has been observed that many researchers have made attempts in the direction of prediction of pressure drop along with Wasp et al. (1977), Doron et al., (1987), Gillies et al. (1991), Sundqvist et al (1996), Mishra et al. (1998), Ghanta and Purohit, (1999), Wilson et al. (2002), to name some of them. Out of these, the approaches and models proposed by Wasp et al. (1977) and Gillies et al. (1991) are more accurate. Kaushal et al. (2002) have made an attempt to modify Wasp et al.'s two layer model. They have also modified the Karabelas (1977) empirical model for solid concentration profiles. They have conducted the experiments with three different flow velocity magnitudes of 2m/s, 2.75m/s and 3.5m/s. The efflux concentration for each velocity magnitude ranges from 4% to 26 % by volume. Like other researchers, they also observed that the solid concentration profiles were functions of particle size, flow

velocity and particle efflux concentration of slurry. In case of pressure drop measurements flow velocities ranged between 1.2m/s to 4m/s. with the efflux concentration ranging between 4% to 26% by volume.

Kaushal et al. (2002) have compared the results obtained for solid particles concentration profiles with those predicted by the Karebelas (1977) model. It has been observed that the model predicts accurately for the finest particle size but as the particle size increase the results predicted vary such that it overestimates the concentration at the bottom of pipe while underestimating the same at the top of the pipe. On the other hand, comparison of the experimental data for pressure drop with those predicted by the Wasp model shows good agreement when the efflux concentration is low at all values of flow velocities. Exceptions are found when the efflux concentration was high along with high flow velocities. The predictions made by Gillies et al' s (1991) two layer model were found to be in good agreement with the experimental results. Kaushal et al. (2002) have made changes by modifying some of the limiting assumptions used in the Karebelas and Wasp models. It has been observed that the modified Karebelas and Wasp models are capable enough to predict accurate results which established fair consensus with experiments.

2.4 Other studies focusing on two phase: This portion will discuss some other studies in which flow is taking place through any other geometry except the pipe.

Wei et al. (2002) have developed a K-ε-T model in order to predict the flow characteristics of dense liquid –solid flows. They have used fluid turbulent kinetic energy and turbulent dissipation rate to describe the turbulent flow of fluid. On the other hand they used turbulent kinetic energy, dissipation rate and pseudo thermal temperature to

describe the random motion of particles. They have explained that random velocity associated with collection of particles is characterized by the turbulent kinetic energy of the particles. In case of an individual particle the random velocity magnitude is defined by the pseudo thermal temperature. They have designed the iterative procedure required to solve the equations involved in the modeling. Their simulation results were found to be in good agreement with the literature. They have concluded that anisotropy dominates in two phase flows.

As discussed in the above paragraphs, Xu et al's (2004) research is inspired from the working of atomic hydrogen propellant feed systems in which the solid hydrogen particles may be transported to engines by using the carrier fluid in the form of liquid helium. They have made use of three dimensional two phase mixture model in order to simulate the flow of the solid hydrogen particles and liquid helium. They utilized the K-ε mixture turbulence model which plays a crucial role in the turbulent mixing of the solid particles and liquid fluid. They indicated that the slurry flow of hydrogen-helium has a high Reynolds number. The Stokes number which is defined as the ratio of the particle response time to the fluid response time also plays an important role. When its value is less than one the particle motion will be tightly coupled with fluid motion. It has been observed that the Stokes number for this two phase flow system is less than or equal to one which is mandatory in order for the hydrogen particles to attain the near equilibrium velocities so that the particles can remain in suspension with the liquid. Different test cases have been discussed on the basis of the governing factors and their influences on the dispersion of hydrogen particles in liquid helium. The governing factors

include the hydrogen particle size, inlet velocities and the inlet particle volume fraction. Table 2.2 shows the cases as identified by Xu et al. (2004),

Test Case #	Inlet velocity (m/s)	Inlet particle volume fraction (%)	Particle diameter (mm)
1	1.0	19.0	1.00
2	1.0	19.0	0.10
3	1.0	19.0	0.01
4	3.0	19.0	0.01
5	3.0	30.0	0.01
6	3.0	10.0	0.01
7	5.0	19.0	0.01

Table 2.1 Cases as identified by Xu et al. (2004)

Effect of particle size: Considering the case 1, 2 and 3 in the above table, contours of particle volume fraction have been obtained as shown in Fig. 2.4 for case 3, which have the smallest particle diameter of 0.01 mm, show the best results of all the three cases for the dispersion of hydrogen particles with a very small amount of particles accumulating at the top which is less than the cases 1 and 2.

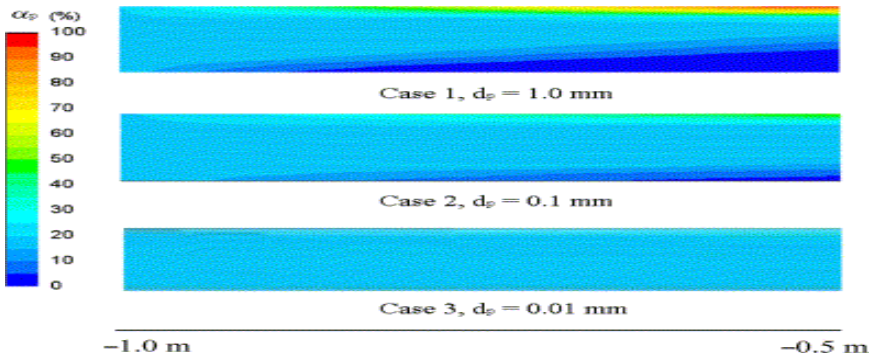

Fig. 2.4.Contour of particle volume fraction in the channels for different particle sizes at elapsed time *t*=2 s. (Influx particle volume fraction $\alpha_{p,0}$=19.0%, flow velocity $\vec{v} = 1.0$) (Source : Xu et al. (2004))

Also, they have plotted the normalized particle volume fraction curves along a channel parallel to the axis at the intersection of y=0.01m and z=0 planes in Fig. 2.5 It has been realized that the closer the normalized particle volume fraction is to 1 that much better will be the dispersion of hydrogen particles. Fig. 2.5 also supports the fact that small particle size is a better choice for better degree of particle dispersion.

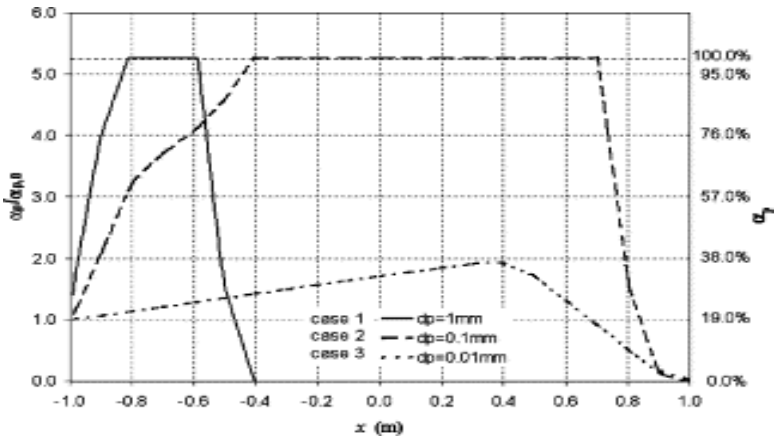

Fig. 2.5 Particle volume fraction at intersection of surfaces *y*=0.01 m and *z*=0 m for different particle sizes at elapsed time *t*=2 s. (Influx particle volume fraction $\alpha_{p,0}$=19.0%, flow velocity $\vec{v}_{in} = 1.0$ m/s.) (Source: Xu et al. (2004))

Effect of Inlet velocities: In Table 2.1, consider the cases 3, 4 and 7 where all the parameters are constant except the influx velocities. The case 7 with inlet velocity as

5m/s. which is the highest of the three cases is found to have better dispersion. Thus, higher the inlet velocity better the particle dispersion achieved.

Effect of inlet particle volume fraction: Here case 4, 5 and 6 from Table 2.1 with respectively 19%, 30% and 10% volume fraction have been discussed. It has been found that higher the influx volume fraction the better the particle distribution in the flow.

Logos et al. (1995) have made an attempt to study the coal water slurries in terms of their rheological behavior. The rheological properties were established to be the functions of solid coal particle size, concentration, and the particle size distribution. These slurries have been formed by mixing water with coal particles with size of the order of 45 μm. For lower concentration of coal particles, slurries exhibit Newtonian fluid properties while for higher concentration they have viscoplastic and shear thinning effects. Their methods involved the mixing of coarser coal particles in the already existing fine coal particles slurry. In the first step they have used the size of coarser coal particles of the order of 208-279 μm for mixing with the fine coal slurry keeping the solid particle concentration constant. This has resulted in a decrease in the slurry viscosity. Furthermore with a ratio of 40% -60% of coarse to fine coal particles in the slurry , slurry viscosity becomes almost five times smaller than that of the slurry with just fine particles with the same solid concentration. Another loss of slurry viscosity by 50% has been observed on adding the coarse coal particles with size ranging between 279-325 μm. They have explained this behavior owing to the effect of spatial rearrangement of the solid particles and an apparent dilution effect. Their results have proved that a coal-water slurry can be formed with a high solid concentration but with a lower slurry viscosity.

Fan et al. (2005) have used an improved inner outer iterative method in order to simulate the two phase solid liquid turbulent flows making use of slender particles instead of the regular spherical one. The inner outer approach mentioned here has been proposed by Brucato et al. (1998) and was later modified by Wang et al. (2002). The improved inner outer approach has been explained later in the discussion of Wang et al. (2002). The set up used in their modeling process consists of a tank which has the stirrer in the form of a Rushton turbine. They have employed the standard K-ε turbulence model. Since the slender particles differ with the spherical particles in the fact that they are dependent on the orientation hence a comparison has been made between the results obtained using the slender particles with those obtained using spherical particles. They have also conducted solid liquid two phase flow experiments in the baffled tank using the digital particle image velocimetry technique. This has been a useful step in order to validate the results obtained from simulation. They have compared the velocity profiles in the experimental and the simulation results following the cylindrical coordinate system. Fig. 2.6 shows the velocity profile of the two results.

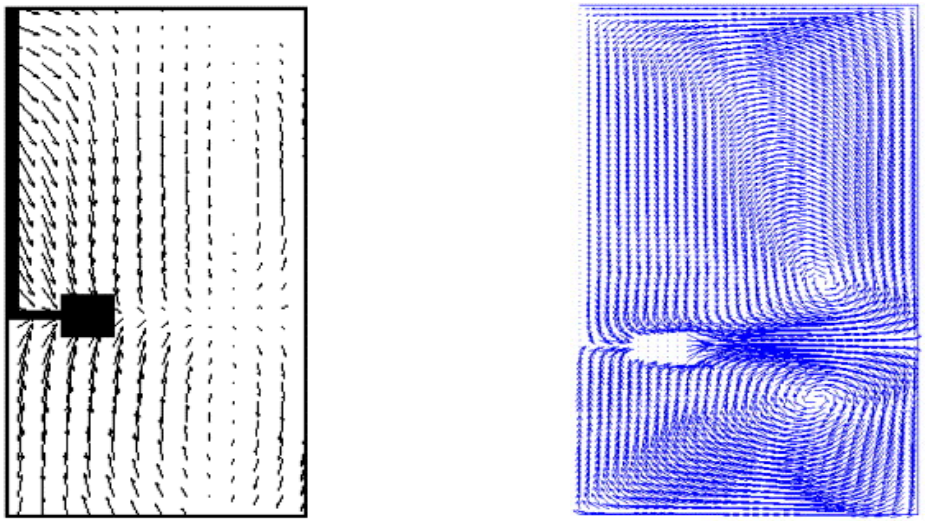

Fig. 2.6 (a) Experimental velocity profile (b) Simulation velocity profile. Both are in r-z plane. (Source: Fan et al. (2005))

They have studied the orientation of slender particles and the effect of impeller speed on the orientation. They used three different speeds i.e. at 200, 300 and 400 rpm of the impeller. It has been observed that the radial and axial velocities as well as the fluctuation velocities are increased due to increase in impeller speed while there is a decrease in the solid concentration in the center of the tank owing to the fact that high impeller speeds result in better and uniform dispersion of particles in the tank. As there is increase in the impeller speed the orientation of the slender particles in the far region from the impeller is not affected. In the near region the orientation decreases with increase in impeller speed due to the particles following the direction of the impeller with large speed. Comparison has been made on the basis of three different velocity components of the flow in case of slender particles and spherical particles of equal volume. Fig. 2.7 shows the comparison curve obtained.

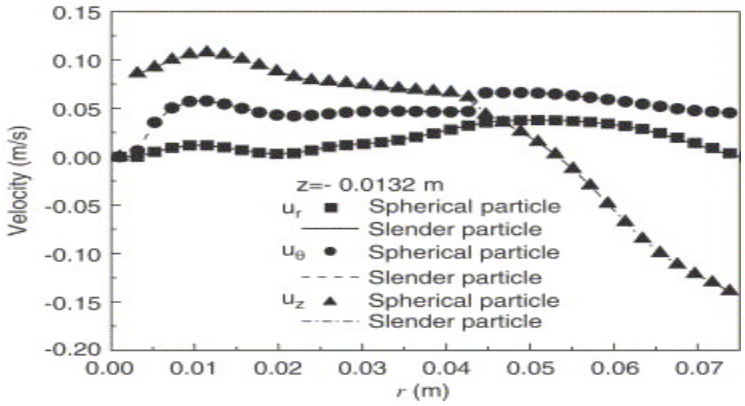

Fig. 2.7 Comparison of simulated velocity between spherical and slender particles. (Source: Fan et al. (2005))

It can be inferred that the velocity components for two types of particles are similar. This can be explained using the fact that due to the high impeller speed, turbulence effects dominate over the particle shape characteristics.

Wang et al. (2003) have also studied the dispersion of solid particles in a solid-liquid baffled stirred vessel with a Rushton impeller. They have also utilized the improved inner outer iterative procedure. They have made an attempt to determine the recirculation below the impeller. They have also used K-ε turbulence model for simulations. According to Wang et al. the main problems encountered in simulation of flow field in stirred vessels involving multiphase flow are the exact representation of the impeller action, the interactions between the participating phases and the turbulent quantities. They have intended to extend this work as a base for the design and modification of solid liquid mixing vessels by numerical simulation. The modified inner outer approach as mentioned earlier subdivides the whole computational domain into two zones which are partially overlapping. Fig. 2.8 shows the two zones of the modified inner outer iterative method.

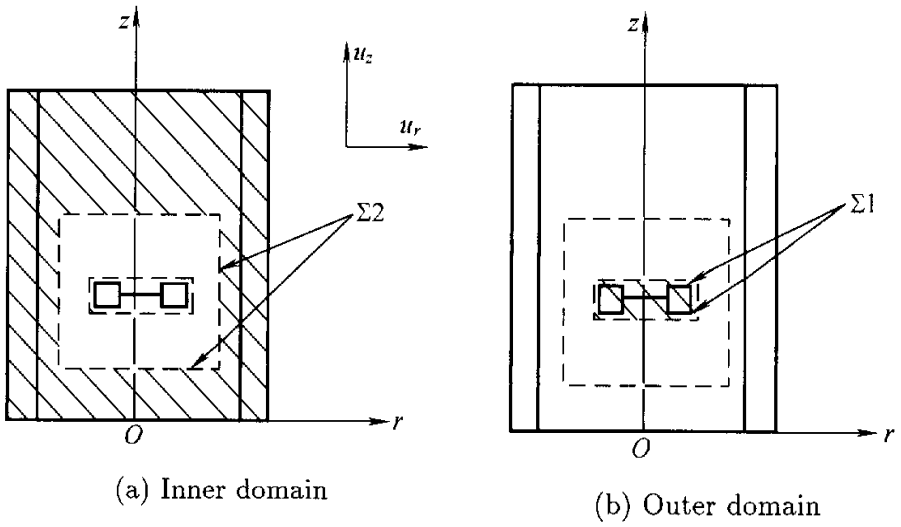

Fig. 2.8.Inner and outer zones in modified inner outer iterative method. (Source: Wang et al. (2003))

The inner zone has the impeller while the outer zone consists of the wall baffles. In the computational process, first the inner domain is simulated in the reference frame that

rotates with the impeller using the arbitrary boundary conditions that are imposed on surface $\sum 2$. This will result in the first trial flow field to be obtained in the impeller region inclusive of the flow parameters distribution on surface $\sum 1$. The flow parameters distribution obtained on the surface $\sum 1$ is used in the form of the boundary conditions to simulate the flow on the outer domain. The flow parameters have not been averaged and hence the information available represents the whole of the computational domain which fortunately also includes flow parameters on the boundary surface $\sum 2$. Further the parameters on the surface $\sum 2$ are used for the second inner simulation as the boundary condition. This will continue until a satisfactory numerical solution is obtained by convergence. Fig. 2.9 shows the computational grid used. It has 36 x 36 x 90 nodes in all. Wang et al. have compared their grid with those used in the previous similar studies by Gosman et al. (1992) with 20 x 15 x 27 nodes and Altway et al. (2001) with 21 x 64 x 45 nodes. They have used a better and denser grid comparatively.

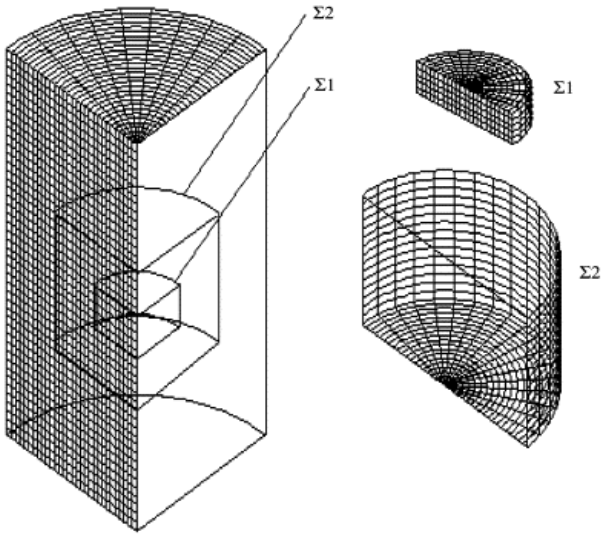

Fig. 2.9 Computational grid of 'inner' and 'outer' domains. (Source: Wang et al. (2003))

The study conducted by Wang et al. (2003) can be used for the systems of solid-liquid flows where the solid loading can be as high as 20%. They have modified the inner-outer approach which can be applied to other systems also where there is an unavailability of the experimental data for the initial boundary conditions.

2.5 Fourier Transformed Infrared (FTIR) spectroscopy: Fourier transform spectroscopy can be defined as a technique used for measurement in which the time dependent coherence of a radiative source is measured in order to collect the spectra. These spectra are required for the study of the material or mixture characteristics. Infrared spectroscopy is the spectroscopy technique that deals with the infrared region of the electromagnetic spectrum. The Fourier transform spectroscopy when combined with infrared spectroscopy brings the Fourier Transformed Infrared (FTIR) spectroscopy into existence. An FTIR method consists of collecting an interferogram with the help of interferometer and then it is Fourier transformed to get the spectra. The FTIR spectrometer is used to digitize the interferogram and does the Fourier transformation to yield the spectrum. Either near infrared or far infrared spectra can be obtained by a FTIR spectrometer. The FTIR spectrometer offers advantages of high spectral resolution, the capability of working with weak signals, high spectral accuracy, quick acquisition of spectra with high signal to noise ratio (S/N ratio) and the capability to work with infrared. FTIR spectroscopy has a wide range of applications. In the current study, FTIR/NIR probes are considered for applications to a turbulent slurry flow. In this section an attempt has been made to review some of the applications of FTIR/NIR methods.

2.5.1 Studies related to FTIR/NIR spectroscopy:

Abebe et al. (2007) have conducted experiments that indicate that Near Infrared spectroscopy is a very good tool while dealing with slurries. According to them the manufacturing processes that involve solid particulates pose a higher degree of difficulties in various chemical, nuclear and pharmaceutical industries as compared to single phase liquids and gases. Lack of effective measurement techniques contributes a lot to the difficulties resulting in optimization and precision manufacturing of particulate solid products. Their experiments demonstrate that NIR spectra can reveal rich and important information about the concentration of solution, solid concentration, particle size and the crystal structure. They have stated that NIR technique has a wide potential for simultaneous measurements of multiple number of solids as well as liquid properties. They have carried out their experiments using a 500 ml jacketed glass reactor. They have used distilled water as the liquid while the chemicals they have employed are L-glutamic acid (L-GA). They have used two different forms of L-glutamic acid namely α and β forms. The experimental set up is shown in Fig. 2.10. The glass reactor consist of a retreat curve impeller, a temperature control bath, a Platinum resistance thermometer (PT 100), a glass condenser and the NIR transflectance probe having 12 mm optical path length. A 2m silica fiber optics cable is used to transmit signal to the FT-NIR spectrometer.

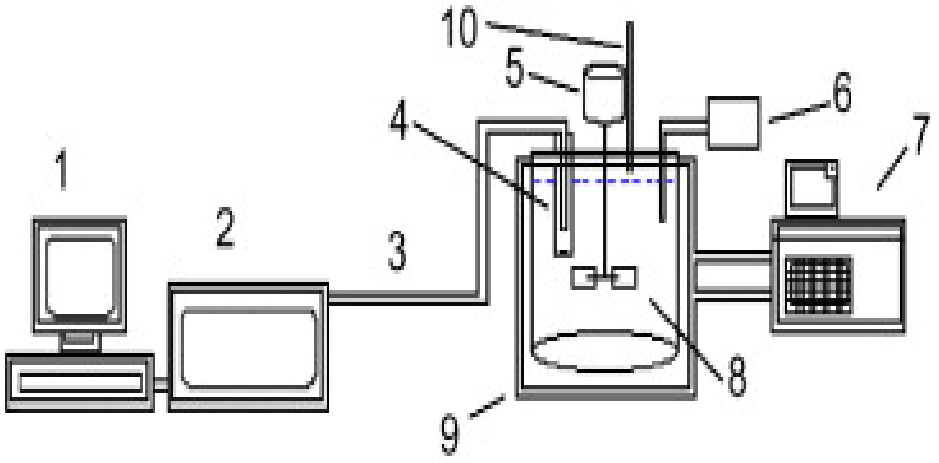

Fig. 2.10.Experimental set up. 1 Personal computer, 2 NIR instrument, 3 Fiber optics cable, 4 Transflectance probe, 5 Stirrer motor, 6, Temperature probe, 7 Reactor temperature control, 8 Stirrer, 9 glass jacketed reactor (500 ml), 10 Condenser.

The slurries were made for both α and β crystals and at different solid concentrations, and over the six particle size ranges for each polymorph. The effect of crystal size on absorbance was explained using the raw spectra plots of the slurries as shown in Fig. 2.11. On the other hand, they have explained the effect of solid concentration using Fig. 2.12. It has been observed that higher the solid concentration the larger will be the baseline shift. The greater solid concentration results in more scattering of radiation and hence less light reaching the detector ultimately resulting in baseline shift at all wavelengths. They have concluded that near infrared radiations are very much effective in predicting the slurry characteristics like particle size, and concentration unlike mid infrareds. NIR spectroscopy can be used as an effective technique in chemical, agricultural and environmental applications owing to the properties such as ability to use fiber-optics for rapid data transmission, good accuracy in measuring both low and high concentrations of solutions, and simple in operation.

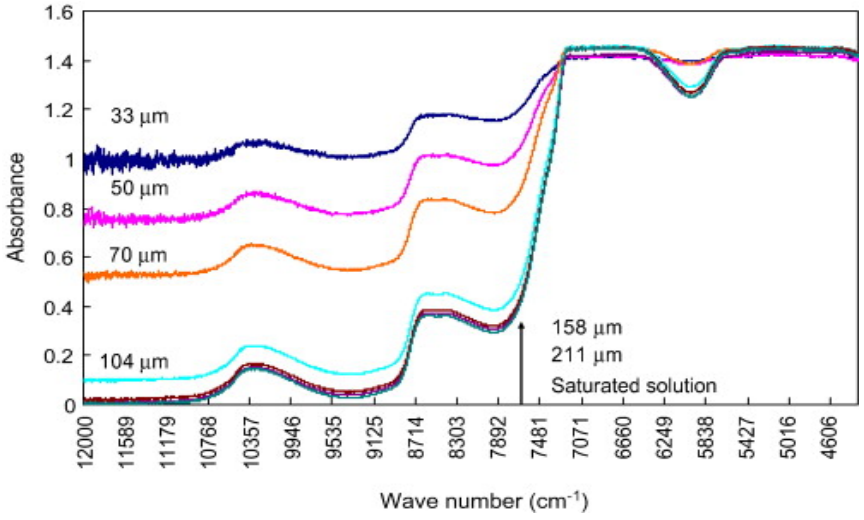

Fig. 2.11. Raw NIR spectra of slurries of α-form L-GA crystals of different particle sizes, under fixed temperature and solid concentration.

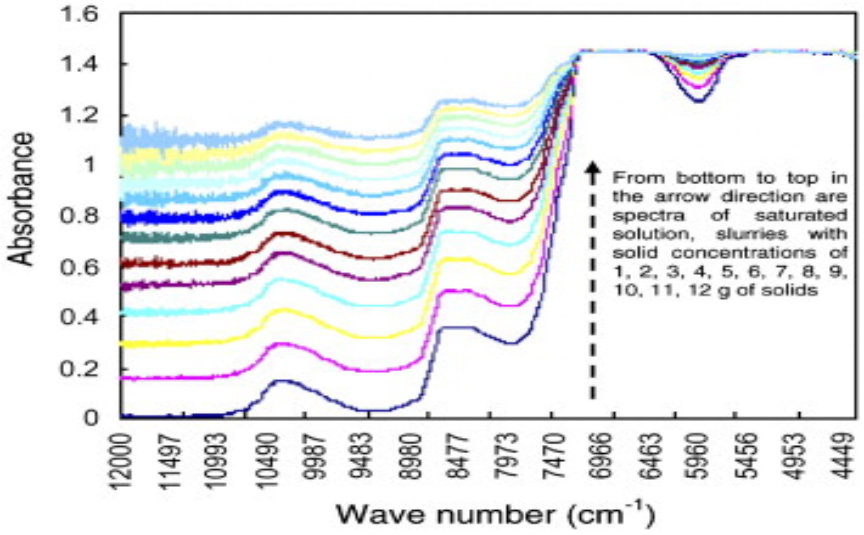

Fig. 2.12. α-form spectra at varied solid concentrations but fixed particle size (70 µm) and temperature (40 °C)

It has been observed that the indoor concentrations of substances like formaldehyde (HCHO) and nitrogen dioxide (NO_2) have increased compared to that outside and these concentrations obviously are capable of producing adverse results. The quantitative measurement for such substances is a must to ensure better quality of ambience though it is not possible to do this accurately with conventional methods. In

such a circumstance FTIR spectroscopy techniques prove to be advantageous. Chen et al. (1999) have studied the quality of the indoor air in a simulated kitchen ambience. They have measured concentrations of major combustion products like carbon dioxide, carbon monoxide and nitric oxide in a room where a conventional natural gas appliance is operated. They have employed FTIR extractive technique in order to measure the combustion products. A comparison has been made further with the results obtained by FTIR technique and those which were obtained from conventional techniques. The FTIR technique was proven to be better. On the other hand they have also furnished the CFD simulations which helped in designing the experimental set up along with interpreting the experimental data. The experimental set up is shown below in Fig. 2.13. It has a room with a conventional four burner stove gas cook top system. The cook top produces a blue flame during the experiments. Air has been taken out using an exhaust fan while fresh air is made to enter using a meshed vent. Three different experiment cases were considered on the basis of different ventilation rates of 2.4, 4.3 and 6.6 air changes per hour (ACH). The total heat generating rate was 3.92kW meter per hour. Similarly while in the CFD simulations three different cases were considered. The grid used for modeling has same

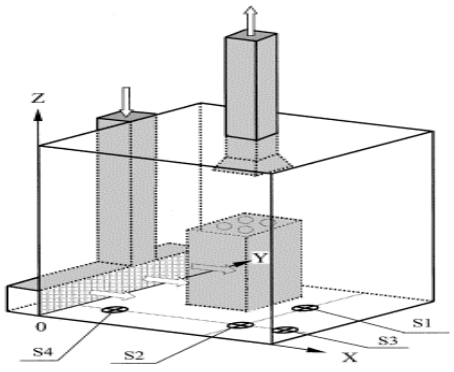

Fig. 2.13.Experimental set up with the measurement locations and cook ups at S1, S2, S3 and S4. (Source: Chen et al. (1999))

dimensions as that of the testing room. It has 29 x 32 x 34 cells in the direction coordinates. The combustion source is modeled on the box shaped obstacle. CFX4 has been used as the CFD package which uses the finite volume methods for solving the conservation equations that govern the problem. A K-ε model with buoyancy correction has been utilized. The simulation results can be depicted as shown in the Fig. 2.14. The results obtained using CFD simulations were able to predict similar qualitative results as obtained by the experiments. The confirmation of stratification of temperature and combustion products concentration has been made. High flow rates were better predicted quantitatively than lower flow rates. This may be due to the use of a less sophisticated turbulence model. Hence, Reynolds flux model can be used. It has been proved that a high flow rate system needs to be positioned above the source to extract the major part of pollutants.

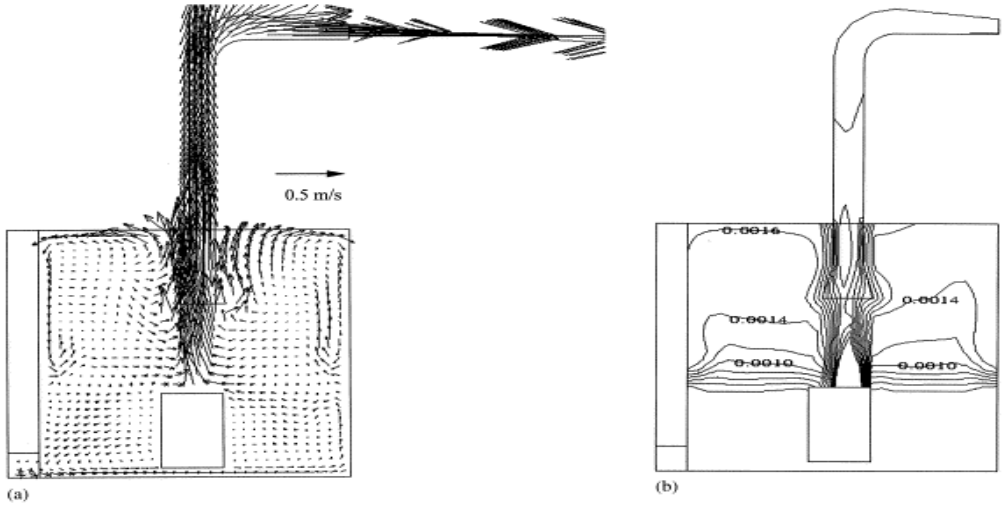

Fig. 2.14. Predicted velocity vectors and CO_2 mass fraction contours at the centre *y* plane for an air flow rate of 2.4 ACH. (Source: Chen et al. (1999))

FTIR spectroscopy can be combined with other techniques to obtain desired solutions. Fabbri et al. (2000) have combined the mid infrared fiber optics (wavelength

ranging between 1100 nm to 2500 nm) technique with FTIR in order to devise a method with the help of which a non-invasive reflectance measurements can be performed. It has a wider area of application in the field of non-invasive analysis of aesthetic works. With this technique measurements can be done with paintings and polychrome sculptures with the view to analyze the composition of painted layers without sampling. This technique uses portable FTIR spectrophotometer using mid infrared fiber optics which enables it to be used on site, i.e., without even moving objects from their places. They have introduced two terms: Surface reflection (R_s) and volume reflection (R_v). Surface reflections are the radiations that have not entered the sample and have suffered single or multiple reflections on the upper surface of the particles of the sample while volume reflections are those radiations that enter the sample and are reflected back after suffering internal partial refractions getting transmitted by the particles.

Friesen (1996) have used an online fiber optic probe in order to collect the spectra of a slurry flowing through a pipe. An attempt has been made to verify the feasibility of the NIR spectroscopy method for developing a reliable method for processing of oil sand slurries in oil sand extraction plants. They have gathered data for a continuous period of nine hours for which there has been a regular variation of the type of ore and the slurry water content. They have utilized a near infrared reflectance analysis (NIRA) technique. They have used an NIR spectrometer installed at a point downstream from the tumbler which is used to mix hot water and sodium hydroxide with oil sand in the first step of hot water extraction. The spectrometer with a protective cover has been mounted on a vibration isolation platform placed on steel table close to the measurement point. A probe with 1m long fiber optic bundle has been inserted into the pipeline having the probe

diameter of 25mm such the window was flush with inside surface of the pipe. The window material is made of sapphire due to high resistance required against abrasion due to sand. This method is used as an efficient method for characterizing the appropriate samples owing to its advantages of being prompt and non destructive technique. Following this method, if there is any need for sample preparation in a specific case, it requires very small amount of sample preparation. This method can be used to analyze large samples.

Switalski et al. (1998) have also tried to investigate the near infrared (NIR) diffuse reflectance spectroscopy as a processing method. Diffuse reflectance carries the merit of analyzing powders having as high as 40% volatility, slurries consisting of as much as 40% solid concentration and emulsions as well. Diffuse reflectance spectroscopy has the capability to examine both the solid and liquid phases on the substance. In this study efforts have been made by researchers to monitor the dryer simulator that is used for the simulation of production rotary dryer in the laboratory. They have mentioned the examples from the industry using NIR diffuse reflectance spectroscopy in monitoring the chemical industry processes of mixing, drying and polymorphism. These are indicative of the fact that many of the other processes can be monitored using this technique.

3 Conclusions:

Thus, from the above discussion some of the points that are eligible to attract our attention include the dependence of multiphase solid-liquid flows on the solid particle inlet concentrations, inlet velocities of the solid and liquid phases and the particle shape and size. It has been observed that smaller the particle diameter better will be the particle dispersion. Spherical particle shapes are likely to disperse more than the slender ones.

Higher inlet velocity and high inlet volume fraction contributes to better dispersion of solid particles. It was also observed that in order for the flow of solid particles with the liquid fluids the velocity of the solid particles should be just above the deposition critical velocity. In order to achieve such a velocity or more precisely to maintain the particles in suspension in the flow the phenomenon of turbulence is a must. Turbulent mixing plays a vital role for the particle dispersion. In order to simulate the turbulent flows K-ε turbulence model is most preferred. Turbulent K-ε model has been found to be the widely used turbulence model. It can be used efficiently in both dilute as well as dense solid liquid flows.

FTIR methods have also been used as efficient technique for non-invasive measurements as well as in the analysis of liquid slurry characteristics. Being a non-destructive technique, it requires little or no sample preparation. An optical probe can be employed which can be used for the detection of the substances. Thus in the present study all these considerations have been taken in to account in order to optimize the quality of obtained results.

CHAPTER III

NUMERICAL APPROACH

3.1 Introduction

Computational Fluid Dynamics (CFD) is classified as a branch of fluid mechanics which deals with the numerical solution of flow of fluids by employing the computational power of modern computers. Computational Fluid Dynamics solves the governing differential equations that are characteristic to the flow. These governing equations consist of the equations of continuity, conservation of momentum also known as Navier Stokes equations and equation of conservation of energy. On the other hand, in case of inviscid flow the Euler equations are momentum equations which govern the flow. In the present study we are dealing with the viscous flow. So the prime concern will be the solution of Continuity and Navier Stokes equation. Some of the advantages of using CFD methods are considered to be the accuracy and reliability of the end results, lower cost of application of CFD compared to the expensive experimental methods, availability of software and graphical tools to visualize the flow without actually making the fluid to flow which results in accurate predictions. In addition, the study of dangerous species can be performed without any risk.

In CFD, a continuous fluid is discretized by considering the flow domain to be constituted of very small units called cells. This cell structure in the flow volume is known as mesh or grid. These cells are used for the analysis of the flow problem. When proceeding with the cell-based analysis approach, a preprocessing is required. For preprocessing, the geometry of the problem should be understood. Mesh has to be constructed in the region where the fluid is going to flow. Further, one should be aware of the governing equations on which the flow properties are dependent. These governing equations may also include some equations which are specific to the problem or type of fluid. Furthermore, the boundary conditions of the flow problem play a major role in determining the accuracy of the simulation process and have to be given attention during the preprocessing of the flow problem. Boundary conditions specify the fluid characteristics at the flow boundaries and the specific properties of viscosity, surface tension that the fluid has.

Computational Fluid Dynamics can be used to model flow with low Reynolds number as well as those with high Reynolds number. Various turbulent modeling and simulation techniques like Direct Numerical Simulation (DNS), Large Eddy Simulation (LES), Reynolds stress model, K-Epsilon model, K-Omega model, Spalart-Allmaras model are available and each one of them can be efficiently used in their specific areas of applications. These will be covered in some detail later in this chapter. In the present study wall bounded turbulent flows have been modeled and the K-Epsilon model with near wall treatment has been employed.

CFD techniques are suitable for the areas of single phase flow as well as multiphase flow. A multiphase phase flow will have the flow consisting of gas-solid,

solid-liquid, gas-liquid phases, liquid-liquid phases or even more than two phases. The point to be considered is that the phases must be non-reacting during the flow. The complexity in the flow arises due to the mutual interaction of different phases. Experimental methods are not capable in every case to completely analyze the flow. Currently, our area of consideration is the flow of solid (particles) and liquid phases where even the clustering of suspended particles depends upon the small scales of turbulence to be resolved. This is very difficult using experimental techniques. Hence numerical simulation plays an important role for the analysis of multiphase turbulent flow problems. Using the computational techniques the role of some crucial physical factors including the effect of gravity and surface tension can be also evaluated in the flow problems.

As it has been mentioned earlier that CFD requires computational power of modern computers in order to give useful results, hence it requires software application codes in order to do the computational work. Many CFD software applications are available that can be used on the basis of the advantages they offer in different fields of applications. In the current research, Fluent has been used as the simulation software package and Gambit has been utilized as the preprocessor. As we mentioned that meshing of flow geometry needs to be done before simulating the flow, Gambit is used for the construction and meshing of the flow geometry. In this case, flow geometry is a pipe with a Fourier Transformed Infrared Reflectance (FTIR) probe placed at half of the length of the pipe inserted through the upper wall of the pipe. The construction and meshing of the probe and pipe geometry are considered later in this chapter.

3.2 Governing Equations

The governing equations are nothing but the mathematical representations of the principles that controls the flow behavior in a particular fluid problem. These principles are the conservation of mass, momentum, and energy. For the present study, one has to deal with the equations of continuity which represents the conservation of mass principle and Navier Stokes equations in three different coordinate axes which respectively represent the momentum conservation principles in the directions of X, Y and Z. Following are the equations as discussed in the preceding lines. The equation of continuity or conservation of mass in three dimensional coordinate systems is expressed.

$$\frac{\partial u}{\partial x} + \frac{\partial v}{\partial y} + \frac{\partial w}{\partial z} = 0 \tag{3.1}$$

Where u, v, w are the velocity components in X, Y and Z directions. This is the continuity equation for incompressible flow. The Navier stokes equation is expressed.

$$\rho \left(\frac{\partial \mathbf{v}}{\partial t} + \mathbf{v} \cdot \nabla \mathbf{v} \right) = -\nabla p + \mu \nabla^2 \mathbf{v} + \mathbf{f}. \tag{3.2}$$

This is the basic form of Navier Stokes equations where each term has its own meaning which is explained as

$$\overbrace{\rho\Big(\underbrace{\frac{\partial \mathbf{v}}{\partial t}}_{\text{Unsteady acceleration}} + \underbrace{\mathbf{v}\cdot\nabla\mathbf{v}}_{\text{Convective acceleration}}\Big)}^{\text{Inertia (per volume)}} = \overbrace{\underbrace{-\nabla p}_{\text{Pressure gradient}} + \underbrace{\mu\nabla^2\mathbf{v}}_{\text{Viscosity}} + \underbrace{\mathbf{f}}_{\text{Other body forces}}}^{\text{Divergence of stress}}. \quad (3.3)$$

Thus, the terms on the left represents the acceleration of the fluid while the terms on the right hand side stand for the forces acting on the fluid. The above equation holds good when talking about incompressible constant viscosity flow. The Navier Stokes equation is a form of conservation of momentum which is explained from Newton's second law of motion and the equation

F = ma (3.4)

is justified as the Navier Stokes equation has acceleration terms on one side and all the existing forces on the other side. The Navier Stokes equation in the Cartesian form for three different coordinate axes for incompressible and constant viscosity flow yields,

$$\rho\left(\frac{\partial u}{\partial t} + u\frac{\partial u}{\partial x} + v\frac{\partial u}{\partial y} + w\frac{\partial u}{\partial z}\right) = -\frac{\partial p}{\partial x} + \mu\left(\frac{\partial^2 u}{\partial x^2} + \frac{\partial^2 u}{\partial y^2} + \frac{\partial^2 u}{\partial z^2}\right) + \rho g_x \quad (3.5)$$

$$\rho\left(\frac{\partial v}{\partial t} + u\frac{\partial v}{\partial x} + v\frac{\partial v}{\partial y} + w\frac{\partial v}{\partial z}\right) = -\frac{\partial p}{\partial y} + \mu\left(\frac{\partial^2 v}{\partial x^2} + \frac{\partial^2 v}{\partial y^2} + \frac{\partial^2 v}{\partial z^2}\right) + \rho g_y \quad (3.6)$$

$$\rho\left(\frac{\partial w}{\partial t} + u\frac{\partial w}{\partial x} + v\frac{\partial w}{\partial y} + w\frac{\partial w}{\partial z}\right) = -\frac{\partial p}{\partial z} + \mu\left(\frac{\partial^2 w}{\partial x^2} + \frac{\partial^2 w}{\partial y^2} + \frac{\partial^2 w}{\partial z^2}\right) + \rho g_z \quad (3.7)$$

3.3 Numerical methods in CFD

In the old days when CFD was discovered, experimental techniques were considered to be advantageous. Nowadays, due to the promptness and accuracy of the computational power, CFD is widely used. The solution of flow problems are obtained by discretizing and then solving the differential equations governing the flow. There is availability of several types of numerical methods for the solution of governing equations such as finite difference, finite volume, and finite element methods. For our area of concern all these three are of interest.

Finite difference method: This method uses the Taylor series approximation at any general point x_i. Thus any term of the PDE can be expressed as,

$$\frac{d^n}{dx^n} f(x_i) \cong \frac{1}{\Delta x^n} \sum_{j=J_1}^{j=J_2} C_j f_{i+j} \tag{3.8}$$

Where Δx represents the mesh size in the grid under consideration and is taken constant. f_k represents the value of the function f(x) at x_k. Taylor's expansion gives the value of coefficients C_J. J_1 and J_2 are the integers which are related with the order n and the desired degree of accuracy. Thus following the above scheme the first and second order derivatives can be represented as follows.

$$\frac{df(x_i)}{dx} \cong \frac{f_{i+1} - f_{i-1}}{2\Delta x} \tag{3.9}$$

(Here n=1 and J_1 =1 and J_2 =1 i.e. first order derivative with first order accurate scheme). And

$$\frac{d^2 f(x_i)}{dx^2} \cong \frac{f_{i+1} - 2f_i + f_{1-1i}}{\Delta x^2} \equiv \Delta_{xx} f_i \qquad \text{…….. (3.10)}$$

(Here n=2 and J_1 =1 and J_2 =1 i.e. second order derivative with first order accurate scheme).

For higher order derivatives the value of n will increase and for higher degree of accuracy the difference between J_1 and J_2 goes on increasing. Similar equations are used while discretizing the time derivatives having the time interval Δt. In finite difference method systems of governing differential equations is converted to a system of algebraic equations in terms of the value of function f at different nodes of the mesh.

Finite element method: In this method the flow domain is discretized by dividing it into smaller divisions or elements and each element is considered while developing the solution using the basis functions. Thus the solution is obtained element wise in terms of the basis functions. As the solution is constructed in terms of the specific basis functions, it explains better about the solution as compared to the finite difference and finite volume methods. But there are always complications in choosing the basis functions which also brings ambiguity in determining the boundary conditions. This method is widely used for structural mechanics problems. It is also applied in areas of fluid studies. One more area of concern is that it requires more memory for computation comparatively. In this method a weighted residual equation is obtained which is represented as

$$R_i = \iiint W_i Q \, dV^e \tag{3.11}$$

Where R^i is the equation residual at an element vertex i, Q represents conservation equation expressed on an element basis, W^i is the weight factor and V^e is the element volume.

Finite volume method: In this method the flow volume is constituted of a number of small volumes and the discretization is based upon the integral form of the partial differential equations (governing equations). The governing equations are discretized such that they can be solved for every volume. The resulting equations obtained consist of fluxes of conserved variables. This method uses the conservative form of governing equations for discretization which ensures that the fluxes through each volume remain conserved. This method is useful for the fact that there is no limitation of using only a structured grid.

Comparison of the three methods: All the three methods have found wide applications in their respective areas on the basis of the ease of applicability. Finite element method provides an end to end continuous solution but it requires lots of programming skills. Similarly finite volume methods are known to provide conservative solutions. Thus on the basis of the qualities and limitations of the three methods they can be chosen to be applied to a given problem. In the current work, Fluent is used as the analysis and simulation software package which is based upon the finite volume method. The discretization in Fluent/Gambit takes place by dividing the flow volume into a number of cells and each has their own volume. Thus the finite volume method comes into picture. Since the finite volume approach uses the integral form of conservation equations, the

equation of continuity expressed in the integral form for a steady and incompressible flow will be,

$$\int_S \vec{\mathbf{V}} \cdot \hat{\mathbf{n}}\, dS = 0 \qquad \text{..... (3.12)}$$

Where S and $\hat{n}$ are the surface of the cell or control volume and the normal to the surface respectively. The above equation represents the net flow in and out of the control volume will be zero. For better interpretation it will be a good idea to look at the following figure.

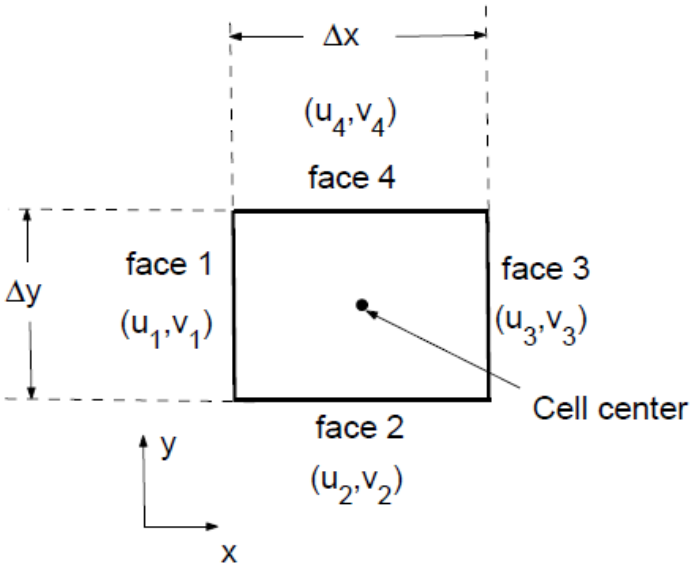

Fig. 3.1 Rectangular cell control volume (Source: CFD Introduction, Bhaskaran and Collins)

The velocity on any face can be expressed as

$$\vec{V}_i = u_i\,\hat{i} + v_i\,\hat{j} \qquad (3.13)$$

Applying the conservation of mass on the cell control volume will result in another equation expressed as,

$$-u_1\Delta y - v_2\Delta x + u_3\Delta y + v_4\Delta x = 0 \tag{3.14}$$

This equation is the equation of continuity applied to a single cell. It explains that the net mass flow in the cell adds to zero. The values at the cell centers are obtained by inverting the discrete system. The values of u_1, v_1, u_2, v_2 are obtained by using the interpolation technique on the cell center values at the adjacent cells. In this way the discrete equations for momentum and energy conservation can also be written. This is how Fluent incorporates finite volume analysis.

3.4 Selection of turbulence model:

A model is defined as a mathematical formulation of the physical and chemical aspects which define the process or product. This does not include the solution of these mathematical formulations. Simulations on the other hand are one of the activities that can be performed with the models. It involves solving a problem using an appropriate model. The observation of turbulent flows is a common phenomenon in various scientific processes that involve fluid motion. Turbulent flows have characteristic velocities that do not have stable behavior rather they are fluctuating in nature. These fluctuating velocities have a vital role to play in the continuity, momentum and energy transport equations. These quantities depict fluctuating characteristics which may vary in magnitude and frequency of fluctuations. Due to the variable nature of the quantities it demands a lot of computational power for calculation of these quantities. By calculating fluctuating quantities shorter length scales of turbulence can be resolved but it becomes extremely expensive in practical problems due to the amount of computational power needed. Such models are the Direct Numerical Simulation (DNS) and Large Eddy Simulation (LES) models. On the other hand, Reynolds averaged Navier Stokes models

(RANS) calculate average quantities. RANS models do not resolve all the turbulence scales. Fig. 3.2 shows the extent of modeling and resolving the turbulence scales in case of different modeling approaches.

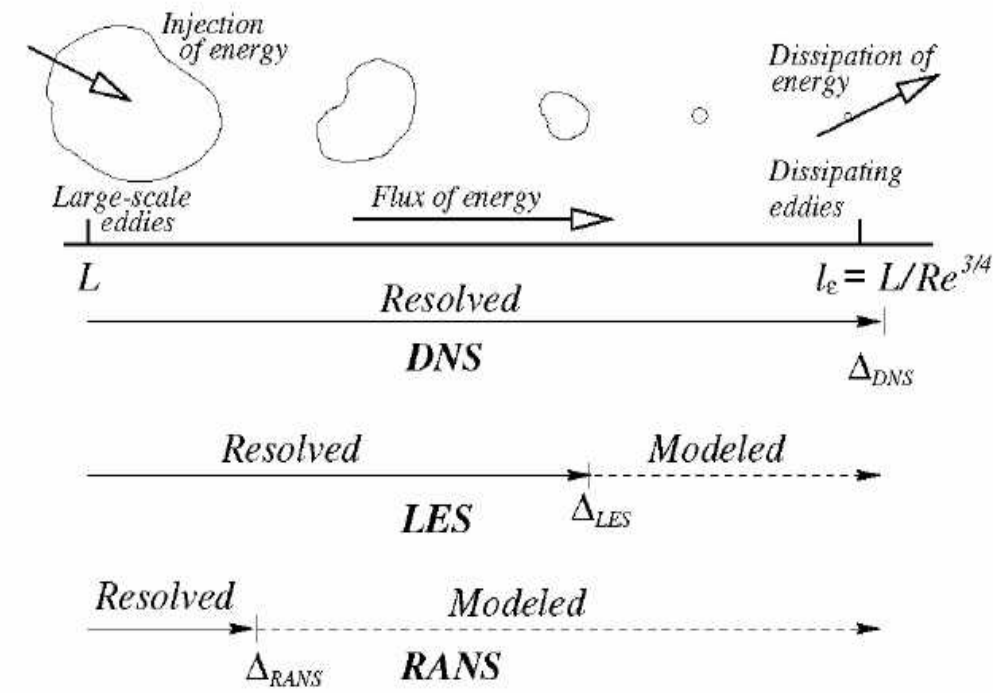

Fig. 3.2 Extent of resolution of turbulence scales and modeling in different turbulence models. (Source: BELL, B. *Turbulent flow cases*, Fluent Inc. 2003)

The selection of a turbulence model for a specific flow problem is based on dynamics involved in the problem, the computational power available, the time available for simulations, the particular practices prevalent for the kind of problem, and also the level of accuracy required. Fluent offers a wide variety of turbulence models and depending on the suitability of the model to the type of flow being considered, it can be

chosen to obtain the solution of the flow problem. The RANS models that Fluent offers consist of Spalart-Allmaras, K-ϵ and its variations, K-omega and its variations and Reynolds stress models (RSM). Fluent also offers the LES and DNS models but the current study does not necessitate talking about those models at length. In the current study we have used K-ϵ model and its variations which is a two equation model (K and ϵ equations) which ensures that turbulent velocities and length scales can be determined independently. The assumptions used behind the model are that the flow should be fully turbulent and the molecular viscosity does not play a significant role in the flow. There are two other variations of this model namely RNG K-ϵ model and realizable K-ϵ. The RNG K- ϵ and realizable K- ϵ models have some modifications compared to standard K- ϵ . To name a few, the RNG K- ϵ model accounts for swirling effects on turbulence and has an extra term for rapidly strained flows in the ϵ equation. Similarly the Realizable K- ϵ model has an improved formulation for turbulent viscosity and a new equation for dissipation rate ϵ.

3.5 Modeling the multiphase flow: A phase can be defined as a particular distinguishable class of material that exhibits unique inertial behavior when interacting with the flow. A multiphase flow has more than one phase in the flow domain. In the present study liquid–solid flow is a concern. Some examples of liquid-solid are slurry flow, hydrotransport, sedimentation etc. The concentration in this study is on the slurry flows. There are two approaches with the help of which multiphase flow can be modeled. They are Euler-Lagrangian approach and Euler-Euler approach. Euler-Euler approach is of relevance in the present issue.

Euler-Euler approach: It is a fact that a phase cannot occupy the volume or content of another phase. Owing to this fact, in this approach the concept of volume fractions of different phases has been introduced. The phases are considered to be interpenetrating mathematically. Each phase has a volume fraction and the outcome of the addition of all volume fractions is unity. These volume fractions are considered continuous functions of space and time and are spatially and temporally dependent. Conservation equations for each phase are obtained to form a set of equations which is solved using constitutive relations. There are three different models under Euler-Euler approach. They are Volume of fluid (VOF) model, Mixture model and Eulerian model. They are described in more detail in the following paragraphs.

Volume of fluid (VOF) model: VOF model is generally used for two fluids that rarely mix with each other or rather are immiscible. The VOF model formulates a common set of momentum equations for all the fluids while each fluid has a different volume fraction equation and the volume fraction is calculated at each cell. The major applications of this model are involved in motion of large bubbles, steady or unsteady tracking of the liquid-gas interface, prediction of jet break up, etc.

Mixture model: The mixture model is an Eulerian multiphase model which is suitable for the modeling of mainly solid particles and liquid fluids flowing together. The solid and liquid should be in strong coupling with each other. The mixture model aims at solving the momentum equations for the mixture. This model can model the phases which are moving with different velocities and hence slip velocity comes into existence. It uses the relative velocities to describe the secondary or dispersed phases. Mixture

model has an advantage that it is independent of the number of phases participating in the flow i.e. it can model any number of phases present in the flow. In this model one can select granular phases also and it enables us to find the properties of granular phases. Since in the current study particles are being dealt with therefore it makes the mixture model most suitable to be used as a multiphase model for the present work. All the related equations and concepts of the mixture multiphase model will be discussed in the next section.

Eulerian model: This model aims at solving different set of continuity and momentum equations for each phase involved in the flow. The coupling between the phases is obtained by using the pressure and interphase exchange coefficients. This induces higher degrees of complexities in this model. The granular and non-granular phases are treated differently and in case of granular phases kinetic theory is used to determine the granular properties. For handling the momentum exchange between the phases, user defined functions are employed. Using the Eulerian model any number of phases can be modeled but one thing to be considered is the availability of sufficient memory. Applications of this model include fluidized bed, particle suspension to name a few.

3.5.1 Modeling with Mixture multiphase model: As has already been mentioned the mixture model uses only one set of continuity and momentum equations for the mixture as a whole and hence it uses less memory. Along with the merits of the mixture model there have been some limitations also. Just for example, while using mixture model one cannot use the density solvers in Fluent. Before moving to the governing equations used

in the mixture model it should be realized that apart from using common set of continuity, momentum and energy equations for the mixture, it solves the volume fraction equation for the secondary phases and algebraic expressions which pertains to the relative velocities if the phases are moving with different velocities.

3.5.2 Equations used in mixture model: The equations that are solved in the mixture model are the following.

Continuity equation-

$$\frac{\partial(\rho_m)}{\partial t} + \nabla.\left(\rho_m \overrightarrow{v_m}\right) = 0 \qquad (3.15)$$

Where $\overrightarrow{v_m}$ and ρ_m represent the mass averaged velocity mixture density such that,

$$\overrightarrow{v_m} = \frac{\sum_{k=1}^{n} \alpha_k \rho_k \overrightarrow{v_k}}{\rho_m} \qquad (3.16)$$

And $$\rho_m = \sum_{k=1}^{n} \alpha_k \rho_k . \qquad (3.17)$$

For α_k being the volume fraction of k^{th} phase.

Momentum equations: The set of momentum equations solved in the mixture model are written as,

$$\frac{\partial\left(\rho_m \overrightarrow{v_m}\right)}{\partial t} + \nabla.\left(\rho_m \overrightarrow{v_m} \overrightarrow{v_m}\right) = -\nabla p + \nabla.\left[\mu_m\left(\nabla \overrightarrow{v_m} + \nabla \overrightarrow{v_m}^{T}\right)\right] + \rho_m \vec{g} + \vec{F} + \nabla.\left(\sum_{k=1}^{n} \alpha_k \rho_k \overrightarrow{v_{dr,k}} \overrightarrow{v_{dr,k}}\right) \qquad (3.18)$$

Here $n, \vec{F}$ and μ_m are the number of phases, total body force and the viscosity of mixture respectively and $\overrightarrow{v_{dr,k}}$ is the drift velocity such that,

$$\mu_m = \sum_{k=1}^{n} \alpha_k \mu_k \tag{3.19}$$

And $$\overrightarrow{v_{d,k}} = \overrightarrow{v_k} - \overrightarrow{v_m} \tag{3.20}$$

Energy equation: The energy equation is given as,

$$\frac{\partial}{\partial t}\sum_{k=1}^{n}(\alpha_k \rho_k E_k) + \nabla \cdot \sum_{k=1}^{n}(\alpha_k \vec{v}_k(\rho_k E_k + p)) = \nabla \cdot (k_{\text{eff}} \nabla T) + S_E \tag{3.21}$$

Where first and the second terms on the right hand side account for heat transfer owing to conduction and miscellaneous volumetric heat sources respectively.

And

$$k_{eff} = \left(\sum \alpha_k (k_k + k_t)\right) \tag{3.22}$$

is the effective conductivity. Subscript t in the conductivity k_t stands for the turbulence and it is the turbulent conductivity and its value depends on the turbulence model.

Slip velocity: In the mixture model the phases participating may have different velocities hence an algebraic slip formulation is employed in Fluent. So the expression for the relative velocity is given as,

$$\overrightarrow{v_{pq}} = \overrightarrow{v_p} - \overrightarrow{v_q} \tag{3.23}$$

Where $\overrightarrow{v_p}$ and $\overrightarrow{v_q}$ are velocities of primary and secondary phase respectively.

The expression for drift velocity is stated as,

$$\vec{v}_{\mathrm{dr},p} = \vec{v}_{pq} - \sum_{k=1}^{n} c_k \vec{v}_{qk} \tag{3.24}$$

Where c_k is the mass fraction of any phase k expressed as,

$$c_k = \frac{\alpha_k \rho_k}{\rho_m} \tag{3.25}$$

Studies reveal that slip velocity is a function of drag function, relaxation time, and acceleration of the particles of secondary phase ($\vec{a}$). When the flow is turbulent, slip velocity will also depend upon the dispersion due to the dispersed phase. Hence Fluent accounts for this by adding a diffusion term in the expression for slip velocity as shown,

$$\vec{v}_{pq} = \frac{(\rho_p - \rho_m) d_p^2}{18 \mu_q f_{\mathrm{drag}}} \vec{a} - \frac{\nu_m}{\alpha_p \sigma_D} \nabla \alpha_q \tag{3.26}$$

Where,

v_m = Turbulent viscosity of mixture.

f_{drag} = Drag function.

σ_D= Prandlt dispersion coefficient.

In Fluent, there are several choices available for the drag functions.

Volume fraction equation for the secondary phase: Volume fraction equations have been obtained from the continuity equation for the secondary phase. It is expressed as follows,

$$\frac{\partial}{\partial t}(\alpha_p \rho_p) + \nabla \cdot (\alpha_p \rho_p \vec{v}_m) = -\nabla \cdot (\alpha_p \rho_p \vec{v}_{\mathrm{dr},p}) + \sum_{q=1}^{n} (\dot{m}_{qp} - \dot{m}_{pq}) \tag{3.27}$$

3.5.3 Limitations and assumptions of Mixture model: Along with the simplicity and ease of using the mixture model it has certain limitations also. Some of these limitations include the use of only the pressure based solver but not the density based one, inability for modeling inviscid flows and the flows involving solidification and melting. Mixture model cannot be used with some other models available in Fluent which include LES Turbulence model, shell conduction model, multiple reference frame (MRF) model (for relative velocity formulation) and Discrete Phase Model (when particles are tracked simultaneously). The mixture model is incapable for modeling streamwise periodic flows with constant mass flow rate and flows consisting of more than one compressible ideal gases. The mixture model uses the assumption of a local equilibrium between the participating phases in order to calculate the relative velocity between the participating phases. This local equilibrium is assumed to be limited to short length scales only.

Apart from the mixture model being used in the current study, Eulerian model can also be a good simulation model. It can also be applied to the current problem. Eulerian model is the most complex multiphase flow model among all the three multiphase flow models. Eulerian model employs as many sets of momentum and continuity equations as the number of phases participating in the flow. In the current case there has been a wide

distribution of particles in the slurry. Owing to this fact, mixture model becomes more feasible over the Eulerian model. The disadvantage that Eulerian model carries is that it demands a lot of computational power. This is also one of the reasons for preferring the mixture model over the Eulerian model.

3.5.4 K-ε Equations used in mixture model: K-ε turbulence mixture model has been used which is by default employed in Fluent when multiphase flow is combined with turbulence. It is suitable for stratified flows. Following are the K and ε equations used in capturing the relevant characteristics,

$$\frac{\partial}{\partial t}(\rho_m k) + \nabla \cdot (\rho_m \vec{v}_m k) = \nabla \cdot \left(\frac{\mu_{t,m}}{\sigma_k}\nabla k\right) + G_{k,m} - \rho_m \epsilon \tag{3.28}$$

And

$$\frac{\partial}{\partial t}(\rho_m \epsilon) + \nabla \cdot (\rho_m \vec{v}_m \epsilon) = \nabla \cdot \left(\frac{\mu_{t,m}}{\sigma_\epsilon}\nabla \epsilon\right) + \frac{\epsilon}{k}(C_{1\epsilon}G_{k,m} - C_{2\epsilon}\rho_m \epsilon) \tag{3.29}$$

Where,

$$\rho_m = \sum_{i=1}^{N} \alpha_i \rho_i \quad , \tag{3.30}$$

$$\vec{v}_m = \frac{\sum_{i=1}^{N} \alpha_i \rho_i \vec{v}_i}{\sum_{i=1}^{N} \alpha_i \rho_i} \tag{3.31}$$

Turbulent viscosity,

$$\mu_{t,m} = \rho_m C_\mu \frac{k^2}{\epsilon} \tag{3.32}$$

And turbulent kinetic energy production is given by,

$$G_{k,m} = \mu_{t,m}(\nabla \vec{v}_m + (\nabla \vec{v}_m)^T) : \nabla \vec{v}_m \tag{3.33}$$

3.6 Incorporation of sensor and pipe geometry using Gambit meshing and formulation:

FTIR probe description: The Fourier Transformed Infrared Reflectance (FTIR) probe consists of a cylindrical section with a gap or slot through its curved surface. The sensing is performed across this slot. The sketch of the probe is shown in the Fig. 3.3. All the dimensions are shown in the figure except one which shows the variable part of the probe whose dimension can be varied in order to vary the slot dimensions.

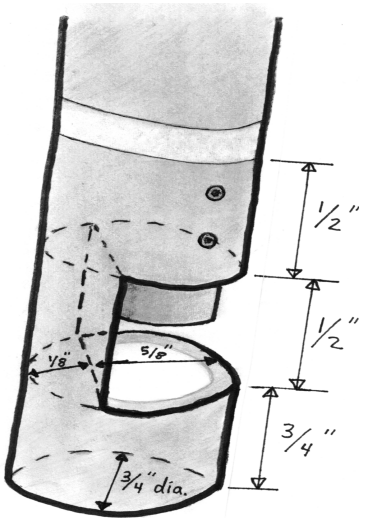

Fig. 3.3 Fourier Transformed Infrared Reflectance probe

The pipe that has been considered for different cases is 7.112 m in length and 0.1016 m in diameter. The probe is placed at distance of 4.064m from the inlet and is 3.048m before the outlet. The Reynolds number of the flow is of the order of 240,000.

In order to design the probe and pipe assembly in Gambit, coordinates of vertices have to be entered using Operation->Geometry->Vertices. After entering the vertices, edges have to be constructed through Operation->Geometry->Edge by using two or more vertices. These edges can be linear, circular or arc. Further edges created will be used for making faces of the assembly design through Operation->Geometry-> Face. And at last by using Operation-> Geometry->Volume, faces are either stitched or swept to obtain three dimensional geometries. It should be pointed that **Stitch and Swept** are two command options in Gambit used to make a volume by stitching multiple faces or sweeping one single face in a direction perpendicular to it and the swept region is converted to volume. For the current case the pipe has been designed in three volumes in inlet, outlet and probe regions.

The next step which is the most important step of the design is the mesh generation or grid formation in the constructed geometry. For the current design Operation-> Mesh-> Mesh volumes have been used. The volume in the probe region has been meshed using the tetrahedral grid meshing with the interval count of the grid points on the faces being 10. The inlet and outlet volume regions have been meshed using hexagonal cooper meshing scheme available in Gambit with an interval count of 40. The total number of cell volumes formed after meshing are 0.68 million. A plain pipe is also designed in order to determine the results of fully developed flow. It has been meshed using the hexagonal cooper scheme and interval count of 50.

The last step of the design process is the specification of boundary conditions. Following Operation->Zones->Specify Boundary Types, desired boundary conditions

can be specified in Gambit. The boundary types specified in the current case are Velocity inlet, Pressure outlet, Wall. Figure shows the boundaries specified.

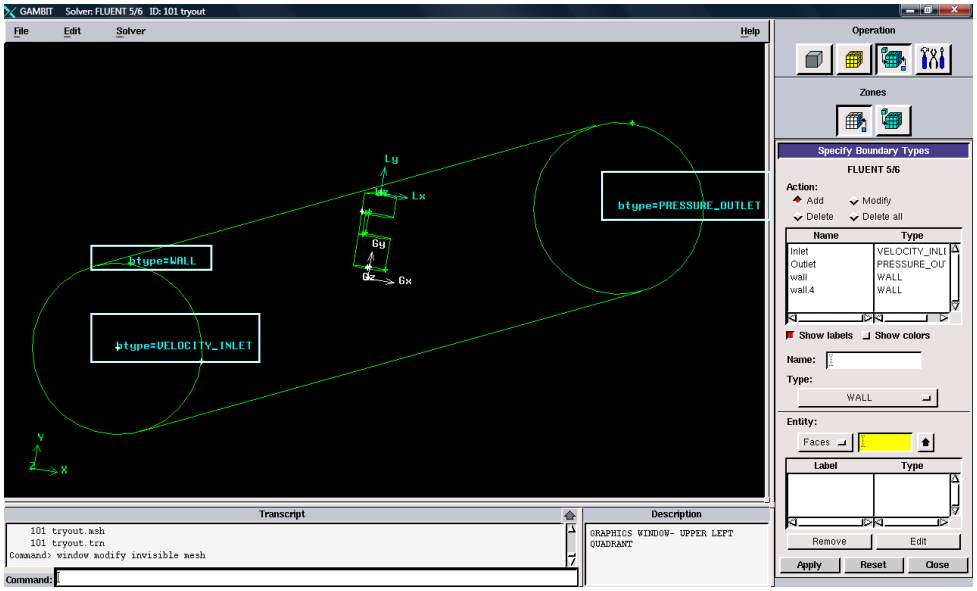

Fig. 3.4 Boundary types shown in Gambit

After when all the above steps are successfully implemented we can expect a meshed geometry similar to as shown in the Fig. 3.5

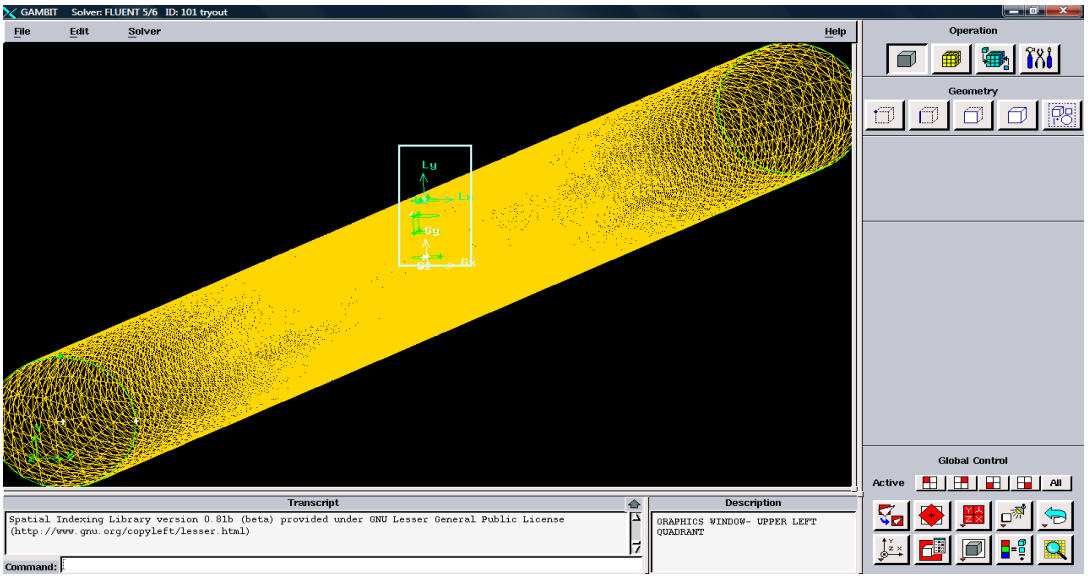

Fig. 3.5 The meshed pipe and probe assembly in Gambit.

The meshed geometry is then saved using File--> Save. Further, the meshed geometry will have to be exported using File-> Export-> Mesh to Fluent where the actual analysis will take place. This will save a **.**msh file in the Gambit working folder.

3.7 Simulations in Fluent: Proceeding with the next stage of the work done in Gambit, click on the Fluent icon to open Fluent. While opening Fluent, 3ddp (Three dimensional double precision) version has to be selected in Full simulation mode. First, the **.**msh file exported in Gambit is imported in Fluent using File-> Read-> Case. Next the Grid has to be checked for discrepancies, if any. This is done using Grid-> Check. Further the problem is set in Fluent by defining the models and input values of the relevant variables. Using the Define panel solver being used, the multiphase model employed and the turbulence model are specified as Define-> Models-> Solver, Define-> Models-> Multiphase and Define-> Models-> Viscous respectively. For the present study, pressure based solver, multiphase mixture model and turbulence K-ε models have been utilized. When mixture model is selected, the user has to specify the number of phases involved in the flow, slip velocity computation if required and any implicit body forces if acting during the flow. The current study makes use of both slip velocity as well as implicit body force which is gravity in this case. Moving ahead the solid and liquid phase materials which are being used in simulation process are selected using Define panel as Define-> Materials. Generally all the materials are available in Fluent database but user can input the materials by adding the name of material along with the required properties. In this case the Table 3.1 shows the input values of the liquids and solid particles. There are two different cases for which two different sets of materials are used.

MATERIAL	DENSITY (in kg per cubic meter)	VISCOSITY (in Kg per second meter)
CASE I		
2-Amino-4,6-dimethylpyrimidine (ADP) particles.	1480	-
Xylene (Liquid)	870	6.2e-04
CASE II		
Calcium carbonate particles.	2800	1.72e-05
Water	998.2	1.003e-03

Table 3.1 Input materials in Fluent

MATERIAL	PHASE
CASE I	
2-Amino-4,6-dimethylpyrimidine (ADP) particles	Secondary
Xylene	Primary
CASE II	
Calcium carbonate particles.	Secondary
Water	Primary

Table 3.2 Input materials phase in Fluent

Using Define-> Phase, one has to define the primary and secondary phases along with their state. Table 3.2 above indicates the phase of the materials used.

For the secondary phase, granular characteristics have been chosen in all the present cases. Further through the Define panel one can choose to select the interactions between the phases which include specifying the drag functions, slip velocities etc. Using the Define panel, Operating conditions and Boundary conditions are provided using Define-> Models-> Operating conditions and Define-> Boundary conditions respectively. In the Operating conditions panel the gravity check box has to be selected and its value is given in Y direction as -9.81m/sec^2. In the Boundary conditions panel different input values have to be provided at different boundaries. Table 3.3 gives a better explanation of the input variables and their values in the current case. The turbulent intensity of the flow is calculated using the following formula which depends upon Reynolds number

$$T.I. = 0.16 \times Re^{-1/8} \tag{3.34}$$

The backflow turbulent intensity is one of the parameters that need to be input. Backflow turbulent intensity refers to the intensity of turbulence if there is any flow taking place in the reverse direction. Backflow parameters are used by Fluent if any backflow occurs during the iterations, otherwise they are not used. A good guess of these parameters will help the solution to run stable if backflow occurs, a bad guess can cause divergence also.

Boundary types	**Primary phase input values.**	**Secondary phase input values.**	**Mixture input values**
Inlet (Velocity inlet)	Flow velocity of liquid phase =2m/sec.	Flow velocity of particle phase =1.5m/sec. and volume fraction =0.4	Specification method (Turbulent intensity= 3.5%. and hydraulic diameter =0.1016m)
Outlet (Pressure outlet)	None.	Backflow volume fraction =0.4	Specification method (Back flow Turbulent intensity= 0.001%. and hydraulic diameter =0.1016m)
Wall	None	None.	Default values
Fluid	None	None	Rotation axis direction Z=1.

Table 3.3 Input variables and their magnitudes.

Further the solution parameters are provided using the Solve panel. Solve-> Controls->Solution controls is used to open the Solution controls panel where the under-relaxation factors, pressure-velocity coupling types and discretization laws are specified. For the current problem as the geometry is complex due to presence of the probe in the flow, hence first order upwind discretization is preferred for all the quantities. One can play with the underrelaxation factors in order to govern the convergence of the residuals. The next step involves the solution initialization using Solve -> Initialize-> Solution initialization. In the current case solution is initialized from inlet. In the next step, convergence criteria are mentioned for all the variables using Solve -> Monitors-> Residuals. Generally it is set at 1e-5 or smaller. Also one has to activate the plot option to enable Fluent to plot residuals. Next step is the one in which iteration parameters like time step size, numbers of time steps, numbers of iterations per time step are specified for a transient flow problem. This is done using Solve -> Iterate-> Iterate. For the present work the time step size has been taken of the order of 0.1. Then iterations are performed to achieve convergence of residuals.

Fluent follows an iterative scheme to find the solution of the flow problem. All the governing equations are solved for each and every time step. This is done until the convergence is achieved in every time step. Once the convergence is obtained in a time step the solution is increased by one time step. This can be expressed as shown in Fig. 3.6. This scheme also considers the non-linear nature of the governing equations as well as the inter-relation between the equations.

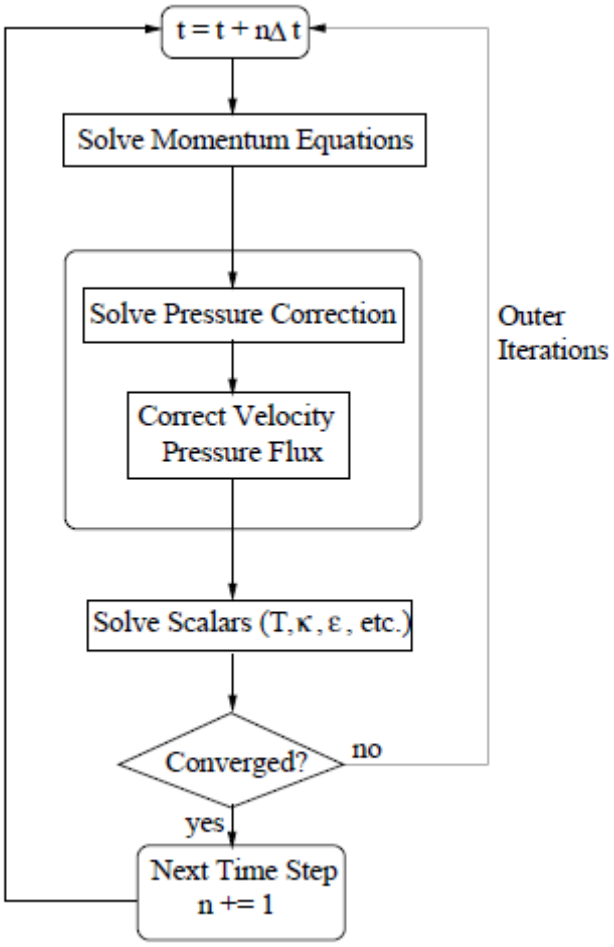

Fig. 3.6 Solution strategy in Fluent (Source: Fluent 6.3 user guide)

Fluent offers versatile post processing tools to visualize and analyze the flow. These tools include XY plots, contour plots, vectors displays etc which can be found under the Display and Plot panels. Post processing has been done and fairly good results have been obtained which have been dealt with in the next chapter.

CHAPTER IV

Results and Discussion

4.1 Brief recapitulation:

It has been discussed in the preceding chapters that Computational Fluid Dynamics is playing an important role in predicting the characteristics of the multiphase flow involving liquid and solid particles. In the current study CFD has been applied to the flow of a chemical slurry in which 2-Amino-4, 6-dimethylpyrimidine (ADP) is used as particles and Xylene is the liquid. In a different case, calcium carbonate particles were made to flow through water forming calcium carbonate-water slurry. The flow has taken place through pipes with the ratio of length to diameter being 70. The modeled Fourier Transform Infrared reflectance probe is placed such that its distance from the inlet is more than that from the outlet of the pipe vertically on the upper surface. The probe is at a distance 40 times the diameter from the inlet and 30 times the diameter from the outlet.

This chapter aims at presenting the important findings of the current research. It has been mentioned that the current research focuses on the application of CFD to visualize the flow over and through the sensing gap of the FTIR/NIR probe. It also aims to determine the profiles of solid particle concentration and velocity through the sensing gap of the probe. The post processing tools of Fluent have been utilized in order to ensure self explanatory and descriptive visualization of the flow. In addition,

Tecplot 260 has been employed for plotting the concentration profiles and velocity profiles of slurry flowing through the sensing gap of the probe. The results obtained by using ADP particles and Xylene are compared with those with the calcium carbonate particles and water. In all the plots shown all distances are in meters and **negative sign on Z velocities represents direction as the slurry is flowing in the negative Z direction.**

4.2 Flow of Xylene (WITHOUT particles) in 7.112m length pipe: In this section, the results obtained by the flow of xylene in a plain pipe (pipe with no probe) are presented. The inlet velocity is 2m/sec. The profiles of Z velocity of xylene have been plotted along different axes. The velocity profiles clearly depicts that fluid flow shows the fully developed behavior.

-Z velocity variation along the centerline:

The pipe coordinate system is shown in Fig. 4.1(a). Fig. 4.1(b) shows the Z velocity variation. The centerline Z-velocity increases as the fluid flow takes place further the inlet. Then it decrease and gradually becomes constant. This shows that the flow has become fully developed.

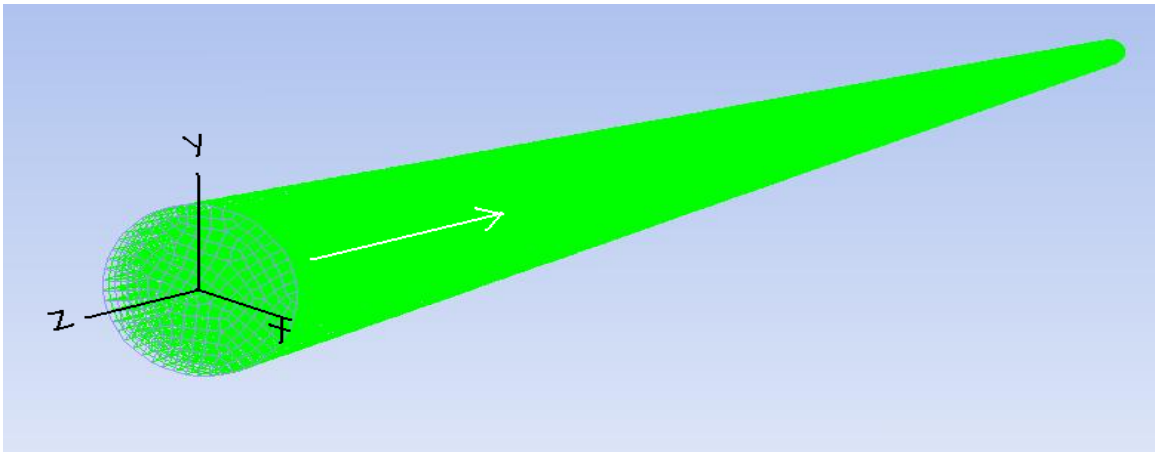

(a)

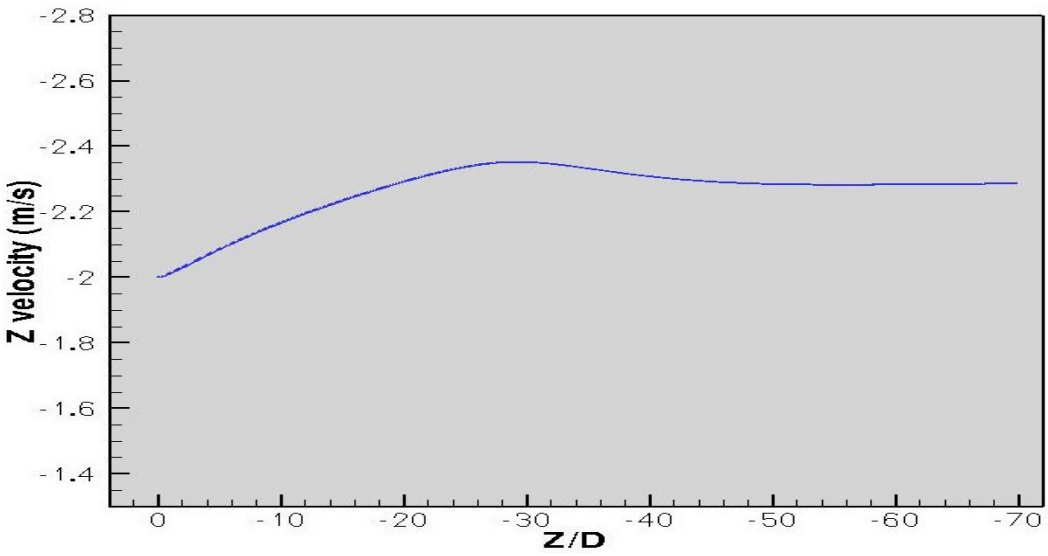

(b)

Fig. 4.1 (a) Pipe coordinate system (plain pipe) (b) Z velocity of Xylene varying along centerline of the pipe.

-Z velocity profiles along the vertical axis along Y direction:

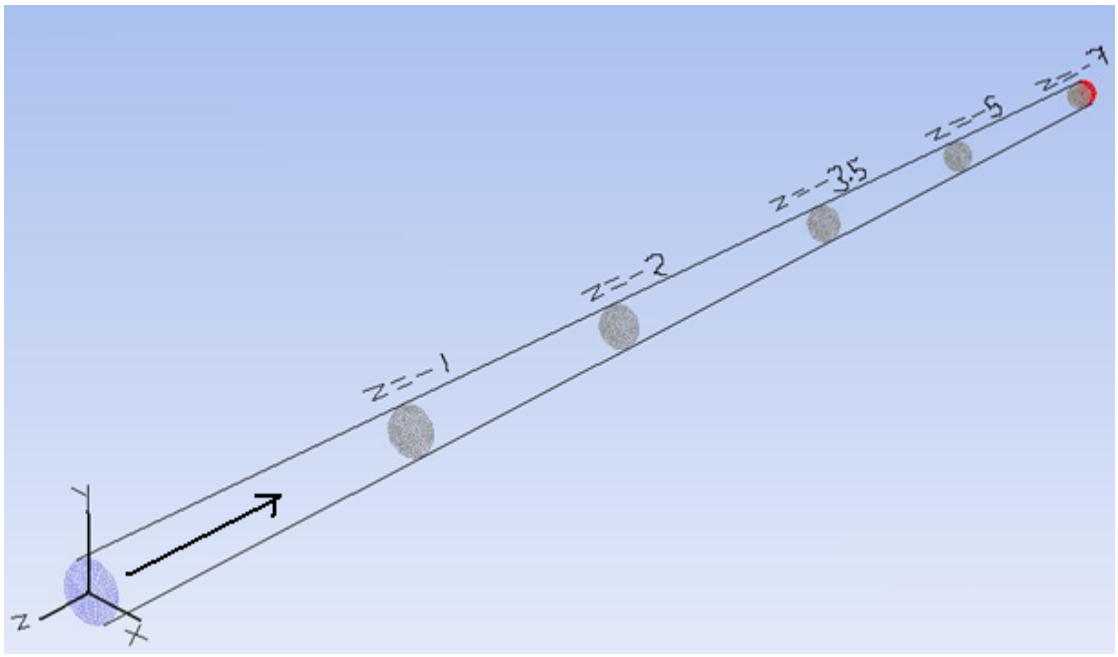

Fig. 4.2 Pipe section showing the location of planes and the respective axes along which Z velocity are plotted. Inlet (hown in blue) is near Z= -1 plane and oulet (shown in red)lies near to Z= -7 plane. Flow direction shown by arrow.

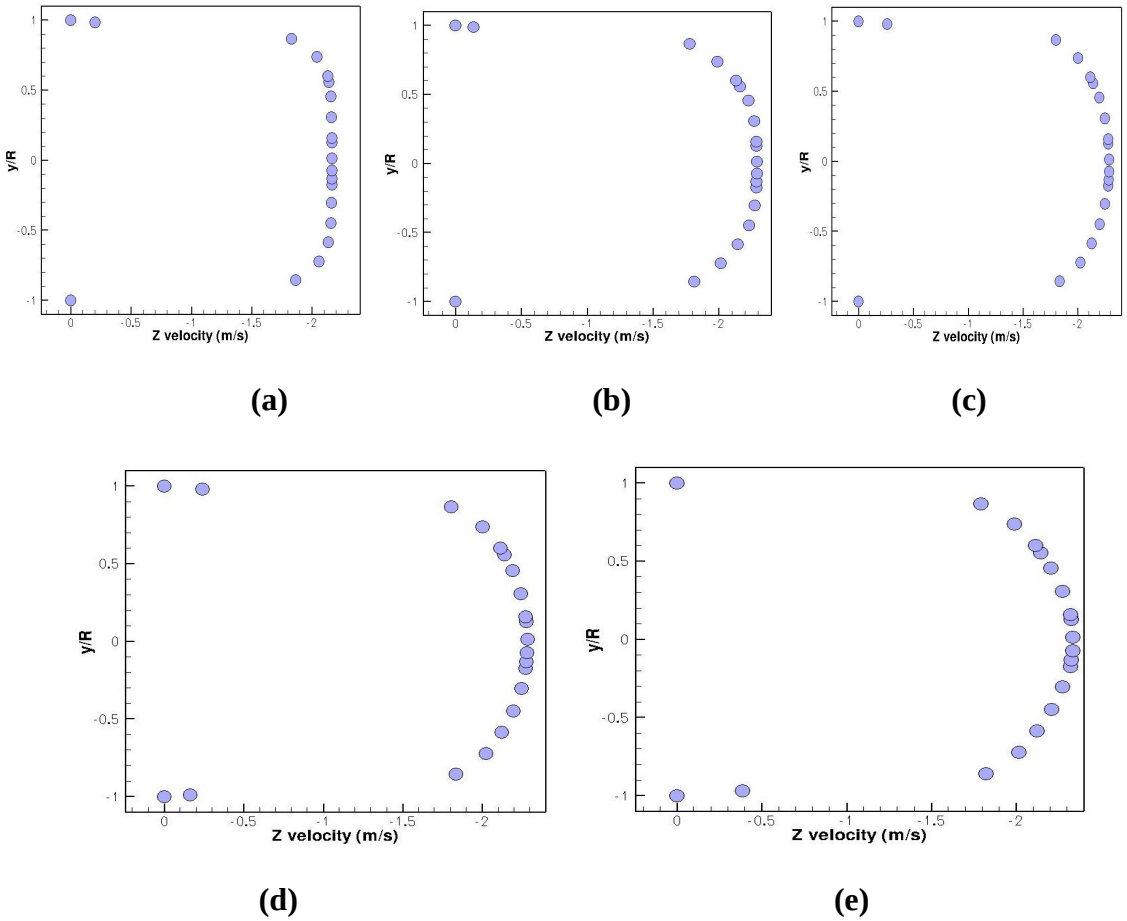

Fig. 4.3 Z velocity profiles along vertical axes in (a) Z= -1 (Z/D=9.84), (b) Z=-2 (Z/D=19.685), (c) Z= -3.5 (Z/D=34.45), (d) Z= -5 (Z/D=49.2) and (e) Z= -7(Z/D= 68.89) cross sectional planes as shown.

Fig. 4.3 shows the Z velocity profiles of Xylene along the vertical axes lying in different cross sectional planes normal to the axis of the pipe. The profiles shown in (a) (b), (c), (d) and (e) are all symmetric with respect to the centerline which is at y/R=0.

The comparison of power law profile for a turbulent plain pipe flow with the non dimensional velocity profiles is shown in Fig. 4.3(f). The inlet velocity is 1.5m/sec. The profile in blue is obtained from Fluent while the one in red is the power law profile. The power law index is 7. The agreement of the profiles is as shown in Fig. 4.3(f). The power law index has been taken from Schlichting (1968).

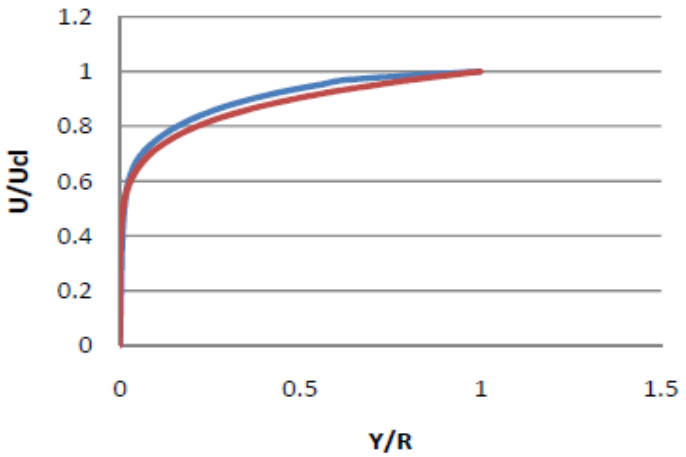

4.3 (f) Comparison of velocity profile in radial direction with power law profile (n=7) shown in red with the fluent profile in blue at Z/D=35.

Z velocity profile along the centerline of a plain pipe WITH particles:

Fig. 4.4 shows the particle Z velocity profile along the centerline of the plain pipe. The particle diameter is 100 microns. Thus in the presence of particles the flow gains fully developed characteristics at around Z/D= -35. Hence placing the probe at Z/D=-40 is worthwhile in order to mount the probe in fully developed flow region.

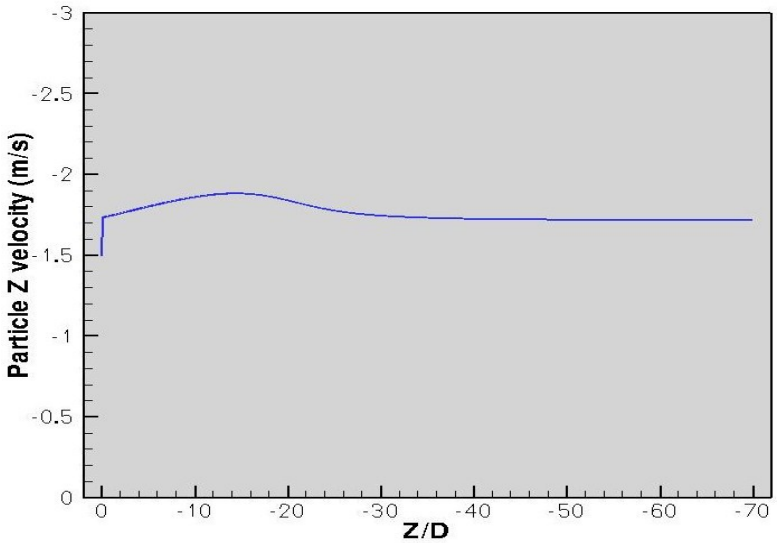

Fig. 4.4 Particle Z velocity profile along centerline of the plain pipe.

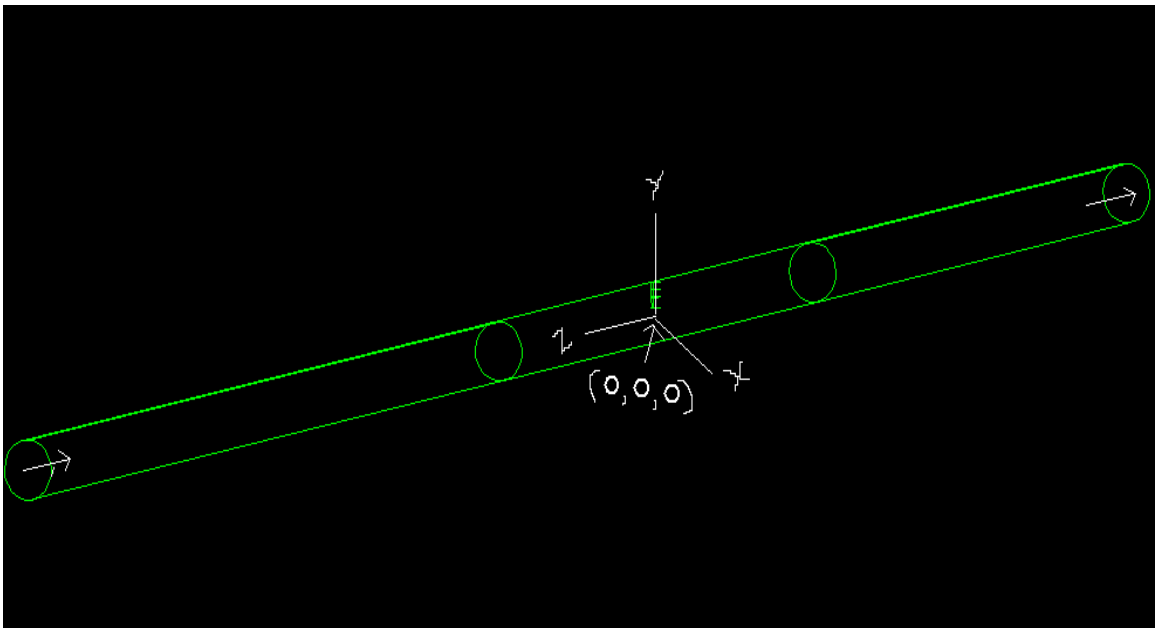

(a1)

4.3 Flow of ADP particles with Xylene in 7.112m (L/D=70) length pipe:

In this section, the data obtained by the simulation of the flow of ADP particles and Xylene have been presented. The data has been presented in the form of plots, contours and vectors of different physical quantities. These quantities are Z-velocity and volume fraction of particles. In order to study the variation of these quantities in particular directions, different lines and planes have been drawn using Fluent post processing tools and then the corresponding physical quantity has been plotted against that line/plane. The pipe dimensions can be expressed in terms of cylindrical coordinates R, θ and Z where R is the radius of pipe, θ being the angular distance and Z being the pipe axis corresponding to the length of the pipe. In the current case R varies from -0.0508 m to 0.0508m, θ varies from 0 to 360 degrees and Z varies from -3.048 m to 4.064 m. Hence the geometry is asymmetrical with respect to Z coordinate. The position of origin is shown in Fig. 4.5(a) as (0,0,0).

4.3.1 Plots of velocity profiles: Velocities have been plotted along the axial (Z/D) and radial (y/R) directions and the conclusions have been drawn. The pipe length ranges from inlet at Z/D=40 and outlet at Z/D= -30 (negative Z direction) with probe at Z/D=0. Y coordinate varies from y/R= -1 to +1. The axes along which the velocity profiles have been plotted are shown in the adjacent figures.

-Particle Z velocity vs. axis (centerline): The axial velocity (Z velocity) has been plotted along the centerline or the axis of the pipe as shown in Figs 4.5. Fig. 4.5(a2) shows the axis along which the velocity has been plotted. Fig. 4.5(b) depicts the variation of Z velocity of particles along the centerline of the pipe. The negative sign on the velocity is indicative of the direction of flow as the flow is in negative Z direction. The particle Z velocity at injection is -1.5 m/sec which suddenly reaches to -1.73 m/sec when comes in contact with the liquid Xylene which has initial velocity of -2m/sec. Thus -1.73 m/sec is the initial velocity of the slurry. The particle Z velocity increases and then comes down to the previous magnitude of -1.73 m/sec as the flow progresses after the inlet. The flow is smooth and the particle Z velocity remains constant till it reaches the vicinity of probe where major fluctuations in the particle Z velocity are observed as shown in Fig. 4.5(c). The particle Z velocity in the probe region shows a zigzag variation. This is attributed to the divergence of the flow in the presence of probe. The fluctuations in Z velocity may be observed owing to 3D flow in y direction (increment in Y component of velocity) as the particles will have the tendency to flow downwards as the probe is approached. After the probe region the particles regain the same velocity magnitude. As the flow approaches the outlet there is a very little decrease in the particle Z velocity. At the outlet the particle Z velocity has the same magnitude of -1.73m/sec.

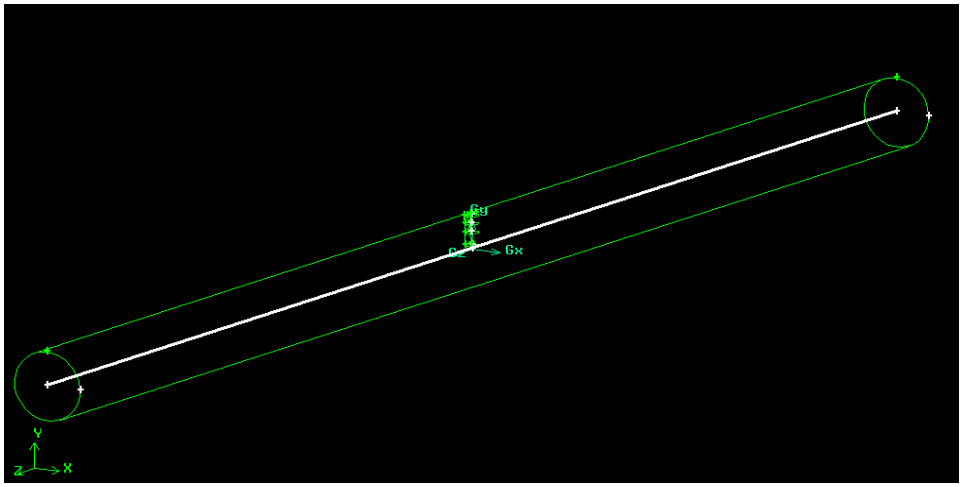
Gy
Gx
Y
Z
X

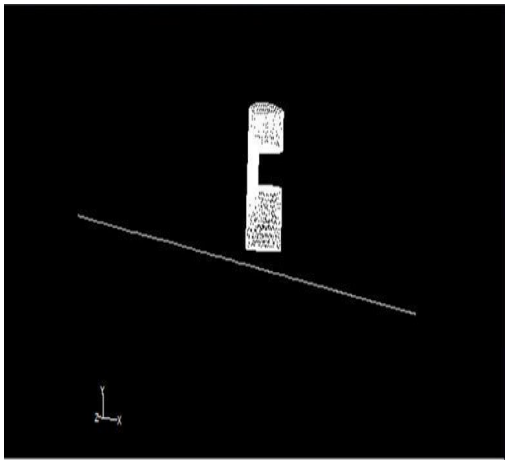

(a2)

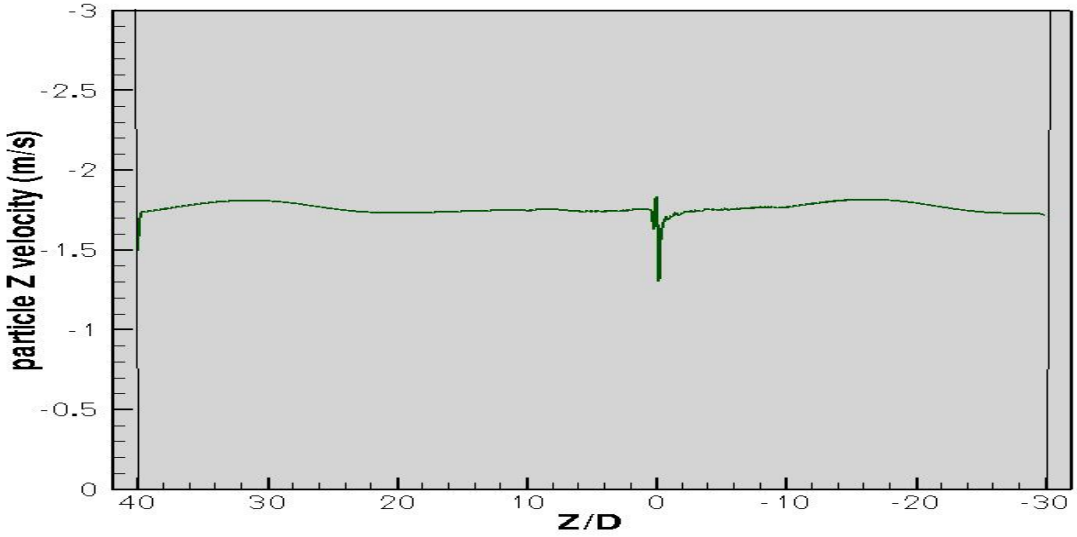
particle Z velocity (m/s)
-3
-2.5
-2
-1.5
-1
-0.5
0
40
30
20
10
0
-10
-20
-30
Z/D

(b)

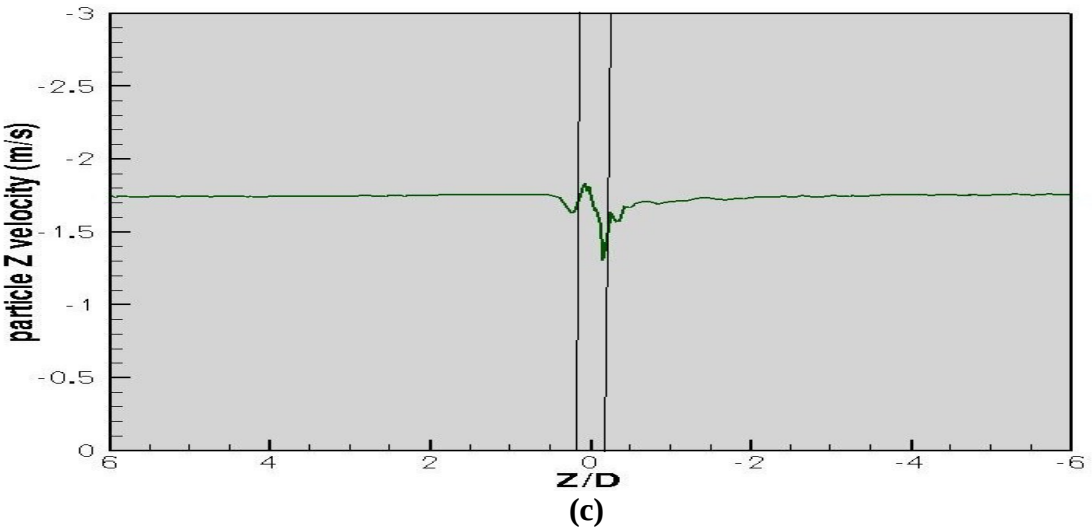

Fig. 4.5 (a1) Probe and pipe assembly with the directional coordinate system (a2) Axis of the pipe (b) Particle phase Z velocity variation along the centerline (c)Flow along the probe vicinity shown between parallel lines.

-Particle Z velocity vs. axis parallel to the centerline and passing through the middle of probe slot: Fig. 4.6 shows the variation of the particle Z velocity along the axis parallel to the centerline and passing through the middle of the probe slot as shown in Fig. 4.6(a). The negative sign on the velocity is indicative of the direction of flow as the flow is in negative Z direction. Along this axis, a similar behavior of particles is observed as along the centerline but as the flow progresses from inlet the particle Z velocity undergo a little decrease in the magnitude and then becomes uniform until it reaches the vicinity of probe slot. Again the major fluctuations in velocity of particles are observed in the probe slot vicinity which is shown in Fig. 4.6(c). After the probe slot vicinity the particle Z velocity starts climbing up to regain the previous velocity. Unlike the variation along the centerline of the pipe, the particles travel more distance in the pipe to regain the same velocity as shown in Fig. 4.6(c). As the flow approaches the outlet the particle Z velocity decreases and ends up at a magnitude of 1.5m/sec.

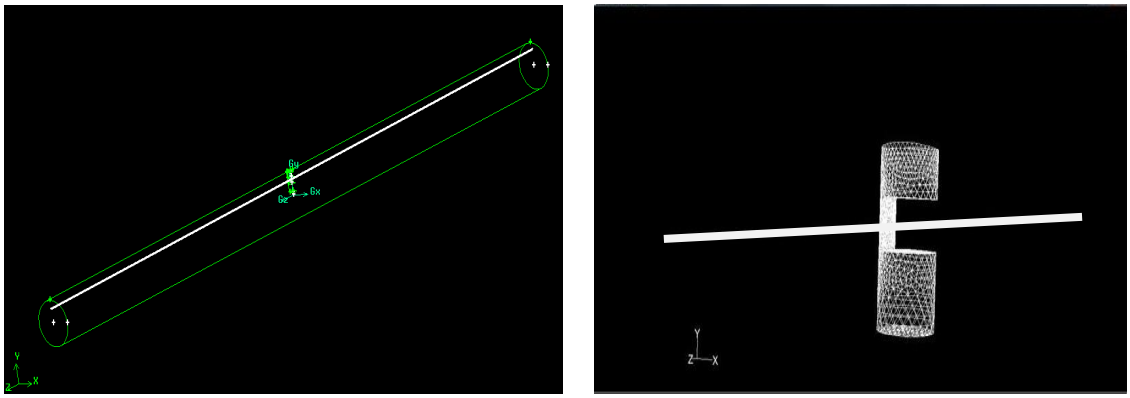

(a)

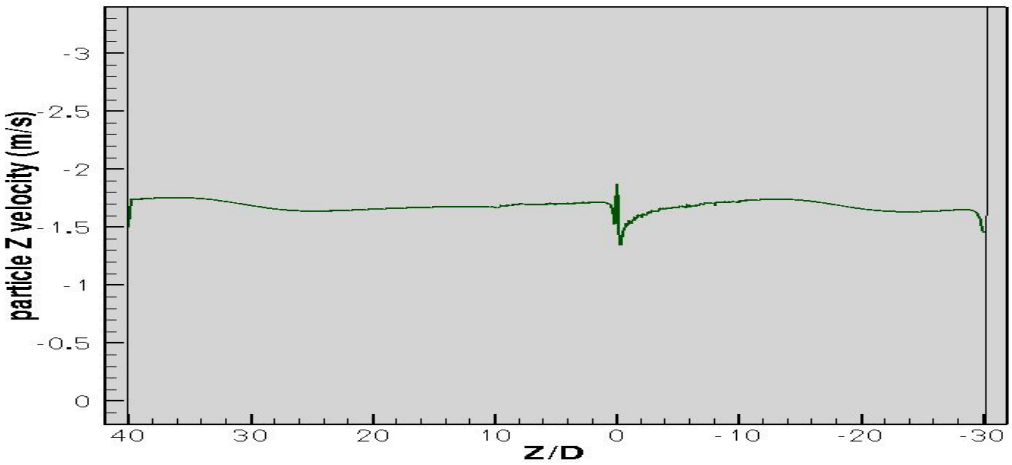

(b)

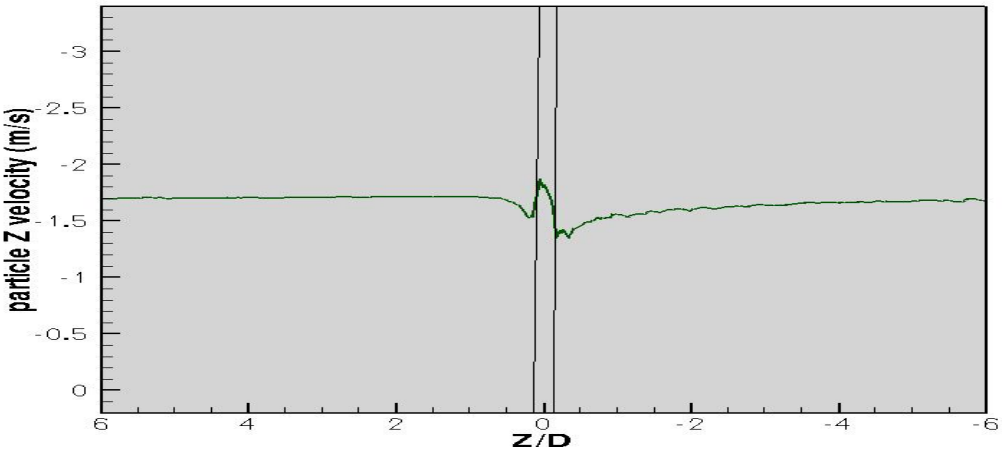

(c)

Fig. 4.6 (a) Axis (b) Particle phase Z velocity variation along the axis parallel to the centerline. (c)Flow along the probe vicinity shown between parallel lines.

-Particle Z velocity vs. axis parallel to the centerline and passing through the lower solid part of probe: Fig. 4.7 shows the variation of particle Z velocity along an axis parallel to the axis of the pipe but passing through the lower solid end of the probe. The particle Z velocity before reaching the probe region behaves similar to the velocity observed along the centerline of the pipe. When it reaches the vicinity of lower solid end of the probe there is immediate drop in velocity to null value due to the presence of

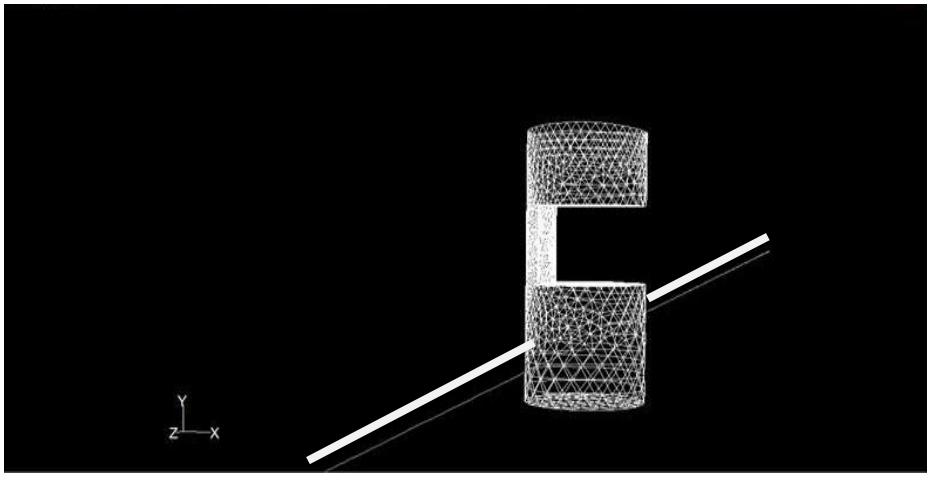

(a)

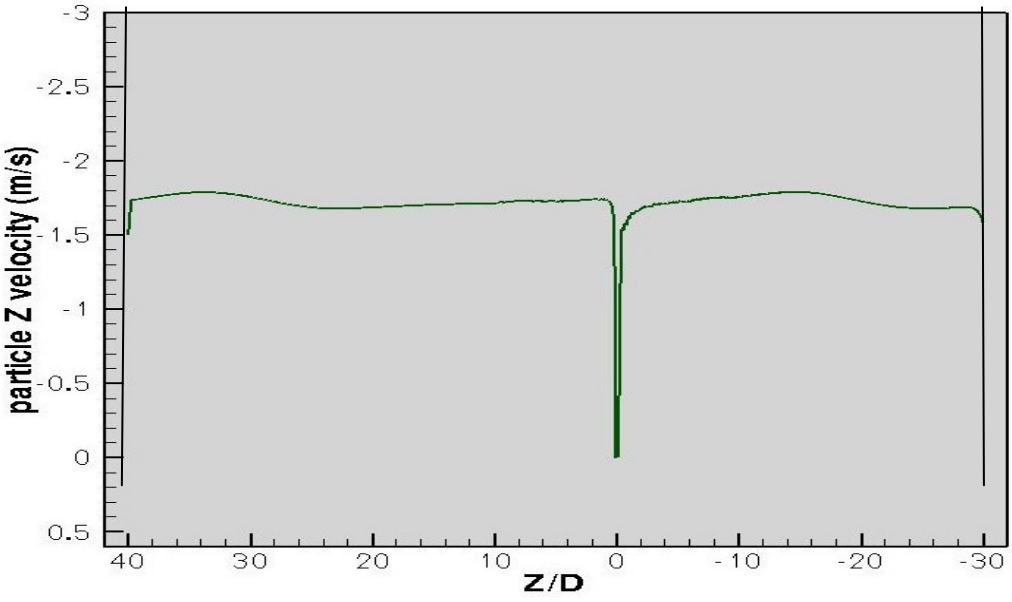

(b)

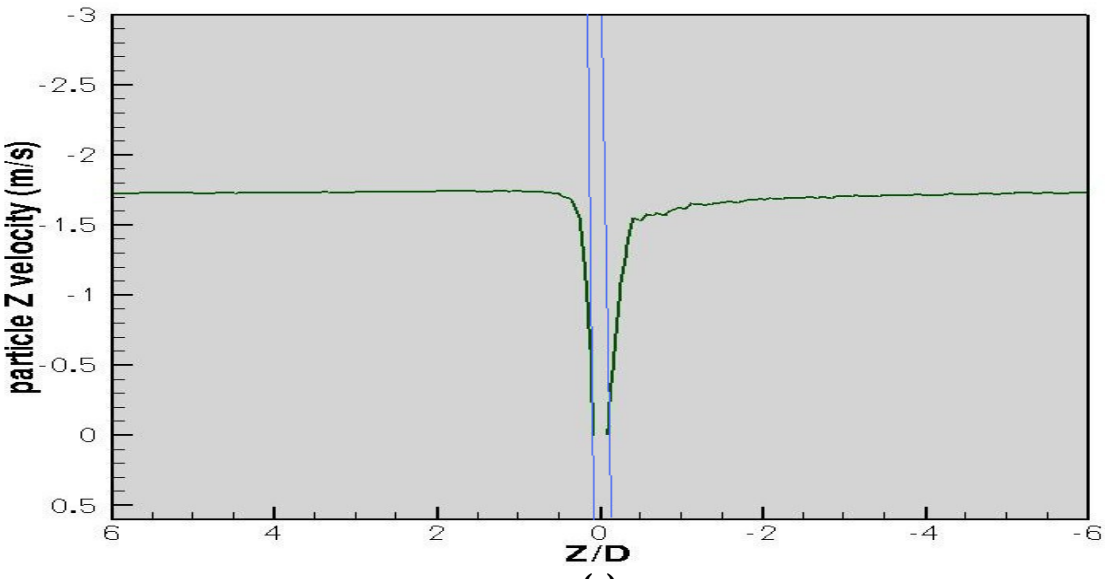

(c)

Fig. 4.7(a) Axis. (b) Particle phase Z velocity variation along the axis parallel to the centerline but passing through the lower solid end of the probe. (c)Flow along the probe vicinity shown between parallel lines.

stagnation point as shown by the curve. Further downstream, the particles attain the usual velocity again which is of the order of -1.73m/sec. The particle Z velocity fall gradually and then becomes uniform as the outlet is approached as shown.

In all the three cases of variation of particle Z velocity (Figs. 4.5(b), 4.6(b), 4.7(b)) it can be noticed that the velocity profile in the region before the probe (Entrance region of pipe) is similar to the profile in the entrance region of the plain pipe with particles (Fig. 4.4) except in the above three cases uniform velocity is achieved earlier Z/D value.

-Particle Z velocity along Y axis (i.e. Along the line through the center of the probe slot circular section and the lines to the left and to the right of it as shown in the Fig. (a)): The variation of particle Z velocity is shown in Fig. 4.8 (b) along the line through the center of the probe slot circular section using the purple □. The negative sign just indicates the direction of flow. The probe slot lies between y/R= 0.5 to y/R=0.75 with

center of slot at y/R=0.625. The points shown explain that the velocity of the particles is zero at the upper and lower surface of the probe slot. The particle Z velocity profile resembles a parabola along the axis through the center of the probe slot.

Fig. 4.8(b) also shows the variation of particle Z velocity along the axis parallel to the Y axis but to the left of it. It is expressed as green triangle ►. There are small variations in the particle Z velocity near the center of the probe slot as shown by the points near the center. They exhibit very small velocity difference.

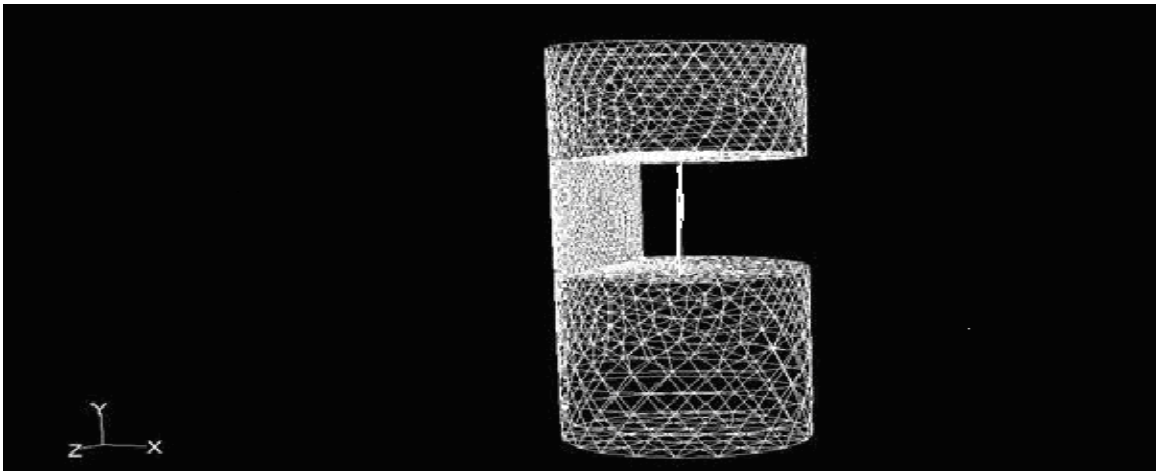

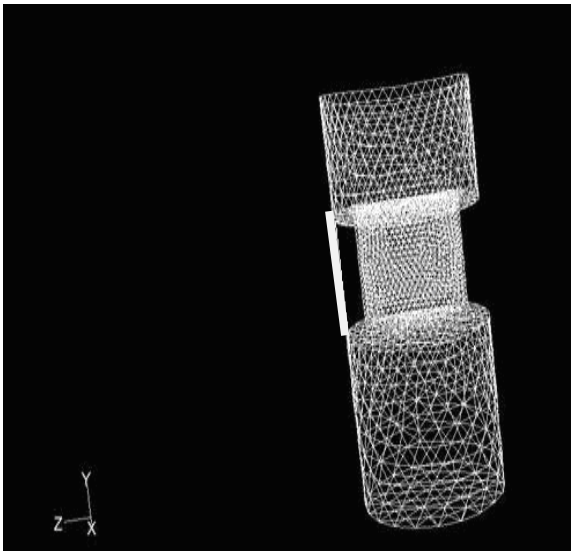

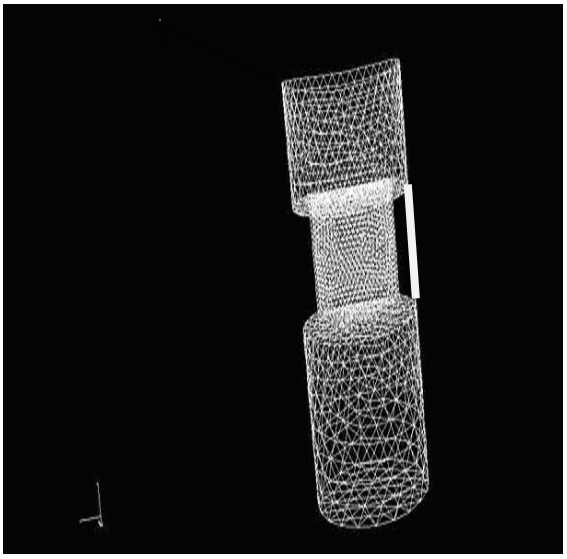

Left **(a)** **Right**

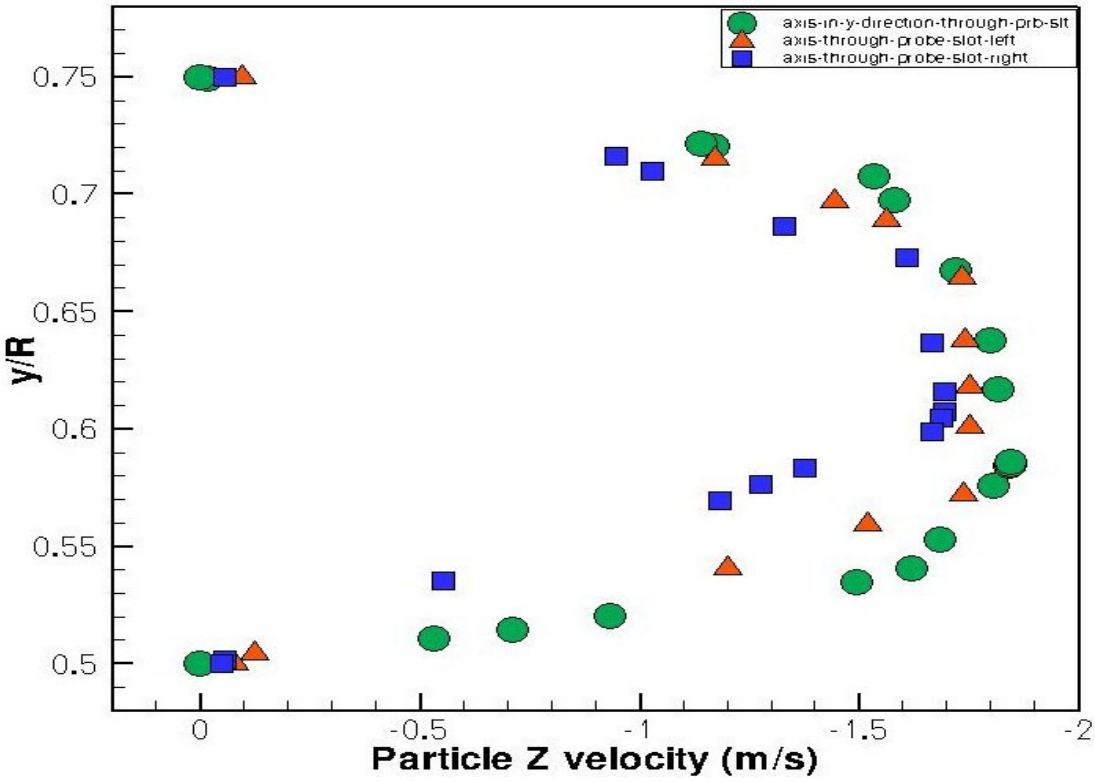

(b)

Fig. 4.8(a) Axes in Y direction and along the lines to the left and to the right of it (b)Particle Z velocity vs. Y axis (Along the line through the center of the probe slot circular section, along the lines to the left and to the right of it.

The variation of particle Z velocity along the axis parallel to the Y axis but to the right of it is also depicted in Fig. 4.8 (b) using blue Δ. The velocity at the lower and upper walls of probe slot is zero. In this case also, the variation resembles a parabola but this time density of velocity points is more near the center of the probe slot. Here the profile defines more curvature near the center compared to the profile obtained for the axis on the left.

4.3.2 Plots of particle volume fraction: This section will focus on the variation of the volume fraction of the particle phase along different axes. This information can be used to predict the particle concentration profiles through the probe slot.

- Particle volume fraction along Y direction (i.e. Along the line through the center of the probe slot circular section and the lines to the left and to the right of it as shown in the Fig. (a)): Fig. 4.9 (b) shows the variation of particle volume fraction along the lines through the center of the probe slot circular section in Y direction and axes to the left and to the right of it as shown in the Fig. (a). The Y axis shows the axis considered with specification as non-dimensional distance y/R while the X axis has the particle volume fraction.

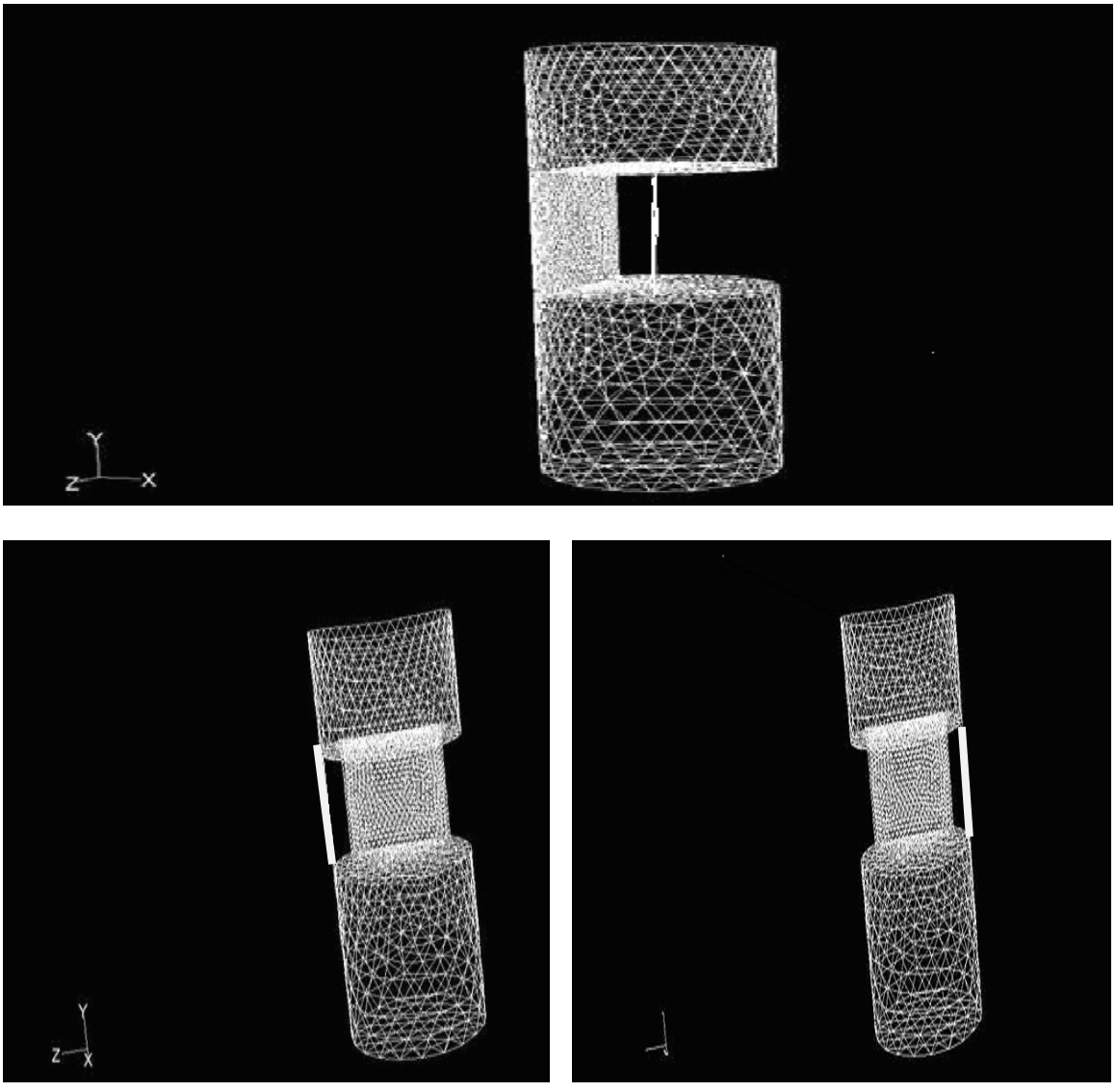

Left **(a)** **Right**

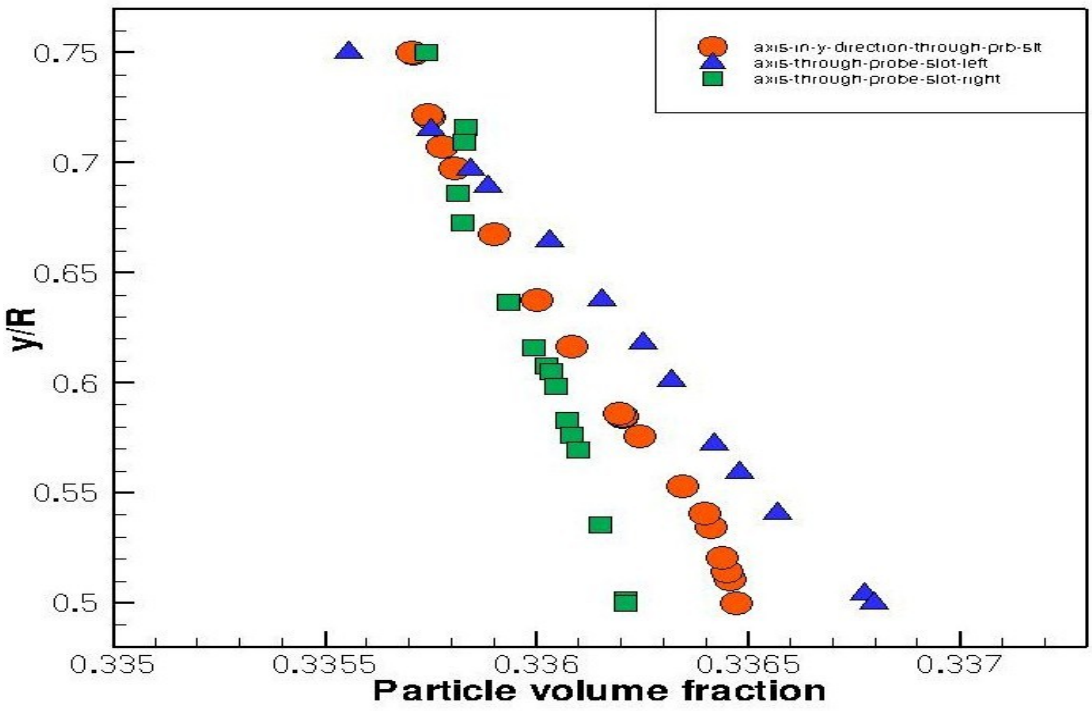

(b)

Fig. 4.9(a) Axes in Y direction and along the lines to the left and to the right of it (b) Particle volume fraction vs. Y axis (Along the line through the center of the probe slot circular section, along the lines to the left and to the right of it.

The variation in volume fraction is of the order of 10^{-3} which can be neglected. Hence the volume fraction of particles can be considered constant along the considered axis. Even though the particle volume fraction is constant, of the three cases the profile obtained for the axis considered on the 'axis through probe slot left' accounts for maximum variation.

- Particle volume fraction along an axis parallel to Y direction but behind it:

The axis is shown in Fig. 4.10 (a) with a red line. Fig. 4.10(b) shows the variation of volume fraction along the axis parallel to Y axis but behind it as shown by the red line in Fig. 4.10(a). It can be inferred that volume fraction decreases as we move from upper wall of the probe slot (y/R=0.75) to lower wall (y/R=0.5). But the magnitude of variation

is of the order of 0.001 hence it can be said that volume fraction is nearly constant along the considered axis.

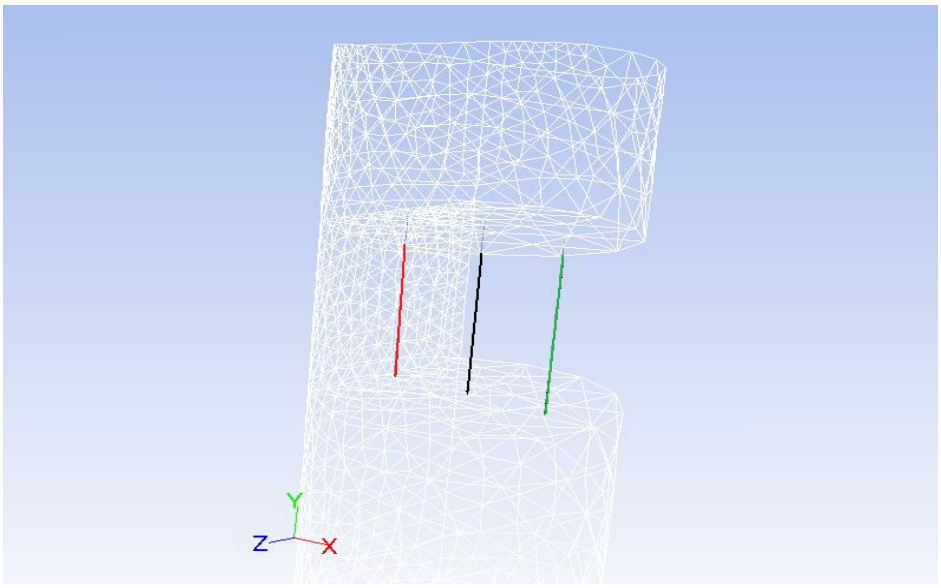

(a)

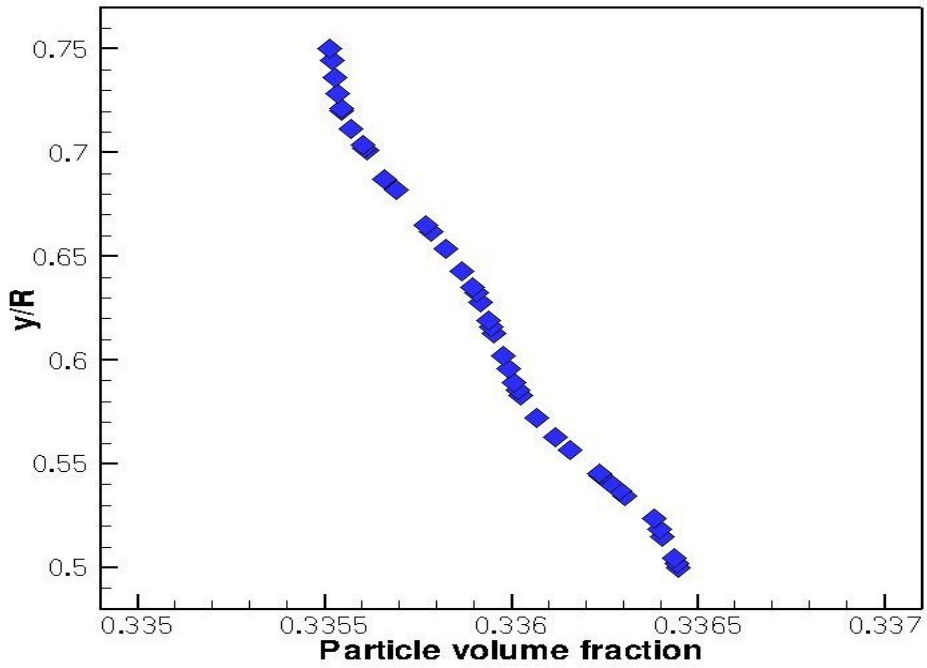

Fig. 4.10(a) Axes. (b) Particle volume fraction variation along the axis behind the Y axis through probe.

- Particle volume fraction along an axis parallel to Y direction but in front of it: Fig. 4.11 shows the variation of volume fraction along the axis parallel to Y axis but in front of it as shown by the green line in Fig. 4.10(a). It can be inferred that volume fraction decreases more steeply in the center of slot as we move from upper wall of the probe slot (y/R=0.75) to lower wall (y/R=0.5). But the magnitude of variation is small and is of the order of 0.001. Hence it can be said that volume fraction is nearly constant along the considered axis.

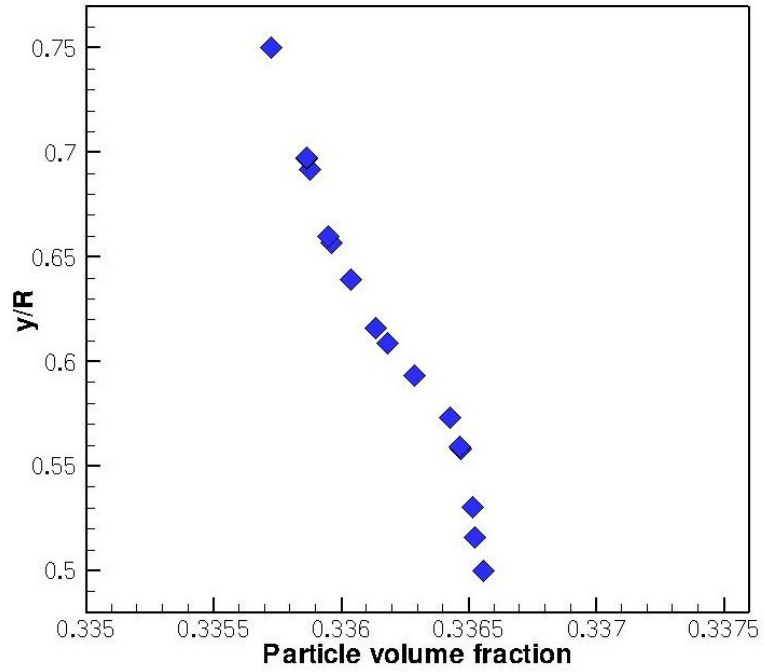

Fig. 4.11 Particle volume fraction variation along the axis in front of Y axis through probe. The axis is shown in Fig. 4.10 (a).

-Comparison of particle volume fraction along the axes shown in Fig. 4.10(a):

Fig. 4.12 shows the comparison of variation of volume fraction along the three different axes as shown by red, black and green lines in Fig. 4.10(a). Though by minute amount, but for comparative study the volume fraction magnitude is highest for the variation along the axis to the front of Y axis (Shown by green in Fig. 4.10(a)). The volume

fraction is lowest along the axis shown in red in Fig. 4.10 (a). This is because the axis shown in red is nearest to the vertical wall and since probe slot has opening just opposite to the wall so a three dimensional flow also takes place. Thus the axes farther from the vertical wall of the probe slot have comparatively more volume fraction magnitude.

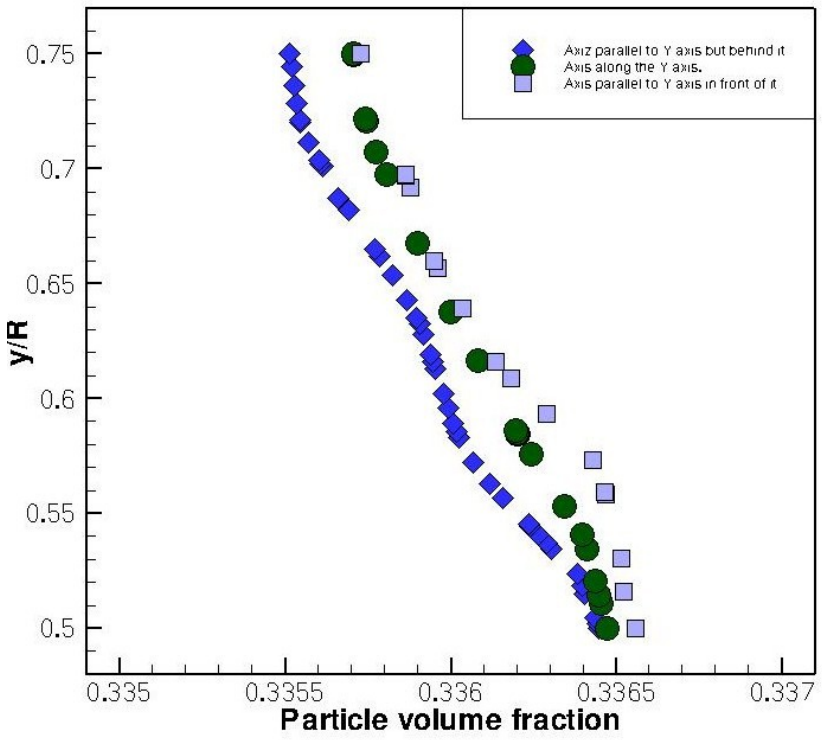

Fig. 4.12 Particle volume fraction variation along the axes shown in Fig. 4.10 (a).

4.3.3 Z velocity of slurry/mixture along the vertical and horizontal (axial) axes.

-Z velocity of slurry/mixture along the vertical axes in Z=3, 2, 1,-1,-2 planes:

Fig. 4.13 shows the variation of particle Z velocity along a vertical axis in Z=3 cross sectional plane as shown by the blue circular section in the probe and pipe assembly in the Fig. 4.13 (a). The end points of the axis lies at y/R = -1 to y/R = 1. The curvilinear profile obtained is asymmetric with respect to the centerline of the pipe which at y/R=0.

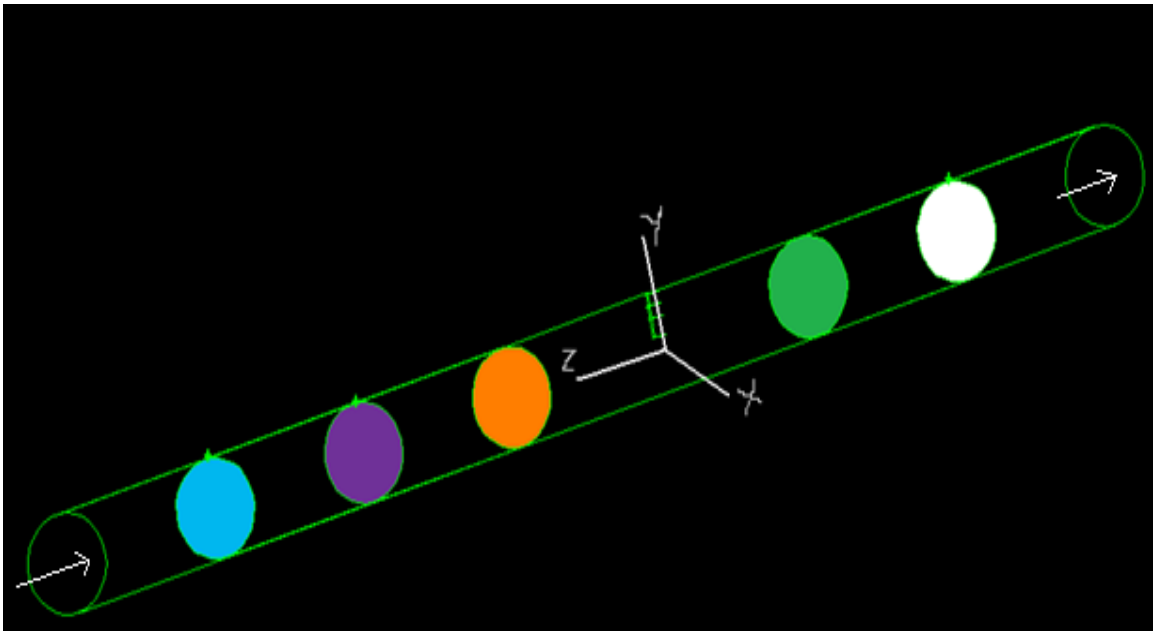

(a)

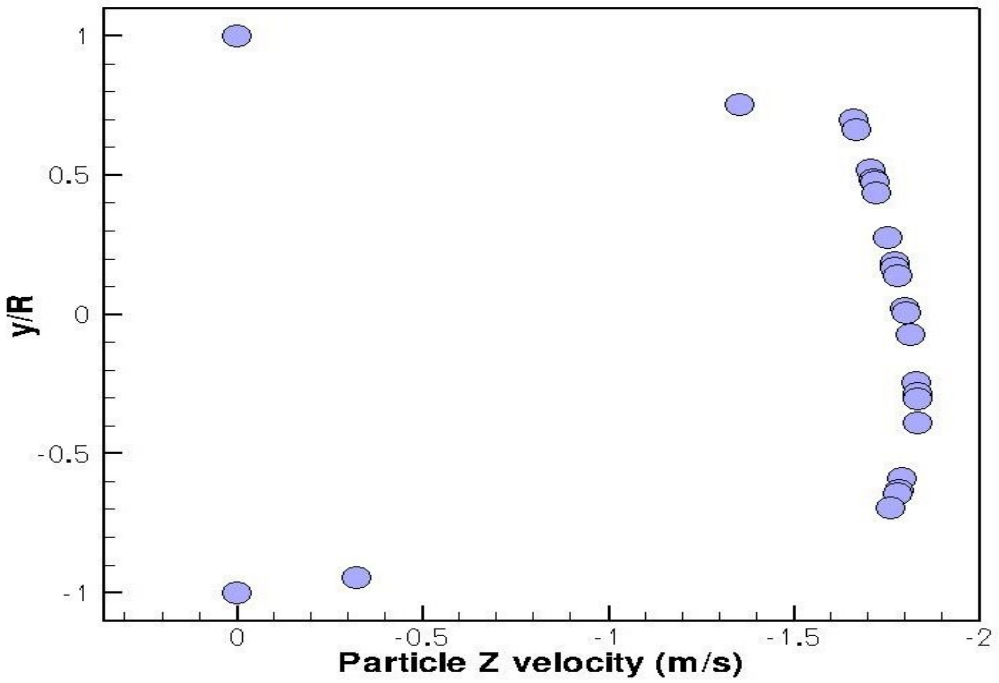

(b)

Fig. 4.13(a) Probe and pipe assembly with the planes Z=3, 2, 1,-1,-2 (left to right) (b) Particle Z velocity along a vertical line in the cross sectional plane Z=3, Z/D=29.527

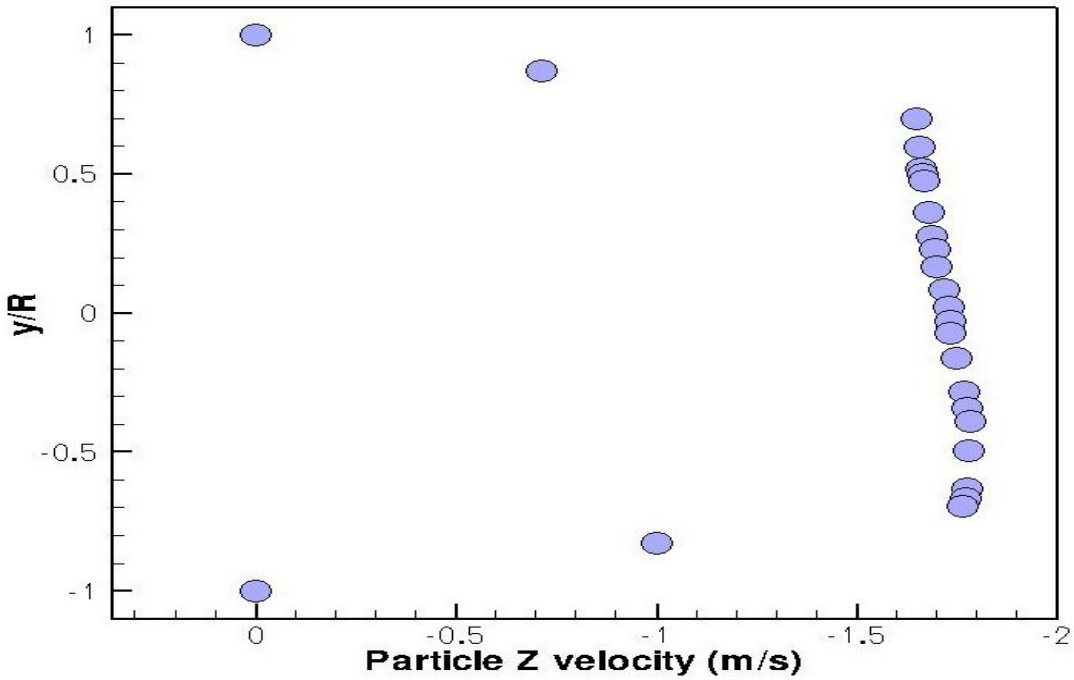

Fig. 4.14 Particle Z velocity along a vertical line in the cross sectional plane Z=2, Z/D=19.685.

Fig. 4.14 shows the variation of particle Z velocity along a vertical axis in Z=2 cross sectional plane as shown by the violet circular section in the probe and pipe assembly in the Fig. 4.13(a).The end points of the axis can be shown at y/R = -1 to y/R = 1. Again the velocity distribution is asymmetric with respect to centerline of pipe which is at point y/R=0. This may be due to the effect of gravity on particles.

Fig. 4.15 depicts the variation of particle Z velocity along a vertical axis lying in Z=1 cross sectional plane as shown by orange circular section in Fig. 4.13 (a). The axis lies along y/R = -1 to y/R = 1. The velocity distribution is less asymmetric with respect to centerline of pipe (y/R=0) compared to the distributions in the planes nearer to the inlet shown in Figures 4.14 and 4.13(b). Also notice that the velocity at centerline (y/R=0) is about -1.75 m/sec.

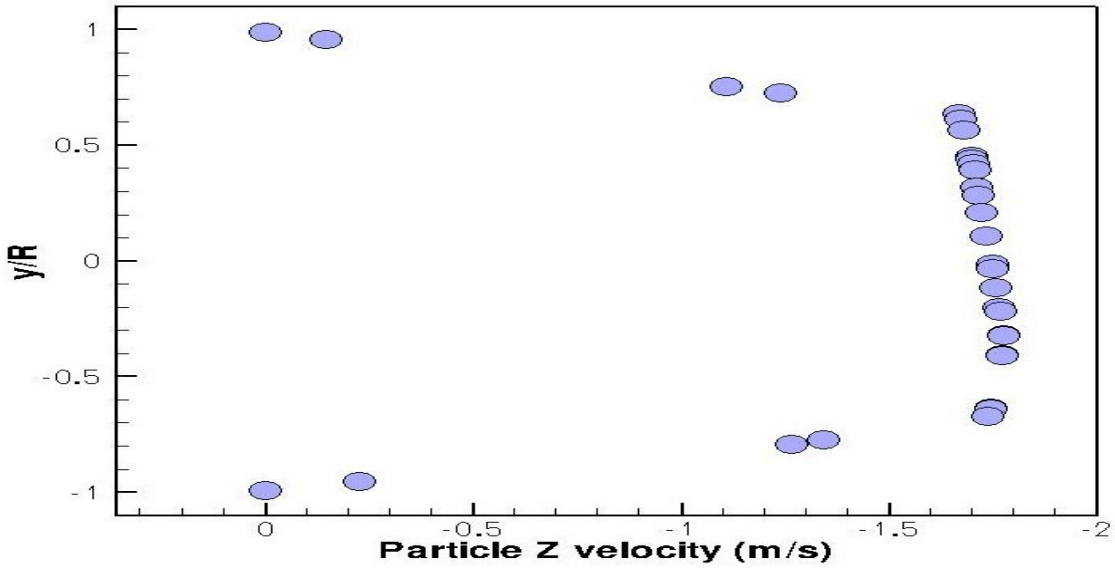

Fig. 4.15 Particle Z velocity along a vertical line in the cross sectional plane Z=1, Z/D=9.84.

Fig. 4.16 shows the variation of particle Z velocity along a vertical axis in Z= -1 cross sectional plane as shown by the green circular section in the probe and pipe assembly in Fig. 4.13(a). The end points of the axis can be shown at y/R = -1 to y/R = 1. The variation is found to be symmetric with respect to the centerline at point y/R=0. The Z velocity is almost 1.75 m/sec. Since the velocity has become constant, hence this marks the presence of fully developed characteristics in the flow. It can be seen that the above results (Fig. 4.13- 4.16) are in agreement with the findings of Lin et al (2007). Here also, the maximum velocity location is moving vertically up as we move downstream.

The variation of particle Z velocity along a vertical axis lying in Z= -2 cross sectional plane is shown by white circular section in Fig. 4.17. It is found that little asymmetricity with respect to the centerline at point y/R=0 has been introduced. This may be due to the presence of gravity. Again the Z velocity at the centerline (y/R=0) is found to be almost -1.75 m/sec which shows that now Z velocity can be considered

nearly constant along the centerline.

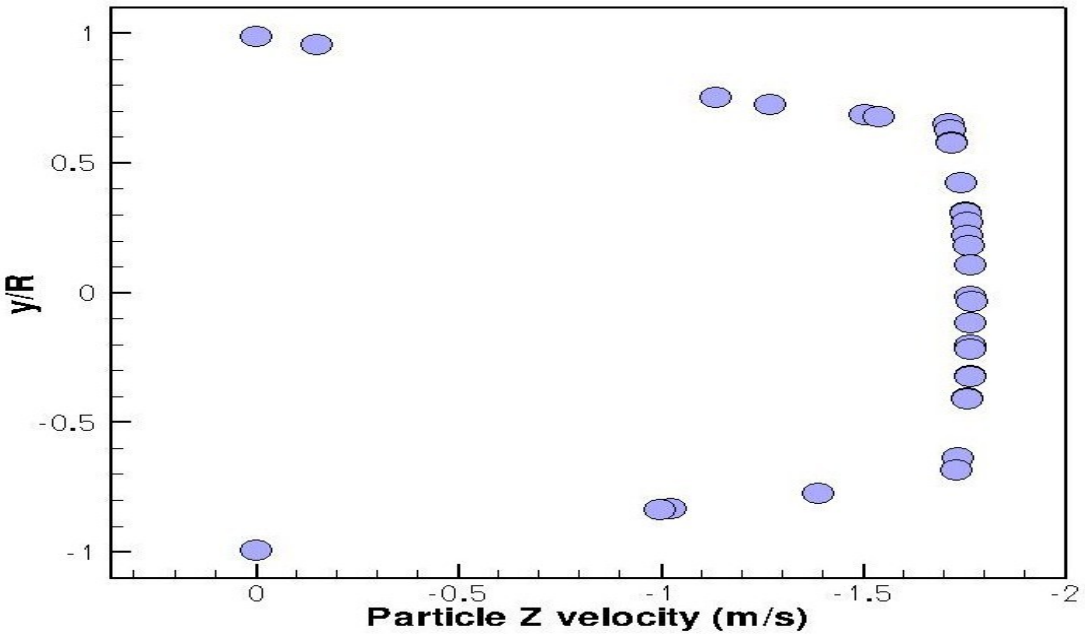

Fig. 4.16 Particle Z velocity along a vertical line in the cross sectional plane Z=-1, Z/D= -9.84.

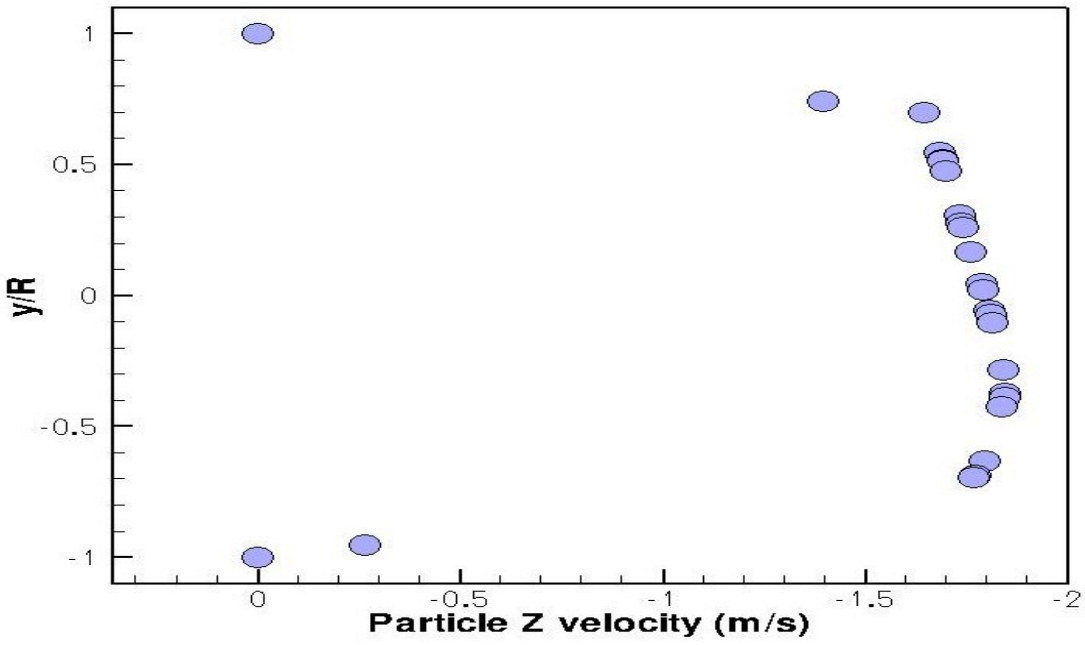

Fig. 4.17 Particle Z velocity along a vertical line in the cross sectional plane Z=-2, Z/D = -19.685

-Z velocity profiles along the axes parallel to Z direction passing through probe slot:

Z velocity profiles along the lines through the probe slot and parallel to Z direction are shown in Figs 4.18. Lines 1, 2, 3 4, and 5 are distributed from upper to lower walls of the slot as shown in Fig. (a'). Hence velocity variations along lines 1 and 5 are very close to zero as they are very near the probe walls. Velocity variations along the lines 2, 3 and 4 which are away from the walls are larger in magnitude. Among all the variations the highest velocity is found along the line 3 (Fig. (c)) which is the centerline of the probe slot and is farthest from the walls.

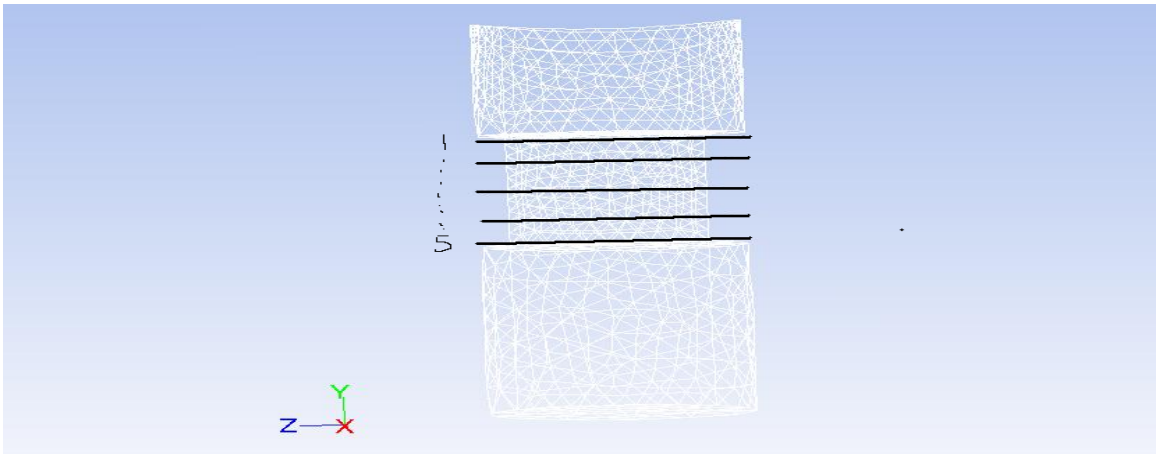

(a')

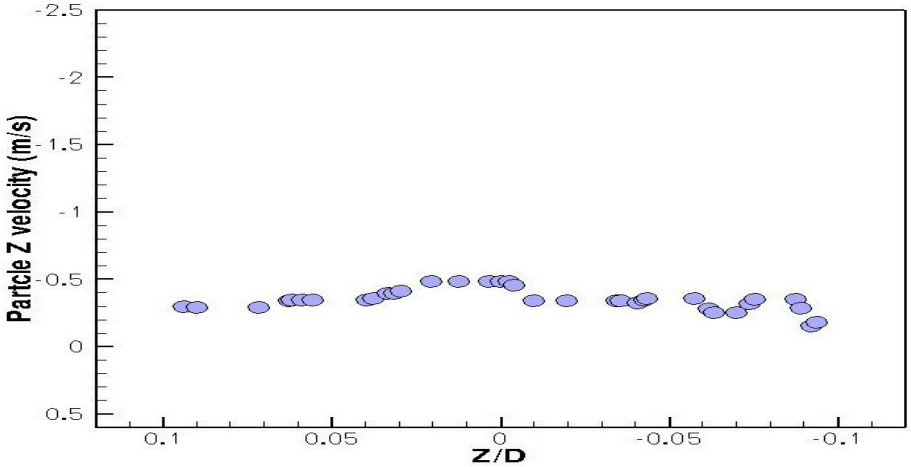

(a)

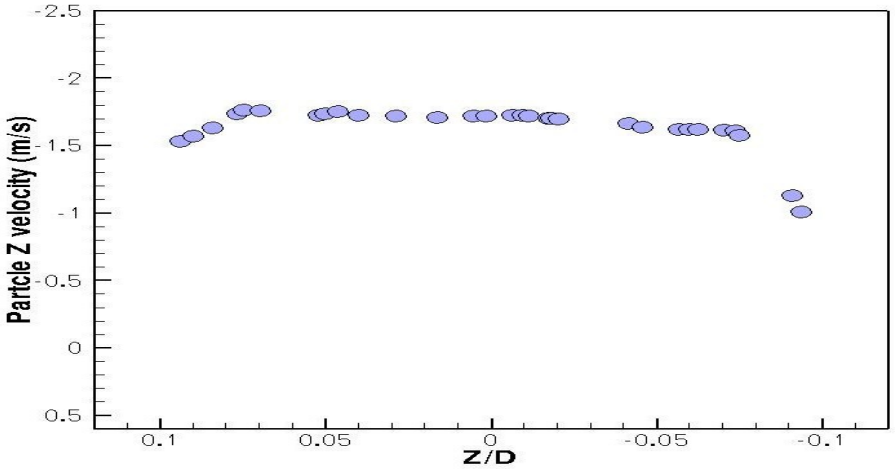

(b)

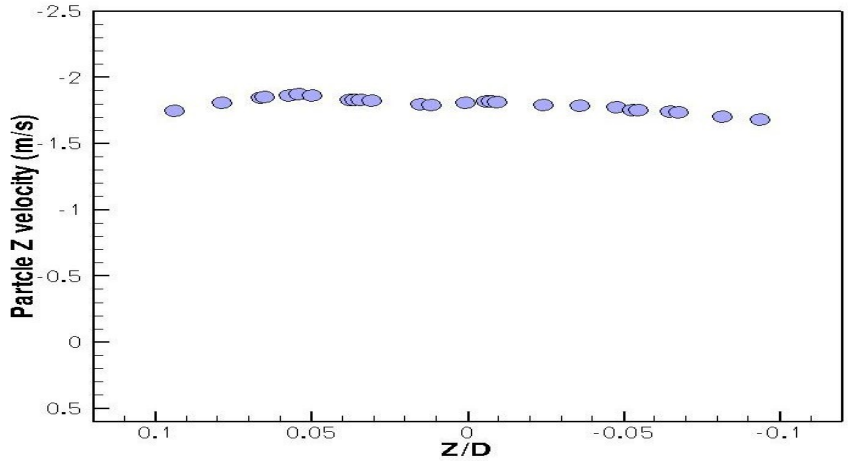

(c)

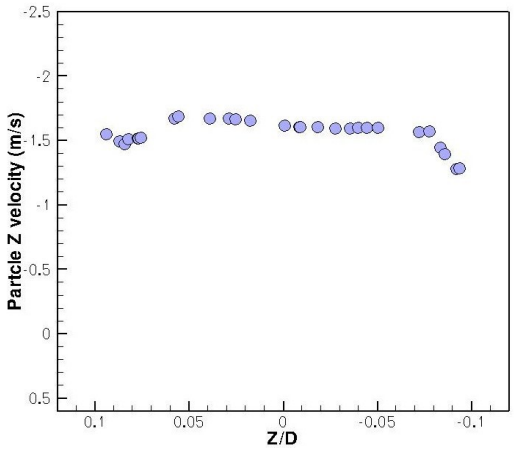

(d)

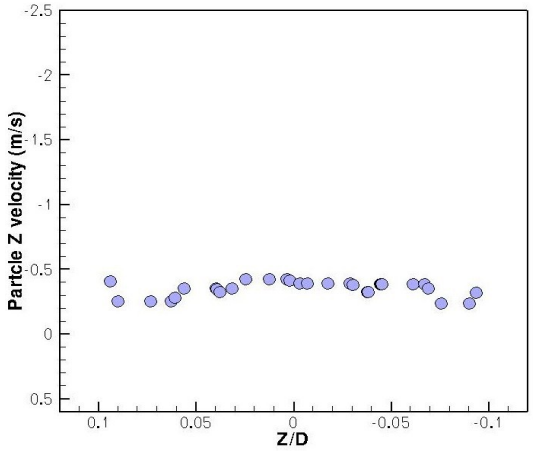

(e)

Fig. 4.18(a') Axes. Particle Z velocity profiles through probe slot along the axial slot lines (a)Slot line 1, y/R= 0.74 (b) Slot line 2, y/R= 0.69(c) Slot line 3, y/R= 0.625 (d) Slot line 4, y/R=0.56 (e) Slot line 5, y/R=0.51.

-Particle volume fraction profiles along the lines parallel to Z direction and passing through probe slot: Z velocity profiles along the lines through the probe slot and parallel to Z direction are shown in Fig. 4.19. The volume fraction variation along these lines are of very small magnitudes and can be assumed nearly constant. However, for comparative study it can be found that the variation of volume fraction along the lines which are nearer to lower wall of probe slot is smaller. This may be due to the effect of gravity on particles at higher elevation from lower wall. That is why volume fraction decreases along the axes which are away from lower wall of probe slot.

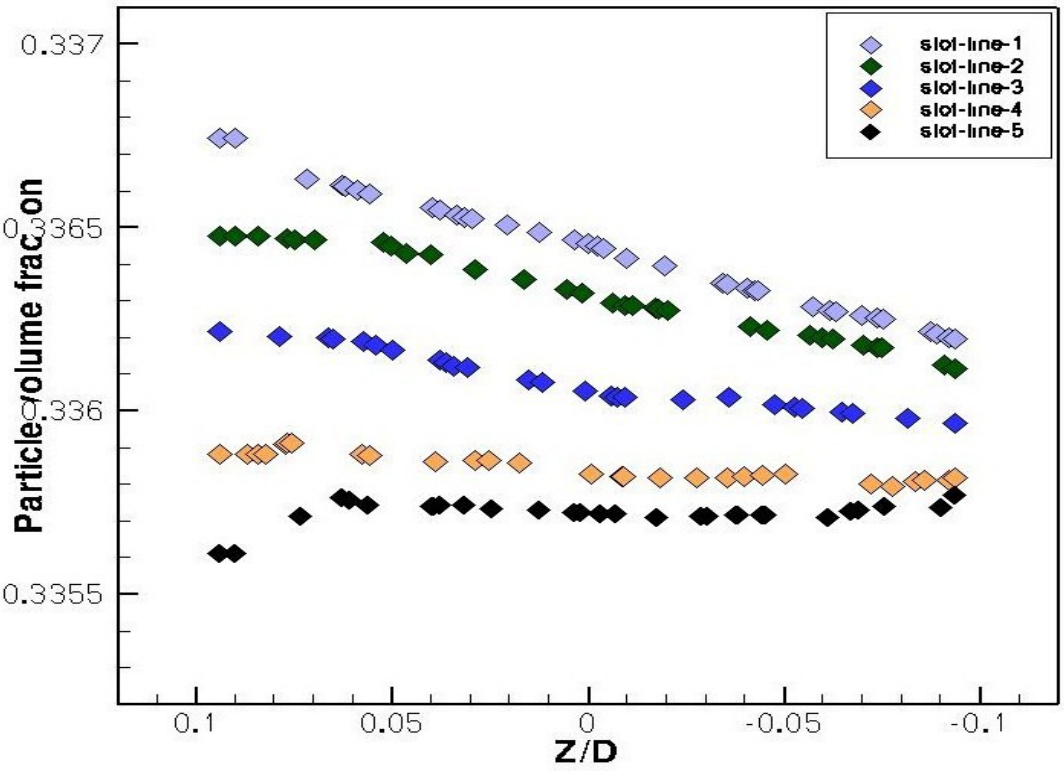

Fig. 4.19 Volume fraction profiles along the axial lines through probe slot.

4.3.4 Visualization of the flow of ADP particles with Xylene: Post processing tools available in Fluent have been utilized to visualize the flow of the slurry of ADP particles

and Xylene over the probe. Vector and contour plots concerning different quantities are presented.

-Contours of Z velocity of slurry/mixture along the plane Y=0.02:

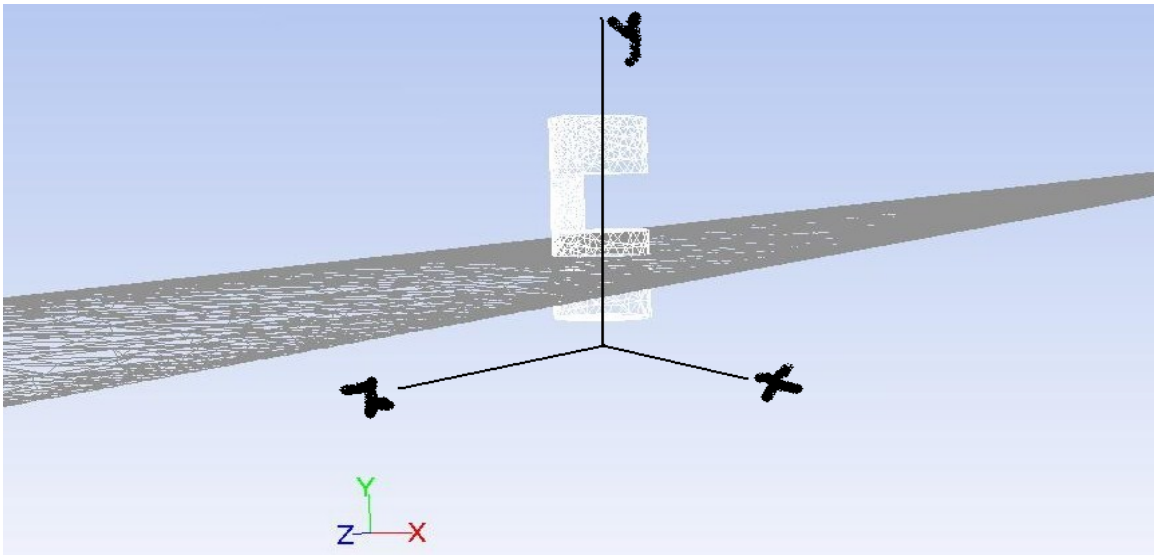

(a)

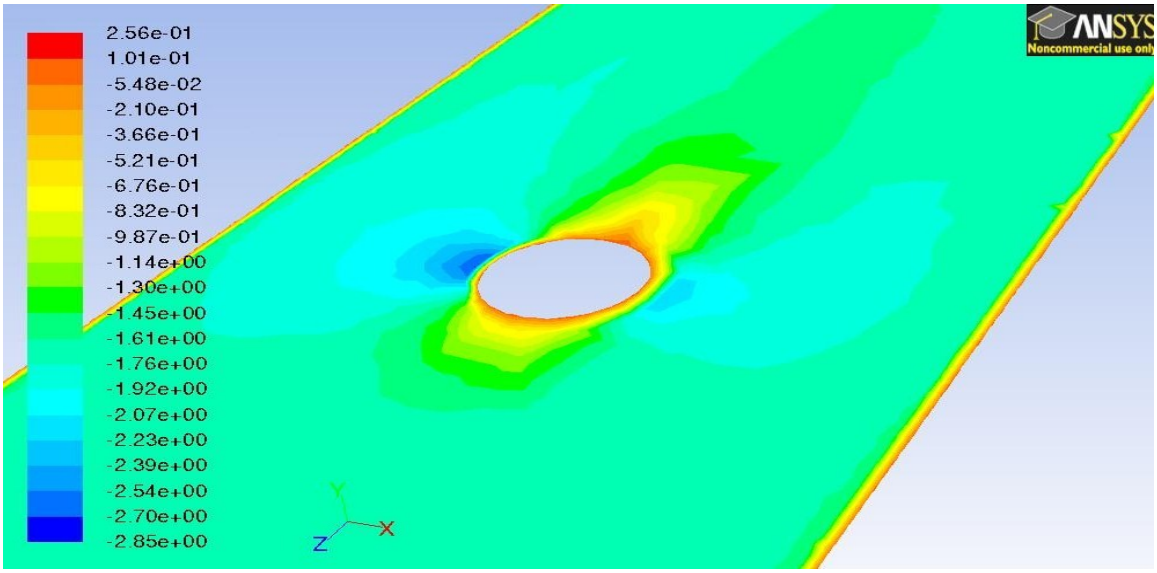

Fig. 4.20(a) Plane Y=0.02 (b) Contours of Z velocity of slurry along the plane Y=0.02, Y/R=0.39.

Fig. 4.20(b) shows the contours of Z velocity along the horizontal plane that passes through the lower solid portion of the probe as shown in Fig. 4.20(a). The contours of

velocity show that the velocity is maximum on the sides of the probe while it is minimum on the front and the back of the probe solid cylindrical portion.

- Contours of Z velocity of slurry/mixture along the plane Y=0.03:

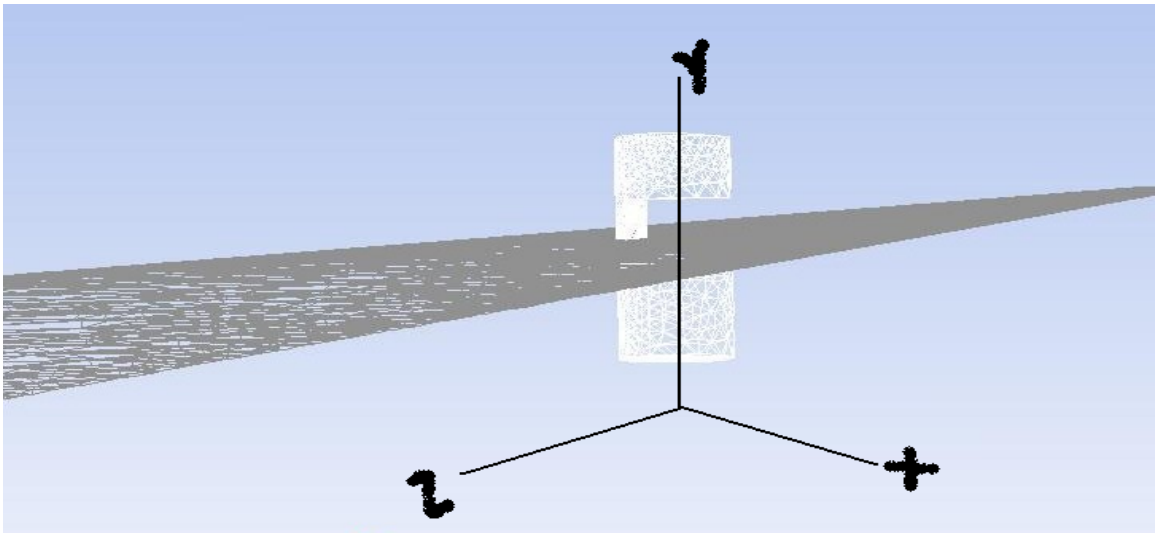

(a)

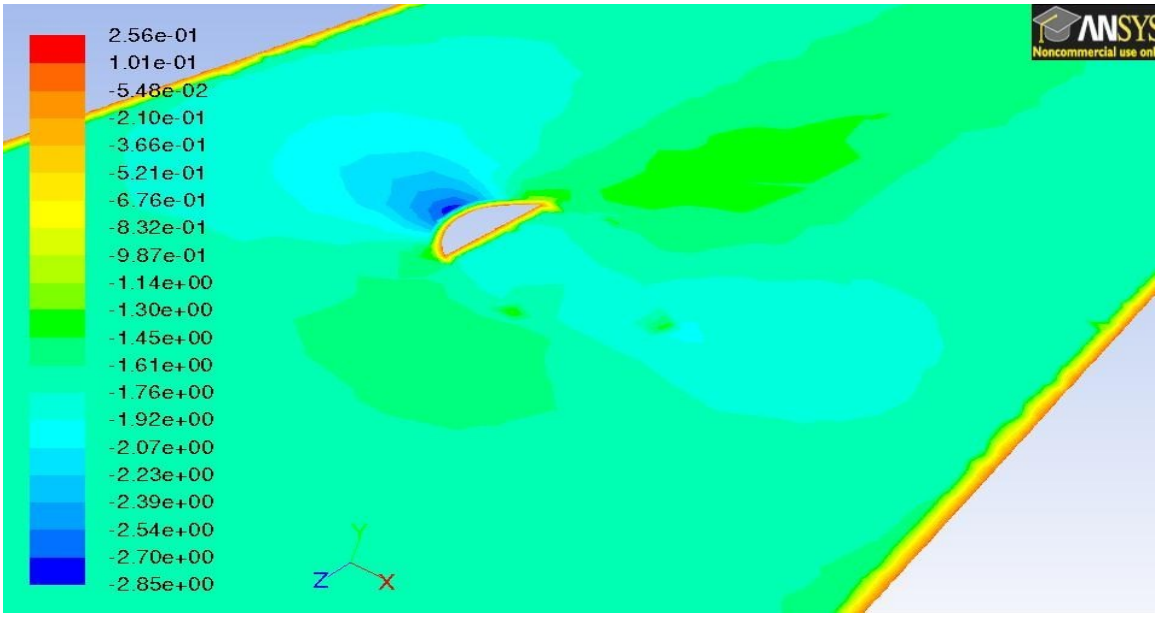

Fig. 4.21(a) Plane Y=0.03(b) Contours of Z velocity of slurry along the plane Y=0.03, Y/R=0.59

Figure 4.21(b) shows the contours of Z velocity along the horizontal plane that passes through solid portion of the probe at the solid semi-circular part adjacent to slot of the

probe as shown in Fig. 4.21(a). Again the Z velocity is maximum on the sides of the probe and minimum on the front and the back of the probe solid portion as shown.

-Contours of Z velocity of slurry/mixture along the plane X=0:

Fig. 4.22 shows the contours of Z velocity of slurry along the vertical plane X=0 with far view. The velocity starts to rise again in vertical direction after it crosses the probe. This is shown with the dark blue flow contours.

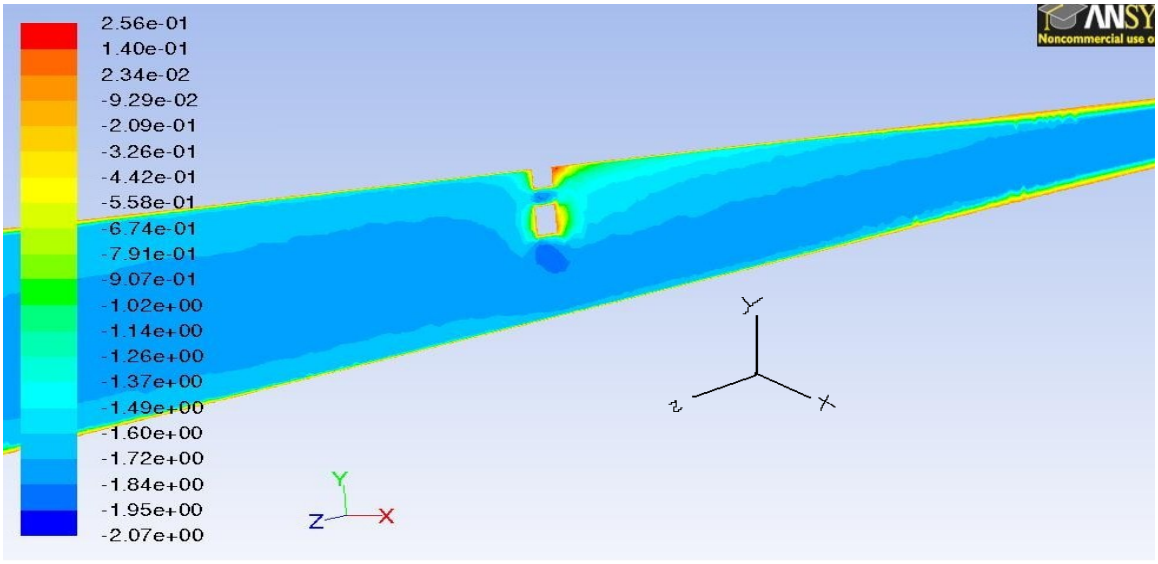

Fig. 4.22 Contours of velocity Z velocity of slurry along the plane X=0 (X/R=0) which the passes right in the middle through the probe section as well as the probe slot.

A closer view of contours along the vertical plane X=0 is shown in Fig. 4.23. The contours show the flow behavior such that after crossing the probe the velocity rises vertically and then falls further downstream as it approaches the outlet of the pipe. The dark blue velocity contours show this behavior.

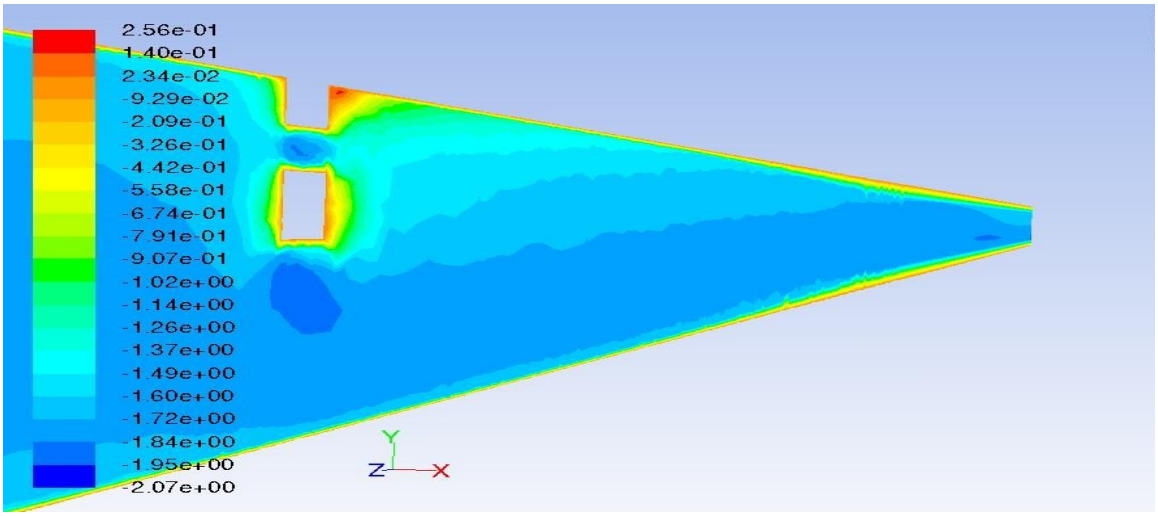

Fig. 4.23 Contours of Z velocity of slurry along the plane X=0 (closer view)

Fig. 4.24 depicts the Z velocity contours in the probe slot vicinity. The contours show that the velocity near the walls of the probe and that of the pipe is zero. The variation of contour colors in the probe vicinity defines the profiles of variation of Z velocity in the probe region. The contours clearly show that there is an abrupt increase in Z velocity when the flow is about to enter the probe slot region.

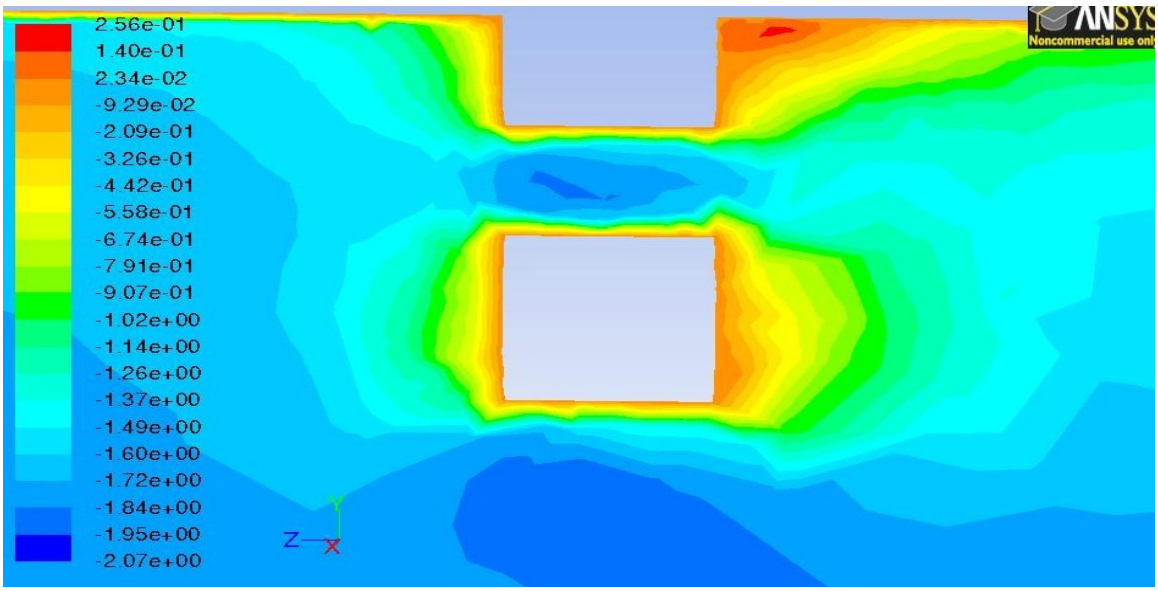

Fig. 4.24 Contours of velocity Z velocity of slurry along the plane X=0, closer look of probe region.

-Contours of Z velocity of slurry/mixture along the plane X=0 passing through the probe slot: Velocity contours are considered for a plane through the probe slot shown in Fig. 4.26.The plane has been separately shown in Fig. 4.25. The plane passes through the slot of the probe and is shown in grey with the probe shown in green.

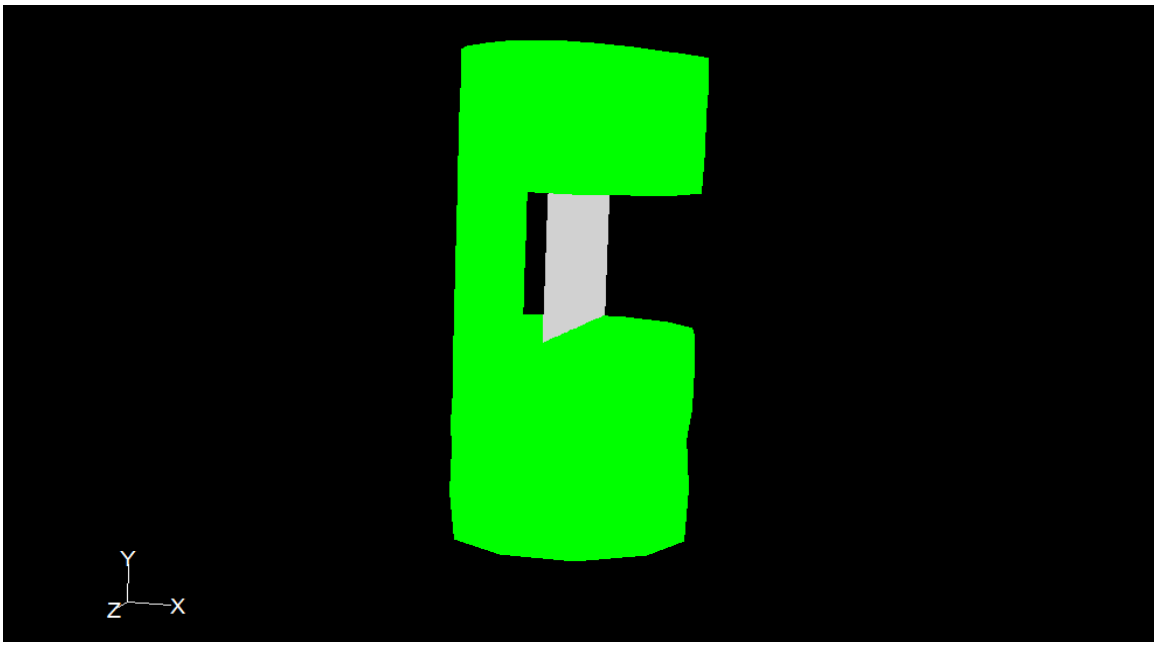

Fig. 4.25 Vertical plane passing through the probe slot shown in grey with the probe shown in green.

The velocity near the wall is zero which is shown with red. Moving away from the wall the velocity increases and is maximum in the central portion of the probe slot. The central region of the probe slot having higher magnitudes of velocity decreases as the flow reaches the end of the probe slot. This can be shown clearly with the region in the dotted box on the right which is less in height than the one on the left. This may be due to the growth of the boundary layer on the upper and lower walls of the probe slot. It can be seen in the portion marked inside the box in Fig. 4.27. As the slot is open from one side hence there will a three dimensional flow. This may result in the fall of Z velocity magnitude.

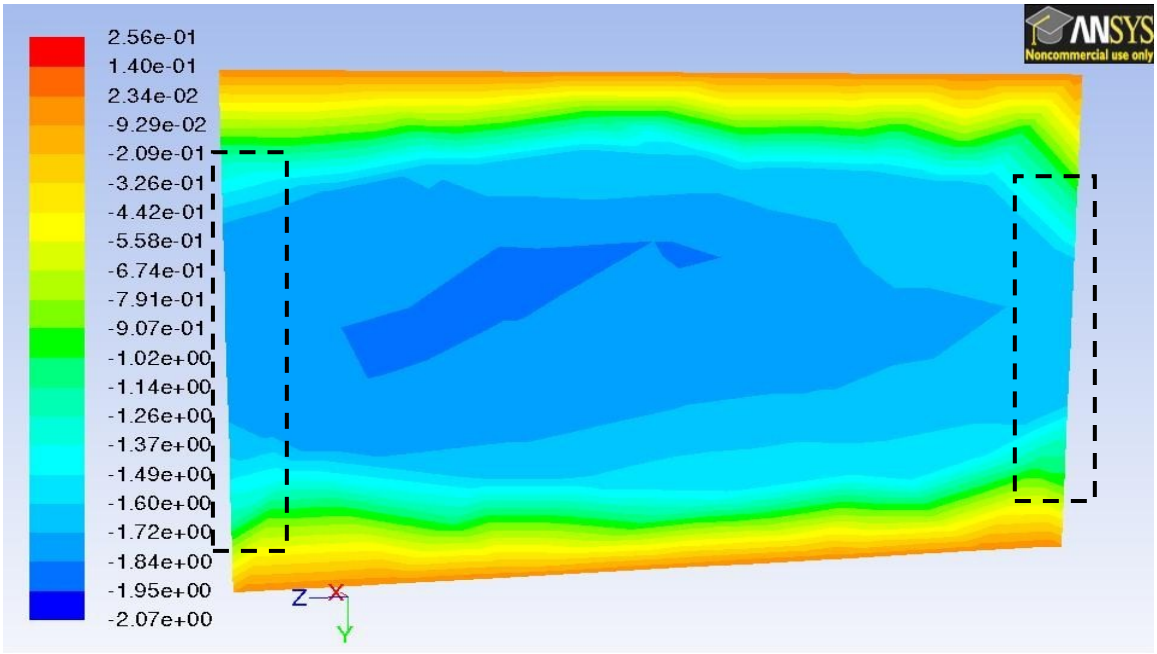

Fig. 4.26 Contours of velocity magnitude of slurry/mixture along the plane X=0, X/R=0 which passes right in the middle of the probe slot.

Contours of Z velocity of slurry/mixture along the plane Z=0 plane passing through the probe slot: Fig. 4.27 shows the variation in Z velocity of slurry with help of contours along Z=0 plane (Z/D=0). The contours depict the region of maximum velocity away from the wall region of the pipe and the probe.

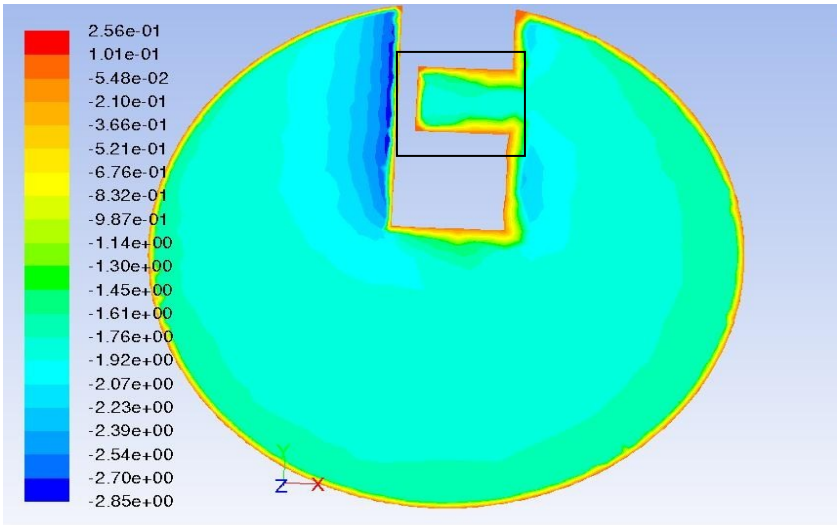

Fig. 4.27 Contours of Z velocity of slurry/mixture along the plane Z=0, where Z/D=0

-Contours of particle volume fraction in the plane X=0:

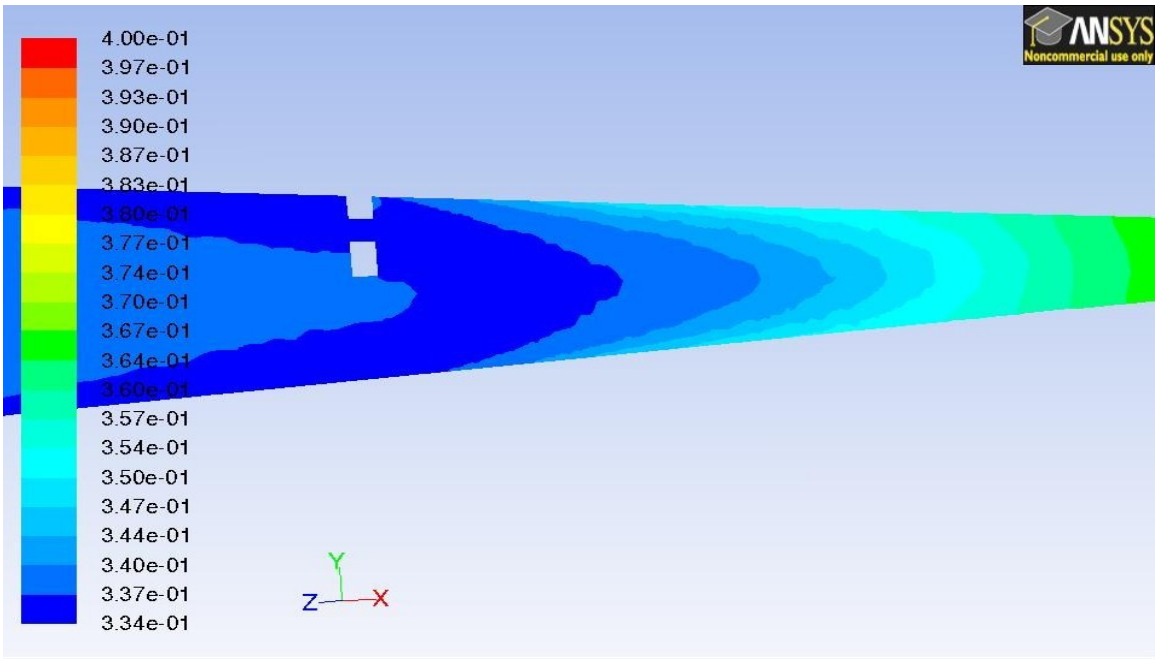

Fig. 4.28 Contours of velocity colored by particle volume fraction in the plane X=0, where X/R=0.

Fig. 4.28 shows the distribution of particle volume fraction along the vertical plane X=0 which passes through the probe region. The distribution of volume fraction is curvilinear in nature. Later on as the flow moves away from the probe region the profiles of volume fraction variation start losing the curvature and tend to become vertical and tend to become normal to the centerline of the pipe.

4.3.5 Comparison of Volume fraction profiles obtained for two different particle sizes: This portion presents the results obtained by using different particle size. Particles of ADP with diameters 100 and 400 micrometers were considered. Volume fraction profiles along the axes through the probe slot as discussed previously are plotted.

- Comparison of volume fraction along Y axis lying in the probe slot:

The volume fraction magnitude for 400 micron particles is slightly less than that for 100 micron particles along the vertical axis between the circular sections of the probe slot. This can be easily inferred from Fig. 4.29 which is owing to more apparent weight of 400 micron particles.

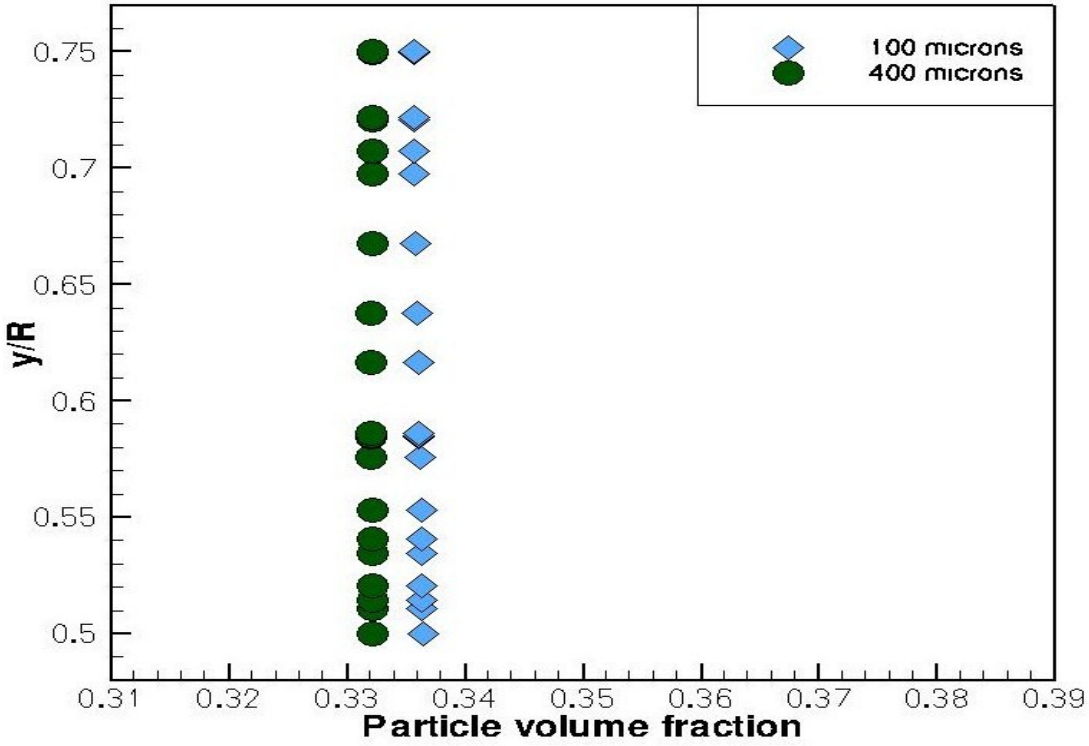

Fig. 4.29 Comparison of volume fraction along Y axis lying in the probe slot.

Comparison of volume fraction along line parallel to Y axis lying in the probe slot but to the left of it: Fig. 4.30 show the volume fraction magnitude along line parallel to Y axis lying in the probe slot but to the left of it for 100 and 400 micron particles. Again,

the 400 micron particles exhibit lower volume fraction than 100 micron particles. This is owing to more apparent weight of 400 micron particles.

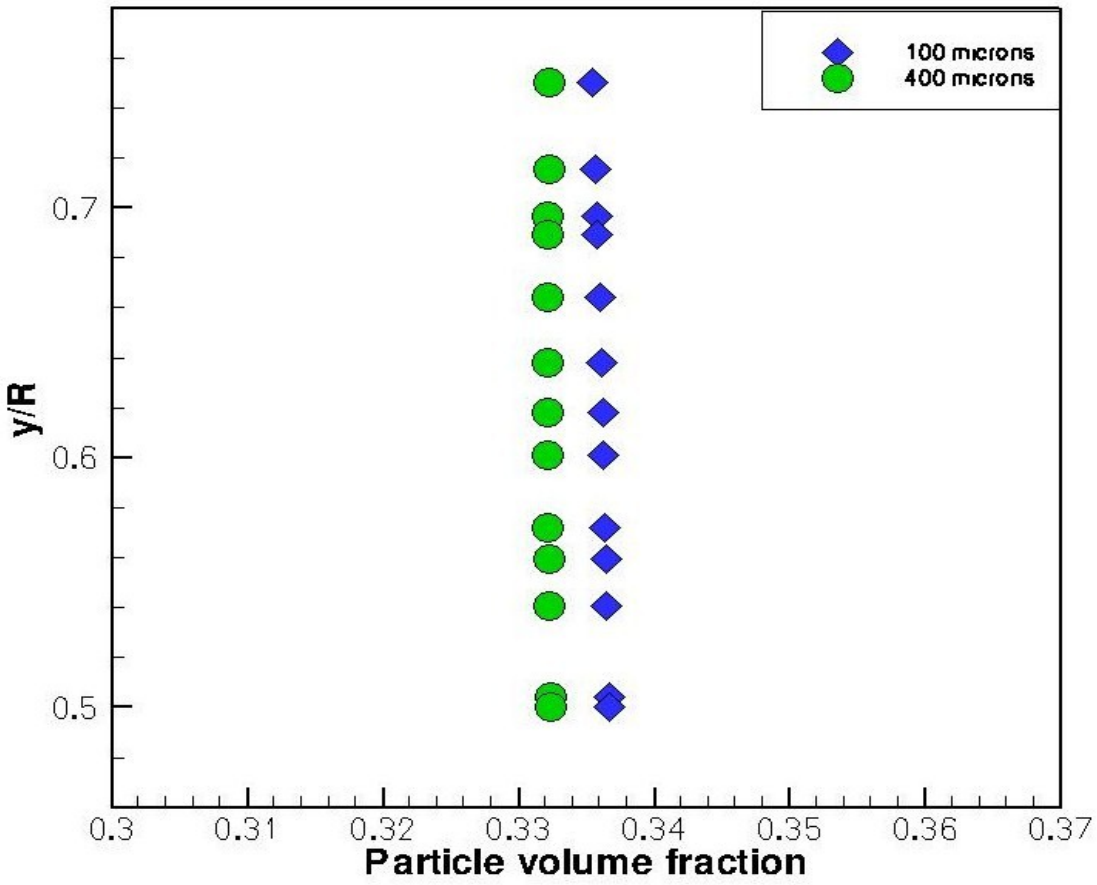

Fig. 4.30 Comparison of volume fraction along line parallel to Y axis lying in the probe slot but to the left of it.

Comparison of volume fraction along line parallel to Y axis lying in the probe slot but to the right of it: Fig. 4. 31 show the volume fraction magnitude along line parallel to Y axis lying in the probe slot but to the right of it for 100 and 400 micron particles. The volume fraction for both the particles is constant along the considered axis. This time also, the 400 micron particles have lower volume fraction than 100 micron particles along the considered axis. This is due to to more apparent weight of 400 micron particles as apparent weight of particles is directly proportional to their diameter.

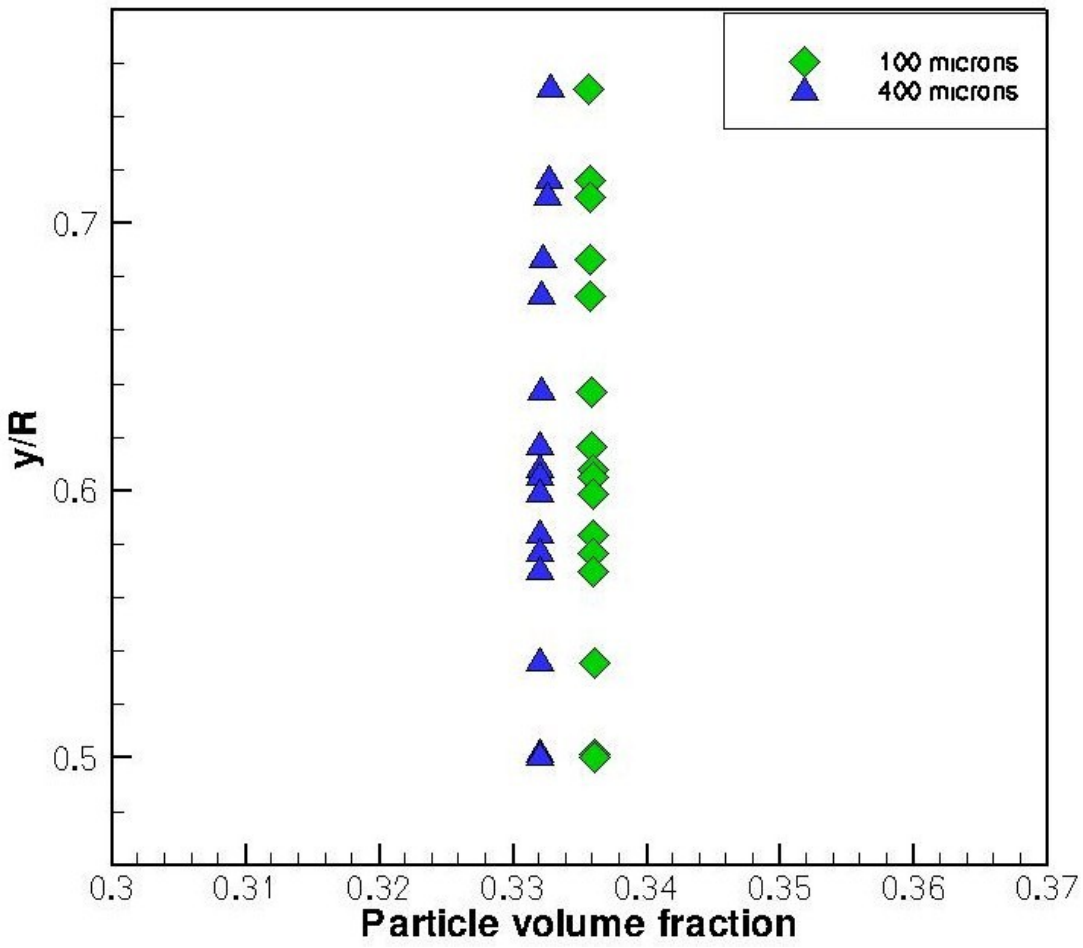

Fig. 4.31 Comparison of volume fraction along line parallel to Y axis lying in the probe slot but to the right of it.

- Particle volume fraction along axes parallel to Y direction but are behind and in front of it: Fig. 4.32(b) and (c) shows the comparison of volume fraction variation of 100 and 400 micron particles along the axis shown in red and green respectively in Fig. 4.32 (a). In this case also, the physics of more apparent weight of 400 micron particles than 100 micron particles holds good. Hence the volume fraction magnitude for 100 micron particles is more than the 400 micron particles ones. Here also the magnitude of volume fraction can be considered constant along the axes shown in Figs 4.32.

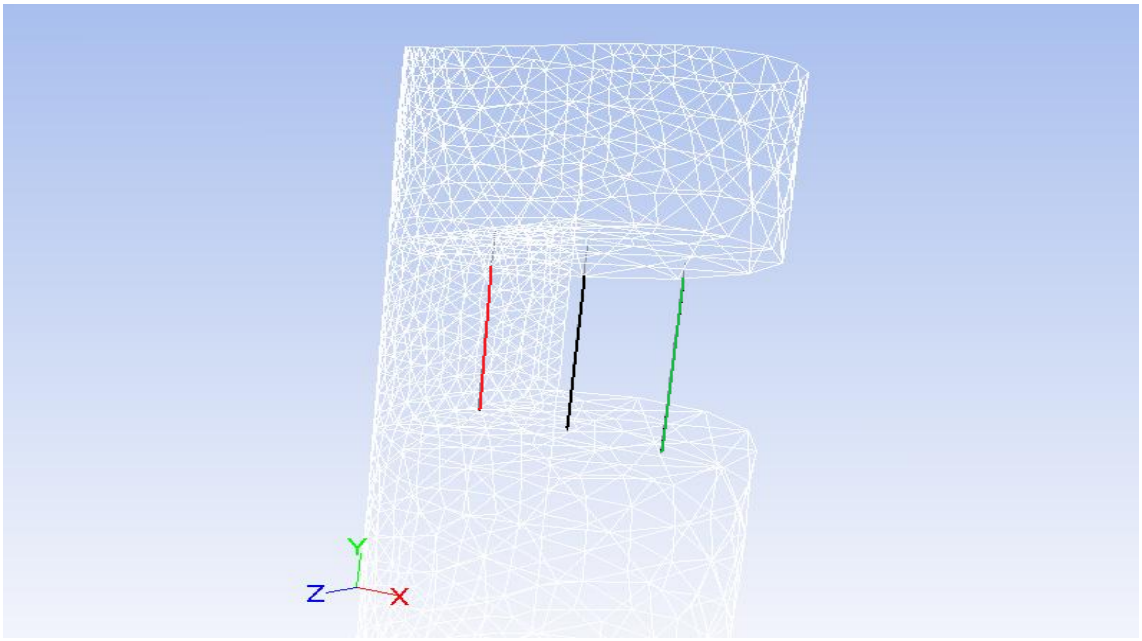

(a)

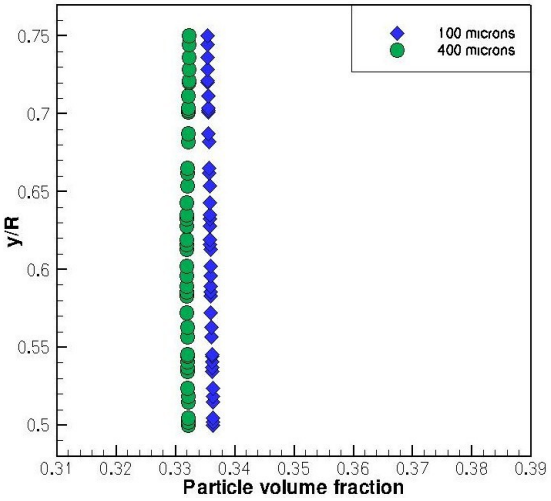

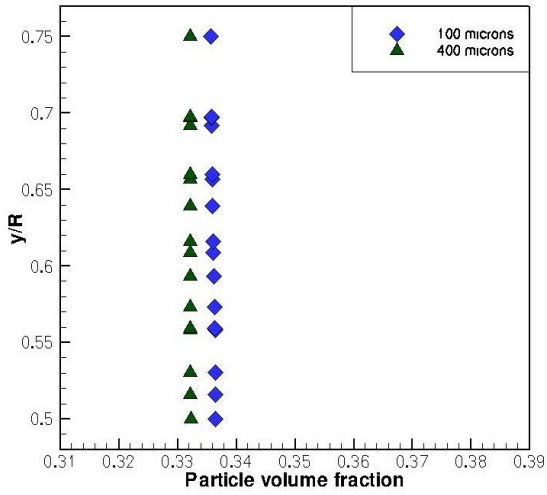

(b) **(c)**

Fig. 4.32 (a) Axes along the probe slot (b) Comparison of volume fraction along line parallel to Y axis but behind it (shown by Red line in Fig. (a)). (c) Comparison of volume fraction along line parallel to Y axis but in front of it (shown by green line in Fig. (a)).

--Comparison of particle volume fraction profiles along the lines parallel to Z direction and passing through probe slot: Fig. 4.33(a) shows the axes A, B and C

along which the volume fraction profiles for 100 micron and 400 micron particles are compared. The comparison is shown in Fig. 4.33 (b), (c) and (d). In each of the three cases along the slot of the probe it can be observed that volume fraction for 100 micron particles are more than the volume fraction of 400 micron particles. This is again due to the larger diameter of 400 micron particles which results in more apparent weight as apparent weight = volume of particle x (density of particles-density of liquid) x gravitational acceleration. In the current cases, the only thing that is different for the two particles is the diameter on which the volume depends. Hence the particles with lesser diameter have greater volume fraction (Provided the same initial volume fraction).

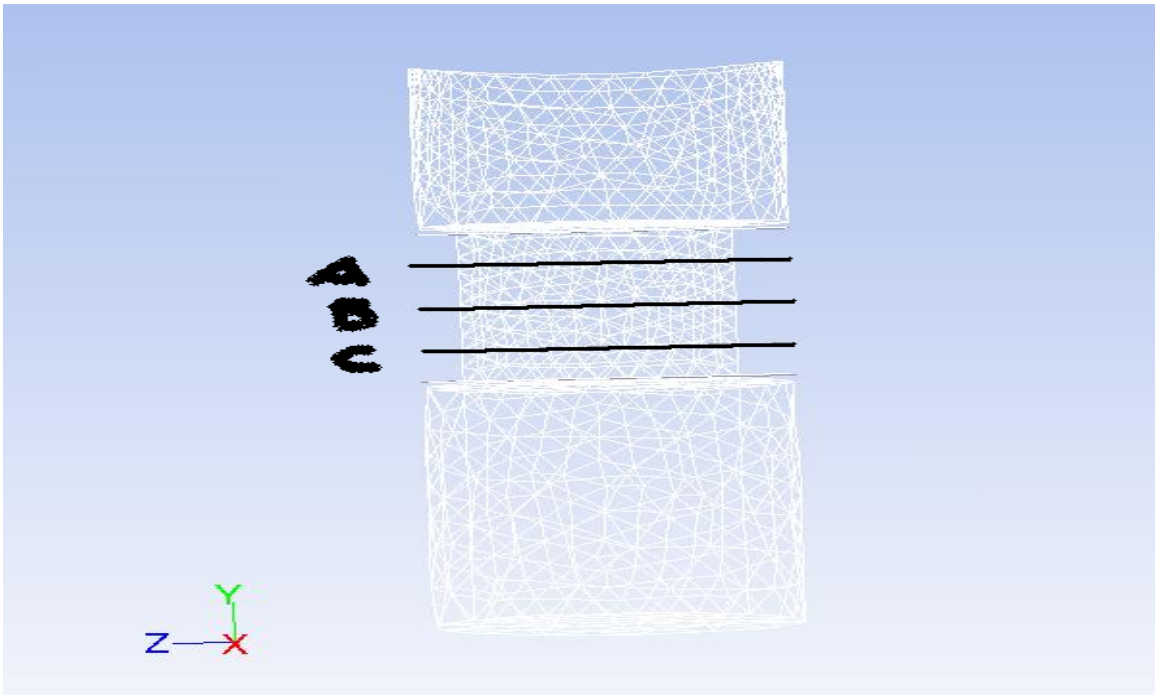

(a)

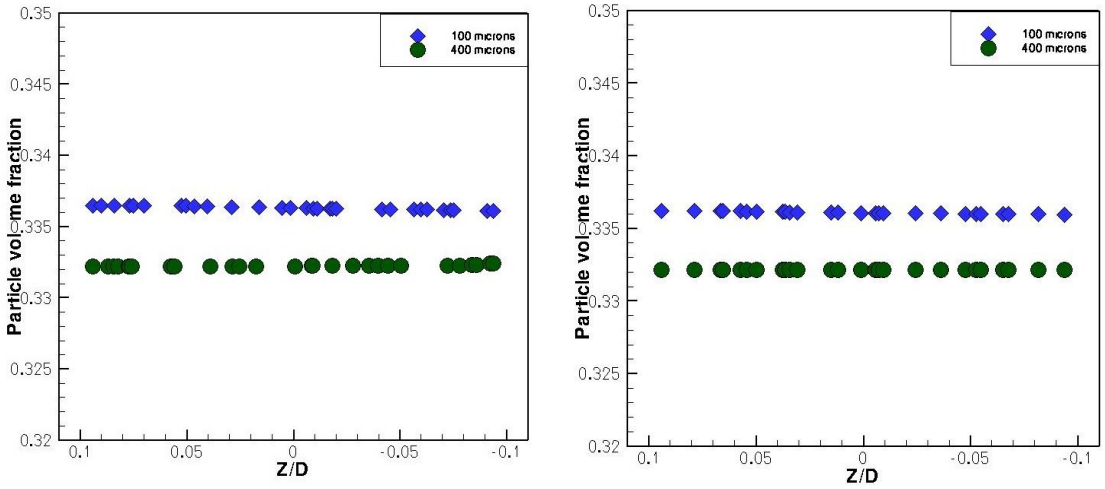

(b) **(c)**

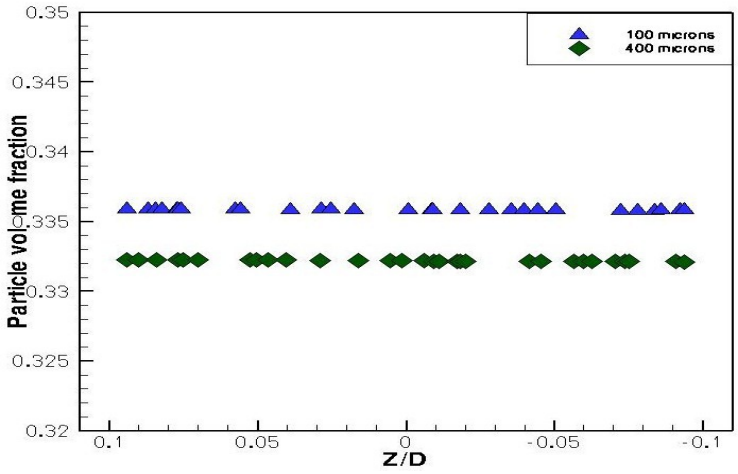

(d)

Fig. 4.33 (a) Axes. Comparison of volume fraction for different particle size along (b) Slot line A, y/R= 0.69 (c) Slot line B, y/R= 0.625 (d) Slot line C, y/R=0.56.

It can be noticed that the results obtained for two different particle sizes are in good agreement with the findings of Hossain et al. (2003). They have discussed that the larger particle size will impart more settling tendency. As observed here, the particles with higher diameter shows lower volume fraction magnitudes along different axes in the probe sensing region (slot).

4.4 Comparison of the velocity profiles obtained for ADP and Xylene slurry to that of calcium carbonate and water slurry: It has been discussed previously that in a different case calcium carbonate particles were made to flow through water as the liquid medium. The axial (z) velocity profiles have been obtained for the slurry mixture flowing through the pipe of length 7.112m (L/D=70). A comparison has been made for the velocity profiles along different axes.

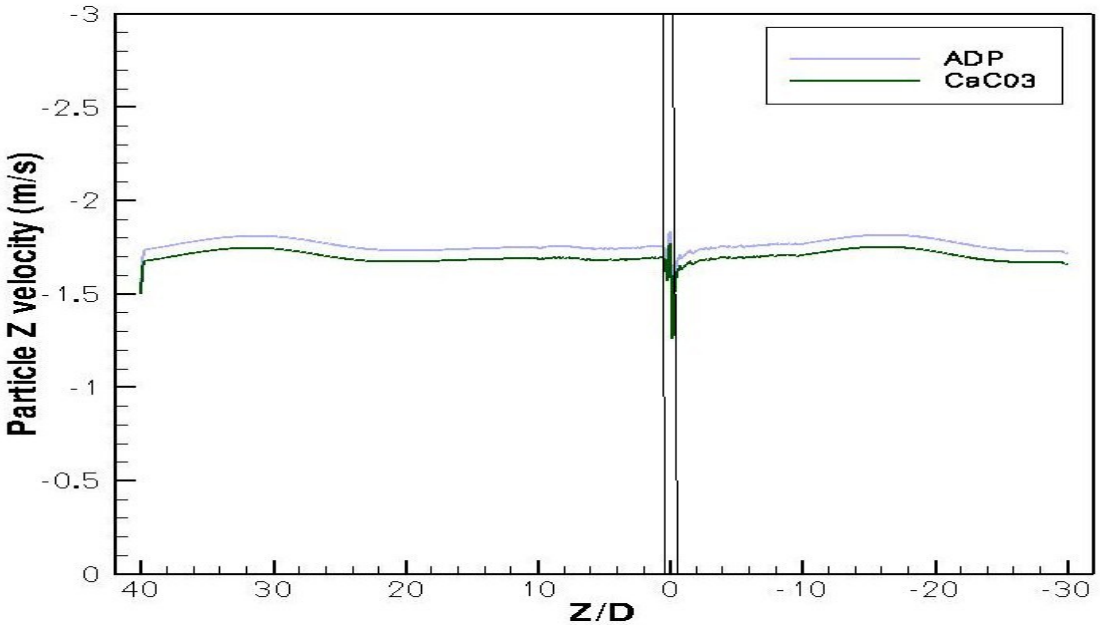

Fig. 4.34 Comparison of ADP and CaC03 particles Z velocity profile along centerline of the pipe. (Probe vicinity shown between parallel lines with 0.09 < Z/D < 0.09)

The Z velocity along the centerline of the pipe for slurry of ADP particles with Xylene is compared with that of the slurry of calcium carbonate particles in water as shown in Fig. 4.34. The Z velocity profile for ADP particles is shown above the calcium carbonate particle profile. This shows that ADP particles are flowing with higher velocity along the centerline than the calcium carbonate particles even though all the conditions are same. These conditions include the particle size, inlet particle volume fraction, inlet

particle and liquid velocities. This behavior can be explained again by means of the buoyancy force applicable on ADP and CaC03 particles. It is a fact that buoyancy force results in the decrease in the actual weight of a body immersed in a liquid. Buoyancy force acting on the body, when subtracted from actual weight of the body results in apparent weight of the immersed body. Thus,

Apparent immersed weight = Actual weight-Buoyancy force

The actual weight and buoyancy force in this case are directly dependent on the densities of particle and liquid (in which particle is immersed). The apparent weight will be directly proportional to the difference in the densities of particle and the liquid carrying it. In case of ADP and Xylene, difference of densities come out to be 610 kg/m^3(1480-870) while in CaC03 and water case it is 1800 kg/m^3 (2800-1000). Thus difference in densities is more for the case of CaC03 and water. Therefore they will have more apparent weight. Due to this their Z velocity component will be suppressed. Hence they have lower Z velocity.

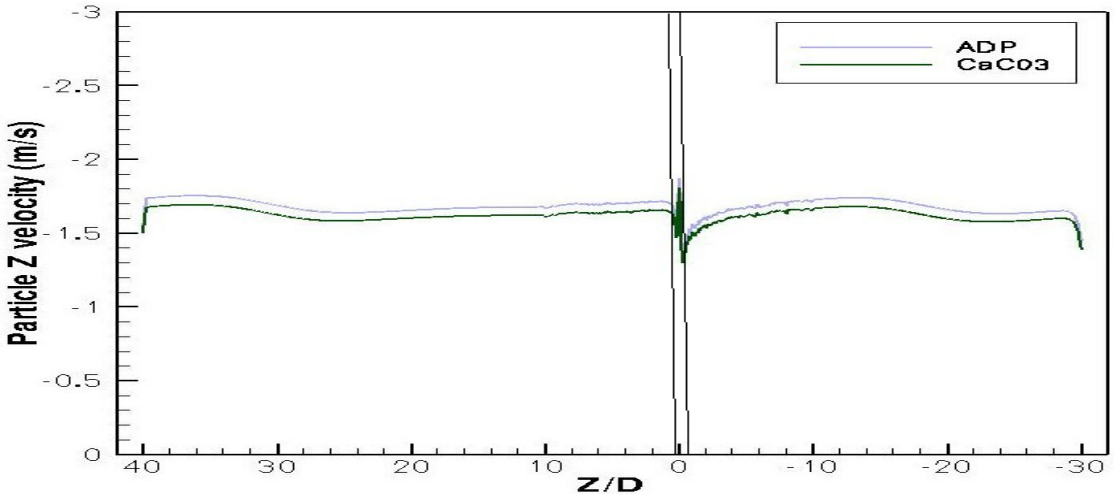

Fig. 4.35 Comparison of ADP and CaC03 particles Z velocity profile along the axis parallel to the centerline and passing through the probe slot. (Probe vicinity shown between parallel lines with 0.09 < Z/D < 0.09)

In Fig. 4.35 the comparison of Z velocity profiles along an axis parallel to the centerline and passing through the probe slot is shown. In this case also, a similar observation can be seen and hence the same reason holds good here also. Calcium carbonate particles being heavier will have lower Z velocity than ADP particles which are lighter.

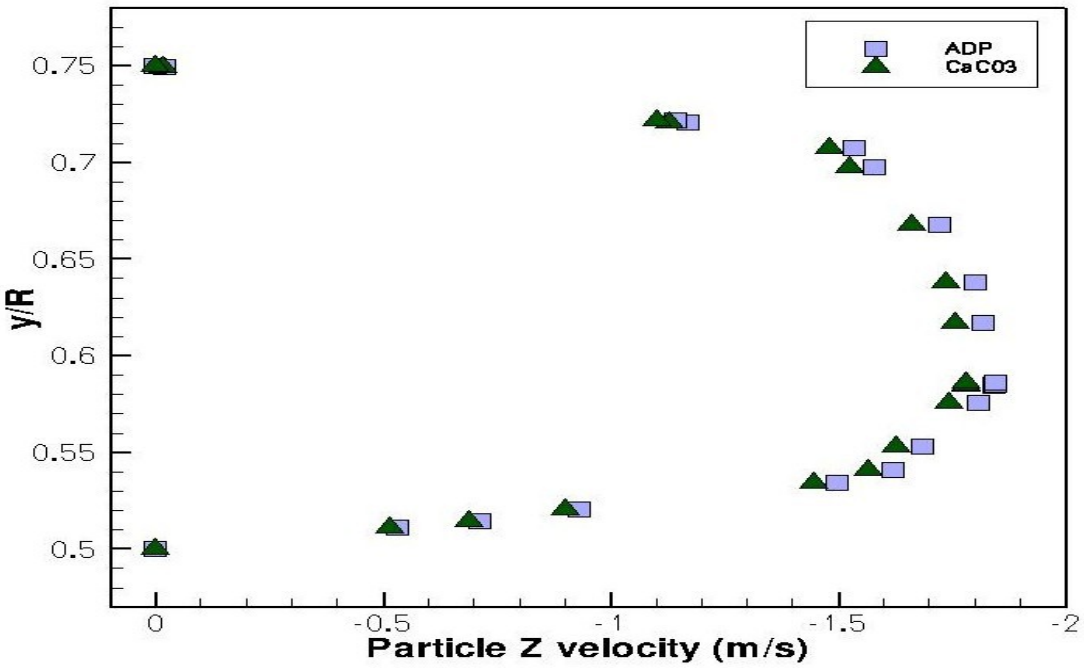

Fig. 4.36 Comparison of Z velocity along the line through the center of the probe slot circular section in Y direction. (Probe slot lying between 0.5<y/R<0.75

In Fig. 4.36, the Z velocity along the line through the center of the probe slot circular section in Y direction has been shown for ADP and calcium carbonate particles. As discussed above similar trend has been observed in this case also with the same reasoning.

The results of velocity profiles obtained by Ling et al. (2001) shows the effects of density difference as they have used two different types of particles with different

densities. Similar observations are observed for the above velocity comparisons owing to density difference. Thus the results show agreement with the findings in the literature.

CHAPTER V

CONCLUSIONS AND RECOMMENDATIONS

5.1 Summary:

In the current research, a chemical slurry consisting of liquid Xylene flowing with ADP particles in a pipe has been considered primarily. Some cases of comparison of slurries of ADP-Xylene and CaC03-water are also considered. The length to diameter ratio of the pipe is 70. A geometric model of an FTIR/NIR probe is mounted asymmetrically on the wall of the pipe. Fluent (Ansys) has been employed as the simulation software to predict the end results of the flow. The K-ε Turbulence model and mixture multiphase model are employed for analysis. Particle sizes of 100 and 400 microns are considered and a comparative study is done based on variation in particle size.

5.2 Conclusions:

The following conclusions are drawn on the basis of results shown in the last chapter.

1. For the plain pipe flow in the pipe with L/D=70, the profiles of axial velocity exhibit fully developed flow characteristics at about Z/D= 45.
2. The axial velocity profile for the slurry of ADP and Xylene is computed for pipe with NO probe. It has been found that the centerline axial velocity becomes constant at

about Z/D=35 and indicating fully developed flow takes place. Since fully developed characteristics are achieved at Z/D= 35, hence with a view to mount the probe/sensor in fully developed region, it is a good idea to mount the probe at a location of Z/D= 40.

3. The axial velocity profiles of ADP particles in the pipe with probe mounted at Z/D= 40 (from the entrance) are plotted along the centerline, an axis parallel to the centerline and passing through the probe sensing region (slot) and the axis parallel to centerline and passing through the probe solid part.

   a) Axial velocity profiles are found similar to the profiles for the plain pipe slurry flow in the entrance region of the pipe.

   b) Fluctuations in the axial velocity are observed in the probe vicinity which require further study.

4. Particle axial velocity and volume fraction along the axes through the probe sensing region (slot) in vertical Y direction and parallel to Y direction are analyzed.

   a) Particle axial velocity magnitudes observed along the axis passing through the probe slot (along y axis) are slightly higher than those for the axes from top to bottom across the gap to the left and right of the probe Y axis in the probe slot.

   b) Volume fraction along these axes is very nearly constant.

5. Volume fractions are compared along the axes in the front and behind the Y axis passing through the probe sensing region (slot). The axis behind is near the probe slot vertical wall. Volume fraction is found to be nearly constant along the considered axes.

6. Particle axial velocity profiles along the vertical axes at different axial locations along the length of the pipe have been computed for ADP-Xylene slurry. The results obtained show that the location of maximum velocity point rises as we move further downstream. The profiles are asymmetric. These results show agreement with the results in literature.

7. Volume fraction profiles along the axes parallel to Z direction (axial direction) and lying in the sensing region (slot) of the probe are computed for ADP and Xylene slurry. The volume fraction variation is very small and volume fraction along the axial direction of probe sensing region (slot) may be considered constant.

8. The variation of volume fraction for two different particle sizes (100 and 400 microns) of ADP are compared along different axes in X, Y and Z directions in the probe sensing region (slot).

a) The volume fraction magnitude is found to be virtually constant along all the axes for both particle sizes.

b) The magnitude of volume fraction for 100 micron particles is found to be somewhat higher than the volume fraction magnitude for 400 micron particles. This difference is believed to be due to the higher settling tendency of larger diameter particles and is in agreement with the literature.

9. Particle axial velocity profiles for the flow of slurry of ADP particle and Xylene are compared with the flow of slurry of CaC03 and water along the three different axes. The magnitude of axial velocity profiles for slurry of ADP and Xylene is found higher than that for the flow of CaC03 and water slurry along all the three axes. This

is due to the higher density magnitude of CaC03 than ADP particles. This agrees with the results in the literature.

5.3 Recommendations:

1. In order to mount in the fully developed flow region the probe can to be mounted at Z/D= 40. Hence the pipe length after the probe for the computations can be reduced. This will result in the decrease in the number of cell volumes formed by meshing the geometry. Hence less computational power will be required for the analysis.

2. The influence of sphericity of the particles should also be modeled as all the particles may not be of the spherical shapes.

3. The discrete phase flow of the slurry of ADP particles and Xylene should be modeled and the results of should be compared with multiphase flow modeling.

REFERENCES

Abebe, S. B., X. Z. Wang, R. Li, K.J. Roberts and X. Lai (2008). "The information content in NIR spectral data for slurries of organic crystals." *Powder Technology* 179(3): 176-183.

Brown, G. J. (2002). "Erosion prediction in slurry pipeline tee-junctions." *Applied Mathematical Modeling* 26(2): 155-170.

Chen, J., B. Duffy, D.F. Fletcher, B.S. Haynes and P. Nelson (2001). "FTIR spectroscopy measurements and CFD simulations of the pollutants arising from unflued combustion in a room." *Building and Environment* 36(5): 597-603.

Doron, P. and D. Barnea (1996). "Flow pattern maps for solid-liquid flow in pipes." *International Journal of Multiphase Flow* 22(2): 273-283.

Doron, P., M. Simkhis and D. Barnea (1997). "Flow of solid-liquid mixtures in inclined pipes." *International Journal of Multiphase Flow* 23(2): 313-323.

Eesa, M. and M. Barigou (2009). "CFD investigation of the pipe transport of coarse solids in laminar power law fluids." *Chemical Engineering Science* 64(2): 322-333.

Eskin, D., Y. Leonenko, and O. Vinogradov (2004). "On a turbulence model for slurry flow in pipelines." *Chemical Engineering Science* 59(3): 557-565.

Friesen, W. I. (1996). "Qualitative analysis of oil sand slurries using on-line NIR spectroscopy." *Applied Spectroscopy* 50(12): 1535-1540.

Karabelas, A. J. (1977). "Vertical distribution of dilute suspensions in turbulent pipe-flow." *AICHE Journal* 23(4): 426-434.

Kasat, G. R., A. R. Khopkar, V.V. Ranade and A.B. Pandit (2008). "CFD simulation of liquid-phase mixing in solid-liquid stirred reactor." *Chemical Engineering Science* 63(15): 3877-3885.

Kaushal, D. R., K. Sato, T Toyota, K. Funatsu, Y. Tomita (2005). "Effect of particle size

distribution on pressure drop and concentration profile in pipeline flow of highly concentrated slurry." *International Journal of Multiphase Flow* 31(7): 809-823.

Kaushal, D. R., V. Seshadri, S.N. Singh (2002). "Prediction of concentration and particle size distribution in the flow of multi-sized particulate slurry through rectangular duct." *Applied Mathematical Modeling* 26(10): 941-952.

Kaushal, D. R., Y. Tomita and R.R. Dighade (2002). "Concentration at the pipe bottom at deposition velocity for transportation of commercial slurries through pipeline." *Powder Technology* 125(1): 89-101.

Kaushal, D. R. and Y. Tomita (2003). "Comparative study of pressure drop in multisized particulate slurry flow through pipe and rectangular duct." *International Journal of Multiphase Flow* 29(9): 1473-1487.

Kaushal, D. R. and Y. Tomita (2007). "Experimental investigation for near-wall lift of coarser particles in slurry pipeline using gamma-ray densitometer." *Powder Technology* 172(3): 177-187.

Logos, C. and Q. D. Nguyen (1996). "Effect of particle size on the flow properties of a south Australian coal-water slurry." *Powder Technology* 88(1): 55-58.

Lin, C. X. and M. A. Ebadian (2008). "A numerical study of developing slurry flow in the entrance region of a horizontal pipe." *Computers & Fluids* 37(8): 965-974.

J. Ling, P. V. Skudarnov, C. X. Lin and M. A. Ebadian (2003). “Numerical investigations of liquid–solid slurry flows in a fully developed turbulent flow region.” *International Journal of Heat and Fluid Flow* 24 (3):389-398

Michaelides, E., (2006), *Particles, bubbles and drops: their motion, heat and mass transfer*, World Scientific Publishing, Singapore.

Oey, R. S., R. F. Mudde, M. Portela and H.E.A. Van Den Akker (2001). "Simulation of a slurry airlift using a two-fluid model." *Chemical Engineering Science* 56(2): 673-681.

Pope, S. B., (2000), *Turbulent Flows*, Cambridge University Press, NY, USA

Seshadri, V., S. N. Singh and D.R. Kaushal (2006). "A model for the prediction of concentration and particle size distribution for the flow of multisized particulate suspensions through closed ducts and open channels." *Particulate Science and Technology* 24(2): 239-258.

Switalski, S. C., T. Colin, N. Redden, E. Stahlecker and V. Parthasarathy, (1999), “Near Infrared Diffuse Reflectance fiber optic spectroscopy for process monitoring applications,” *Proceedings of SPIE – The International Society for Optical Engineering*, 3538:158-166.

Wei, J. J., C. B. Hu, P. Jiang (2000). "K-epsilon-T model of dense liquid-solid two-phase turbulent flow and its application to the pipe flow." *Applied Mathematics and Mechanics*-English Edition 21(5): 519-528.

Xu, J., A. Rouelle, K.M. Smith, D. Celik, M.Y. Hussaini and S.W. Van Sciver (2004). "Two-phase flow of solid hydrogen particles and liquid helium." *Cryogenics* 44(6-8): 459-466.

APPENDIX

Snapshots taken from FLUENT 6.3

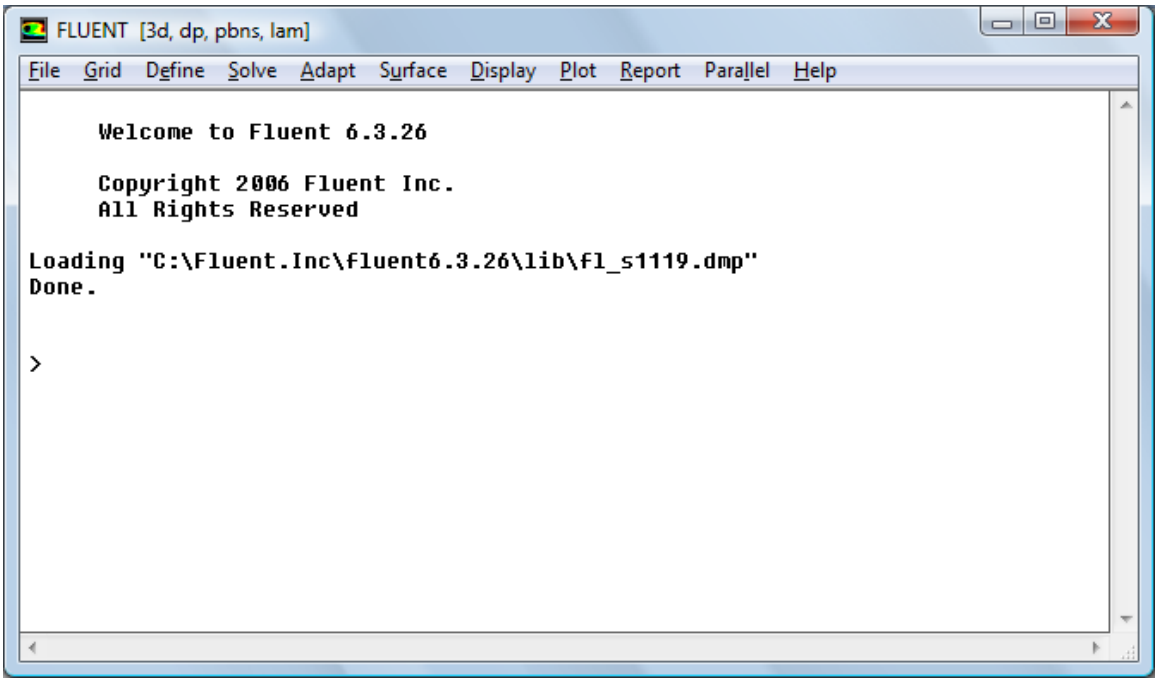

Main pull down menu of FLUENT. Version 3ddp stands for 3D-Double Precision.

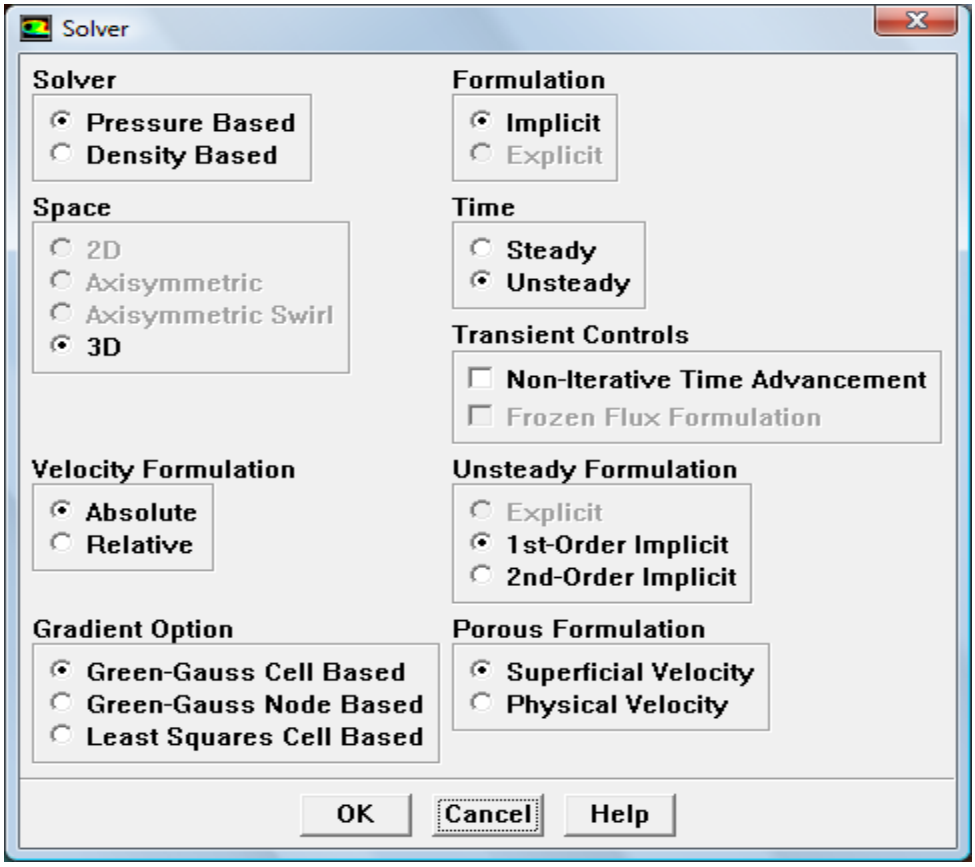
Solver
Solver
Pressure Based
Density Based
Formulation
Implicit
Explicit
Space
2D
Axisymmetric
Axisymmetric Swirl
3D
Time
Steady
Unsteady
Transient Controls
Non-Iterative Time Advancement
Frozen Flux Formulation
Velocity Formulation
Absolute
Relative
Unsteady Formulation
Explicit
1st-Order Implicit
2nd-Order Implicit
Gradient Option
Green-Gauss Cell Based
Green-Gauss Node Based
Least Squares Cell Based
Porous Formulation
Superficial Velocity
Physical Velocity
OK
Cancel
Help

SOLVER MENU

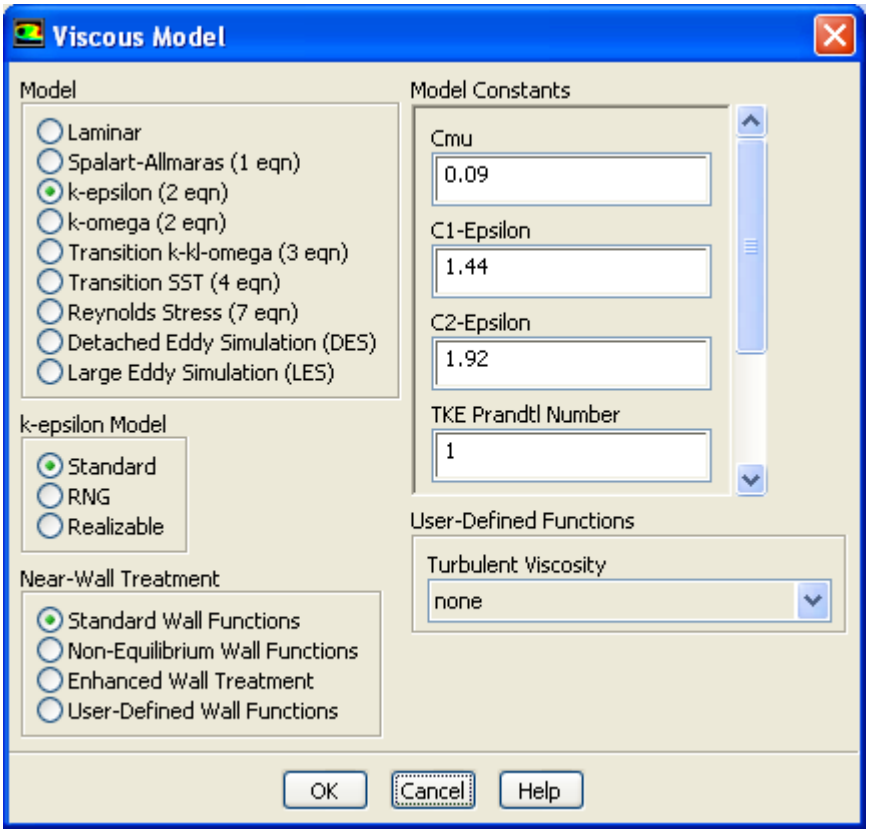

Selection of Turbulence model in FLUENT. Default values of model constants are used.

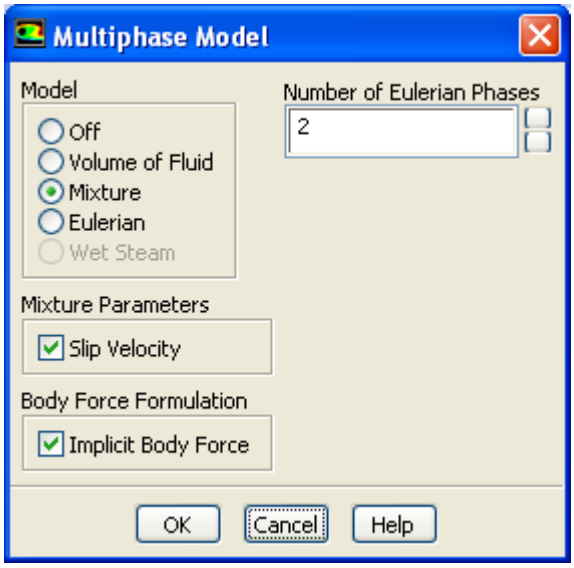

Selection of Multiphase model.

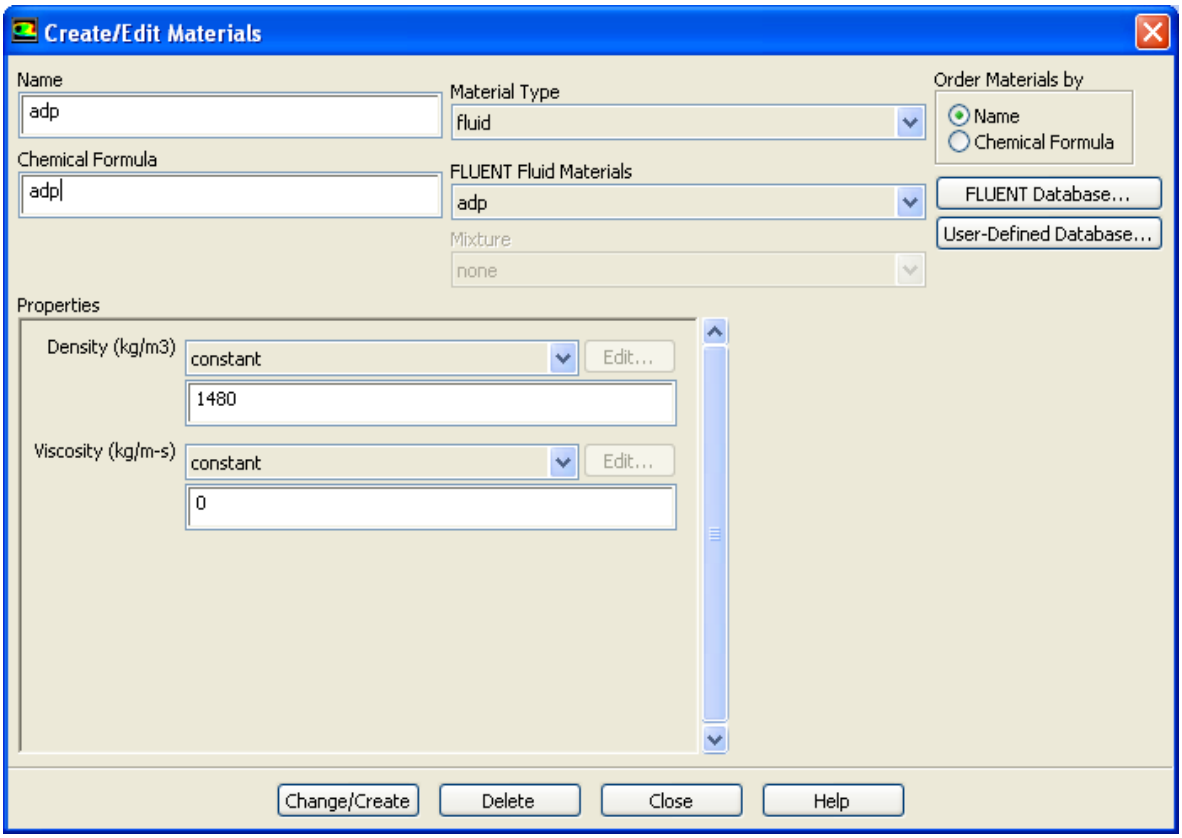

MATERIAL PROPERTIES OF ADP

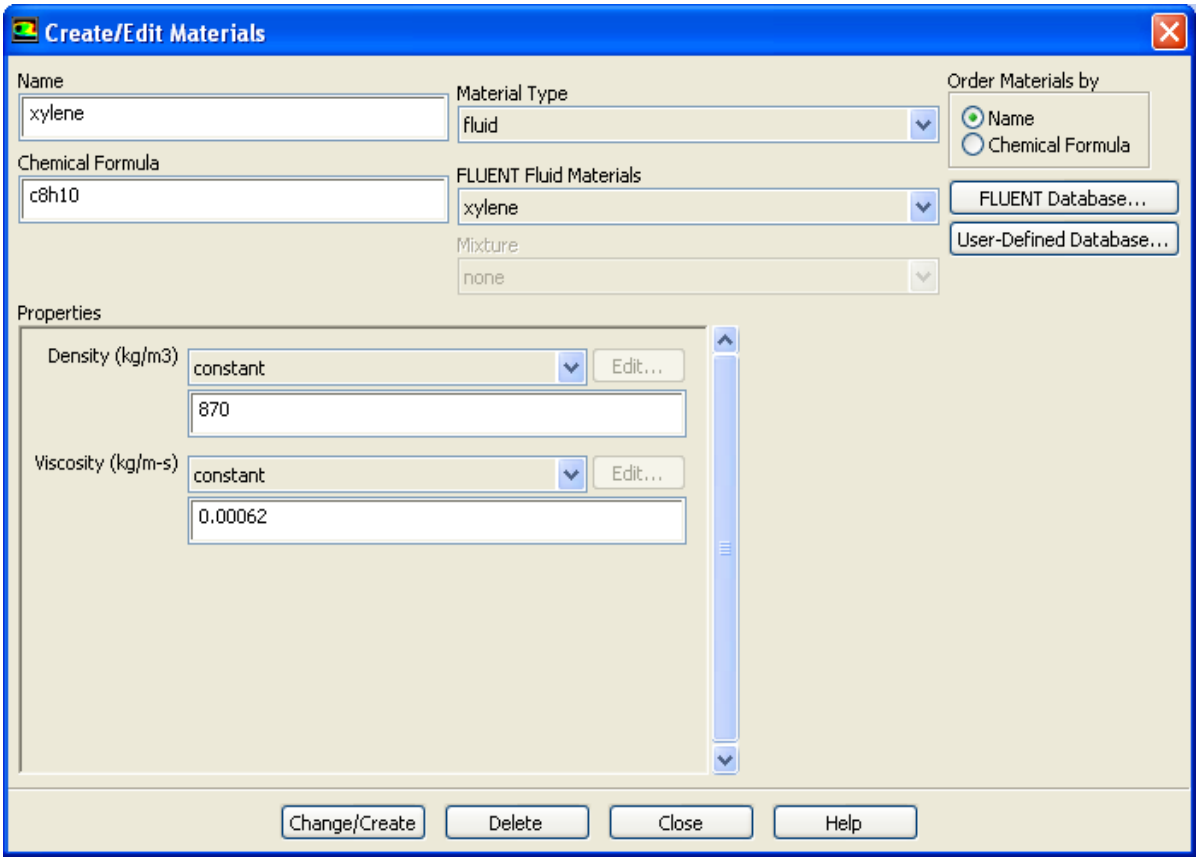

MATERIAL PROPERTIES OF XYLENE

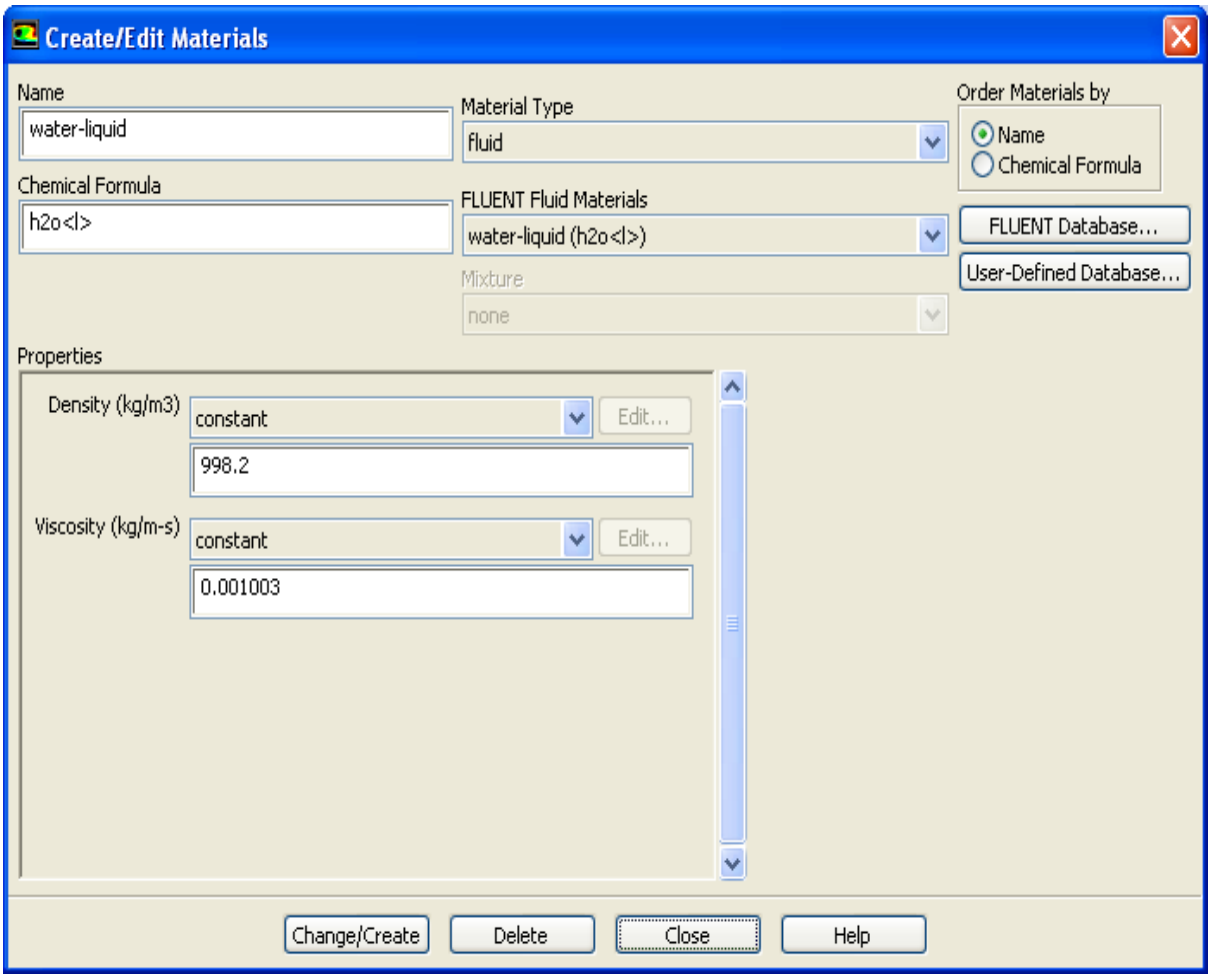

DEFAULT PROPERTIES OF WATER.

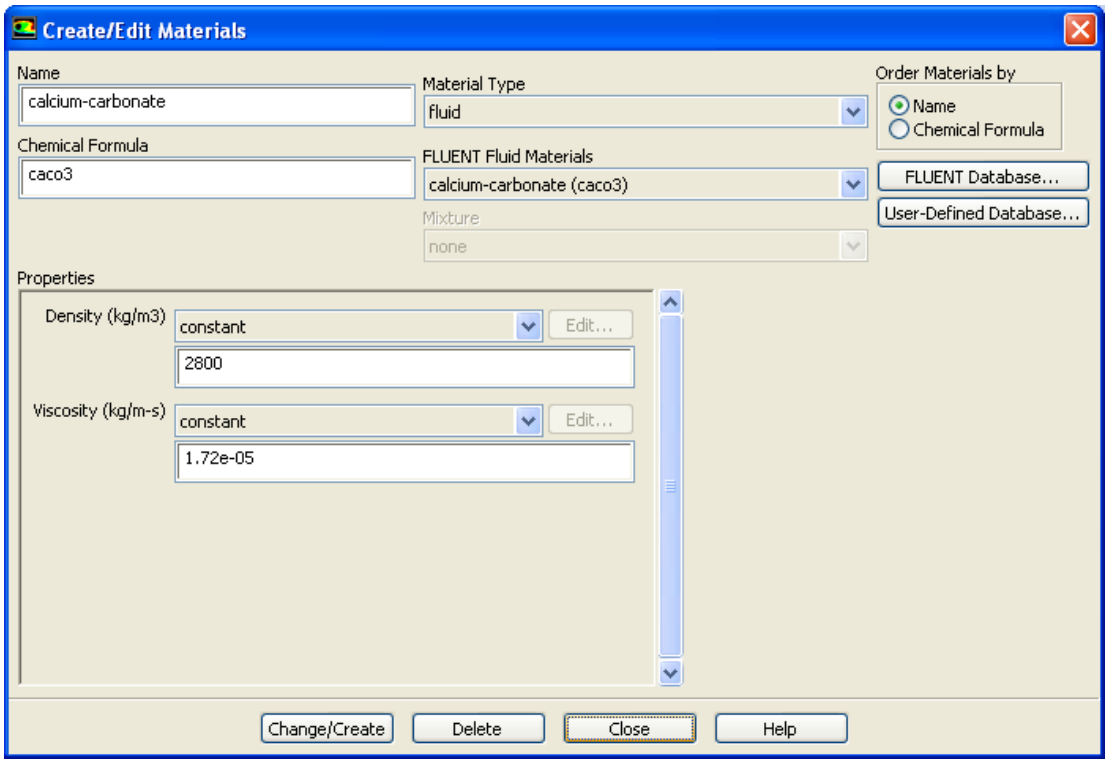

DEFAULT PROPERTIES OF CaCO3

VITA

GAURAV SHARMA

Candidate for the Degree of

Master of Science

Thesis: CFD ANALYSIS OF TURBULENT SLURRY FLOW THROUGH THE SENSING REGION OF NEAR IR DIFFUSE TRANSMISSION AND REFLECTANCE PROBE MOUNTED IN A PIPE FLOW

Major Field: Mechanical and Aerospace Engineering.

Biographical:

Personal data: Born in Gwalior, India on 21st June 1983, son of Mrs. Kamlesh Sharma and Mr. H.K. Sharma.

Education:
Completed the requirements for the Master of Science in Mechanical and Aerospace Engineering at Oklahoma State University, Stillwater, Oklahoma in December, 2009.
Received Bachelor of Engineering (B.E.) degree in Mechanical Engineering at MITS (RGPV), Gwalior, Madhya Pradesh/India in July 2007.

Experience:
Software Engineer: Sep 2006 to Aug 2007
Patni Computer Systems, India.

Teaching Assistant: Aug 2007 to April 2008,
Department of Mechanical and Aerospace Engineering, Oklahoma State University.

Research Assistant: May 2008 to Dec 2009,
Department of Mechanical and Aerospace Engineering, Oklahoma State University.

Name: Gaurav Sharma Date of Degree: May, 2010

Institution: Oklahoma State University Location: Stillwater, Oklahoma

Title of Study: CFD ANALYSIS OF TURBULENT SLURRY FLOW THROUGH THE SENSING REGION OF NEAR IR DIFFUSE TRANSMISSION AND REFLECTANCE PROBE MOUNTED IN A PIPE FLOW

Pages in Study: 118 Candidate for the Degree of Master of Science

Major Field: Mechanical and Aerospace Engineering

Scope and Method of Study: In the current research, CFD analysis of a chemical slurry consisting of liquid Xylene flowing with 2 amino, 4, 6 dimethyl pyrimidine (ADP) particles in a pipe has been considered primarily. Some cases of comparison of slurries of ADP-Xylene and CaC03-water are also considered. The diameter of the pipe is 0.0508 m. The length to diameter ratio of the pipe is 70. A geometric model of an FTIR/NIR probe is mounted asymmetrically on the wall of the pipe and major concentration was given to the flow in the sensing region of the probe. Fluent (Ansys) has been employed as the simulation software to predict the end results of the flow. K-ε Turbulence model and mixture multiphase model are employed for analysis. Particle sizes of 100 and 400 microns are considered and a comparative study is done based on variation in particle size.

Findings and Conclusions: In the probe vicinity, fluctuations are observed in axial velocity profiles along the centerline and the axes parallel to centerline and passing through probe sensing region. Axial velocity profiles are analyzed along vertical axes at different axial position. These profiles hold fair agreement with the literature. Particle volume fraction profiles are analyzed along different axes parallel to x, y and z directions but lying in the probe sensing region. It has been noticed that variation in particle volume fraction magnitude is negligible. Thus volume fraction is nearly constant in the probe sensing region. The particle volume fraction for 100 and 400 micron particles size are compared along the axes in the sensing region of the probe. It has been found that 100 micron particles have higher particle volume fraction magnitudes than 400 micron particles. This is in good agreement with literature. Axial velocity profiles of ADP-Xylene slurry is compared with that of CaC03-water slurry. The axial velocity of ADP particles is found to be higher than that of CaC03 particles due to density difference between the particles. This agrees well with the literature.

ADVISER'S APPROVAL: Dr. Frank W. Chambers